When AI Changes Work: A Machine Learning Analysis of AI-Related Job Concerns and Mental Health Discussions on Reddit

James Cao[1], Haixia He[2], Weiguo Fan[2]

[1]La Jolla High School, San Diego, CA; [2]Department of Business Analytics, University of Iowa, Iowa City, IA

Background

- AI is **transforming** work. In 2024, **417,000** employees were **laid-off** from technology companies globally.
- Many workers express **uncertainty** and **stress** in work environments.
- Reddit provides **large-scale** discussion of these experiences.
  - **2.2 billion** visits per month [6], **anonymous users**, **no personal information**

Objectives

Purpose: To examine how Reddit users perceive the impact of artificial intelligence on jobs and careers.

RQ1: How do Reddit users discuss the impact of AI on work and mental health?

RQ2: What mental health experiences are most commonly discussed in AI/job-related Reddit posts?

RQ3: How can machine learning models detect and classify AI-related job concerns and mental health impacts?

Methodology

1 Data Collection

4000 posts and comments were collected from subreddits

AI:
- r/singularity
- r/dataengineering
- r/ai

Job/Work:
- r/careerguidance
- r/jobs
- r/layoffs

Mental Health:
- r/mentalhealth
- r/depression
- r/anxiety

2 Data Annotation

Four annotators separately labeling:

1. **Discussion topic** (AI, Job/Work, Mental Health)
2. **Sentiment** (Positive, Mixed, Negative)
3. **Personal experience** (Yes/No)
4. **Employment disruption** (Yes/No)
5. **Demographics** (Age, Gender, Occupation)

High agreement was reached (**Cohen's κ > 0.70**)

Methodology

3 Data Preprocessing

Duplicate texts were removed, lowercased all letters, and the dataset was sorted by author's name.

4 Emotion and Topic Analysis

- Used a roBERTa model trained by GoEmotions to identify 28 emotional categories
- BERTopic on both the complete dataset and exclusively "Mental Health"-related texts
- Compared emotion and topic distributions across AI-related employment discussions

Model	Purpose
CardiffNLP	Pre-trained sentiment model
Bartlarge-MNLI	Zero-shot classification
fine-tuned roBERTa	Pre-trained Transformer model
VADER	Baseline classifier
Random Forest Model	Classic machine learning algorithm
LinearSVM (TF-IDF)	Supervised machine learning algorithm specific to classification

5 Statistical Analysis

- Frequency distributions were found for attitude and topic labels
- Chi-square tests of independence
- Cramer's V effect sizes

6 Machine Learning Classification

Six machine learning models were trained or tested:
- twitter-roBERTA-base (CardiffNLP)
- Bartlarge-MNLI
- fine-tuned robERTa
- VADER
- Random Forest Model
- LinearSVM (TF-IDF)

Results

Discussion Themes

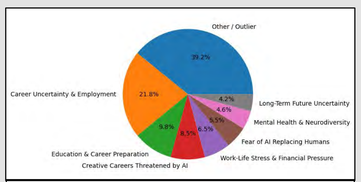


Figure 1: Seven themes found by BERTopic.



Figure 2: Most common words in mental health texts.

Mental Health Patterns

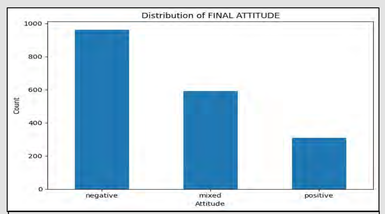


Figure 3: Sentiment distribution. RQ2

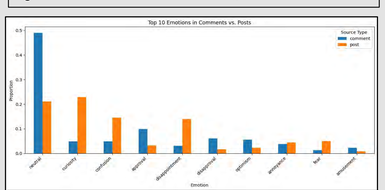


Figure 4: Top 10 most frequent emotions

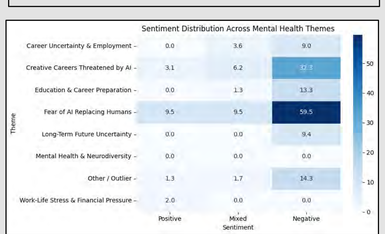


Figure 5: Sentiment Distribution across Mental Health Themes

Model Performance

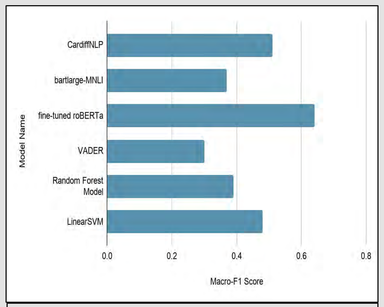


Figure 6: Sentiment classification performance by Macro-F1 scores.

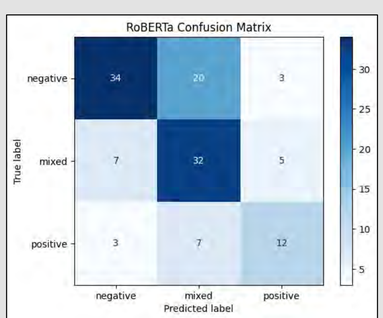


Figure 7: Confusion matrix of the fine-tuned RoBERTa sentiment classifier.

Conclusion

Key Findings

- Topic modeling identified **recurring themes**, including **career uncertainty**, **education** & career preparation, and **creative careers** threatened by AI.
- **Negative** and **mixed** sentiments were more prevalent than positive ones.
- Emotion analysis revealed a predominance of **pessimistic** emotions (confusion, disappointment).
- There were **significant associations** between **discussion themes** and **sentiment** (χ^2, $p < 0.001$).
- The **fine-tuned roBERTa model** achieved the best sentiment classification performance
  - **Macro-F1 = 0.64**
- The findings suggest that concerns about **AI extend beyond employment**, with many users expressing **emotional and mental health** impacts alongside **career-related challenges**.

Future Directions

- Expand the dataset to include additional **social media platforms** or **subreddits**.
- Improve classification performance using **larger** or **domain-specific** language models.
- Apply **time series analysis** to examine **temporal trends** in discussions across online communities.

Acknowledgements

- Secondary Student Training Program (SSTP)
- Tippie College of Business, Haixia He and Dr. Weiguo Fan
- Kai Seifan, Elizabeth Wang, and Sarah Li

For any questions, please email: ohjamescao@gmail.com

References

1. Baholli, I., Hidri, F., & Tigno, G. (2026). Sentiment and Topic Dynamics in Reddit Discussions on AI and Automation Innovation in the Workforce. Communications in Computer and Information Science, 2669 CCIS, 334–342. https://doi.org/10.1007/978-3-032-07373-0_24/TABLES/2
2. Mahdavimoghaddam, J., Saha, K., Hui, J., Dillahunt, T., & Bagheri, E. (2026). A Social Media Lens on the Needs and Concerns of Information Workers. ACM Transactions on Social Computing, 9(2), 1–44. https://doi.org/10.1145/3811241
3. More than half of U.S. workers say job insecurity causing stress. (2025). Retrieved July 14, 2026, from www.apa.org/news/press/releases/2025/05/job-insecurity-causing-stress
4. Ocal, A., & Crowston, K. (2024). Framing and feelings on social media: the futures of work and intelligent machines. Information Technology & People, 37(7), 2462–2488. https://doi.org/10.1108/ITP-01-2023-0049
5. Reddit Statistics 2026 | Traffic, Users, Ads and Revenue. (n.d.). Retrieved July 14, 2026, from https://www.interteammarketing.com/blog/reddit-statistics-2026
6. Shekhar, A., & Saurombe, M. D. (2026). Algorithmic anxiety: AI, work, and the evolving psychological contract in digital discourse. Frontiers in Psychology, 17, 1745164. https://doi.org/10.3389/FPSYG.2026.1745164/TEXT

Turning Tumors "Cold": SETDB1 expression correlates with immune exclusion in endometrial cancer

Adrian Chan[1,2], Kiarash Salari[2], Shujie Yang[1, 3]
University of Iowa Department of Pathology,[1] Phillips Exeter Academy,[2] Holden Comprehensive Cancer Center,[3] University of Iowa Carver College of Medicine

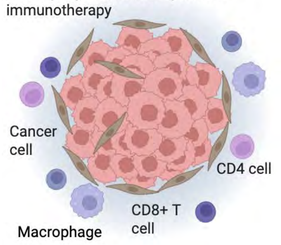
IOWA HEALTH CARE | Holden Comprehensive Cancer Center

Introduction

1. Endometrial cancer(EC) mortality has continued to rise despite advances in treatment.[1]

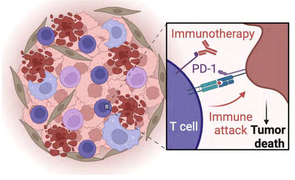
Cold Tumor

- Exclusion of CD8+ T cells, CD4 T helper cells, and macrophages
- Poor prognosis and response to immunotherapy



Hot Tumor

- Immune cells are present in tumor
- Improved killing of tumor cells with immunotherapy treatment



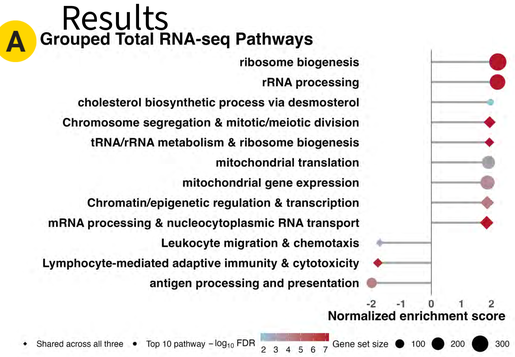
2. SETDB1 is an epigenetic gene silencer. In mouse models, it has been shown to promotes oncogene transcription and creates a “cold” tumor microenvironment.[4]
3. Is high SETDB1 expression associated with immune exclusion and worse immunotherapy outcomes in EC?

Methods

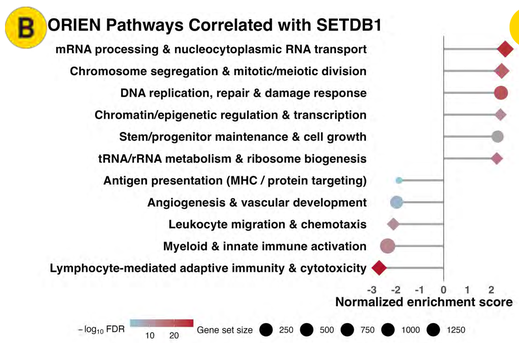
2 Cell Models: EC ISH and PDC10 cell lines(n=3 per sample)
2 Tumor Cohorts: ORIEN-UCEC(n=1127), TCGA-UCEC(n=553)

1. Associated pathways identified by Gene Ontology(GO) pathway analysis of Gene Set Enrichment Analysis(GSEA)
2. Kaplan-Meier curves and Cox models evaluated overall survival. High/low groups based on maximally selected cutpoints.
3. Bulk-RNA immune-marker scores were correlated with SETDB1 expression.

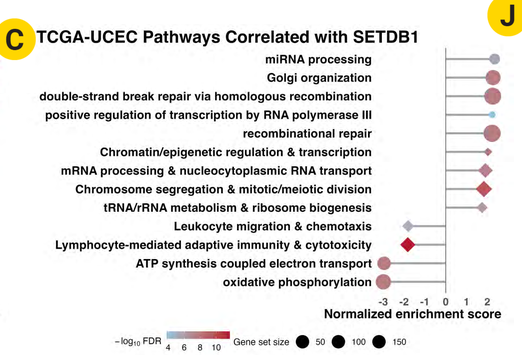
Results



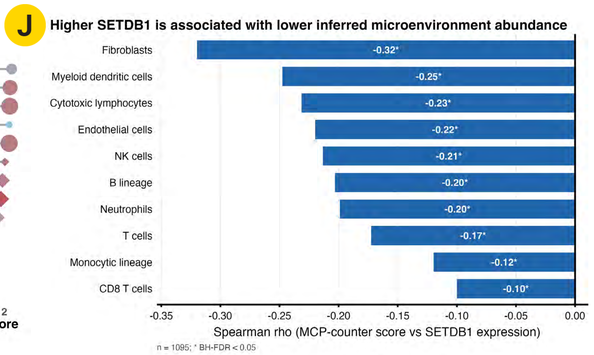
A. Initial SETDB1-loss RNA-seq identifies cell-cycle and RNA-processing pathways and inversely correlated with and lymphocyte-mediated immunity.



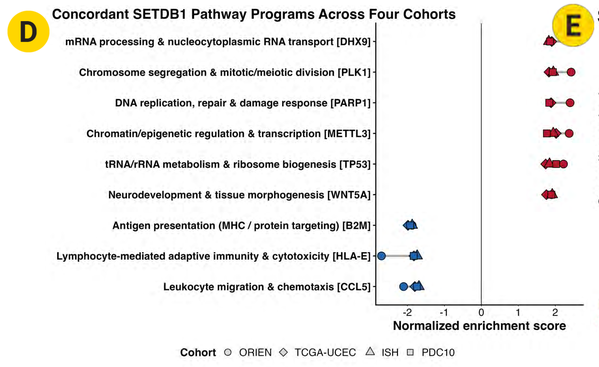
B. SETDB1 co-expression is associated with proliferative and immune-suppressive pathways in the ORIEN EC cohort.



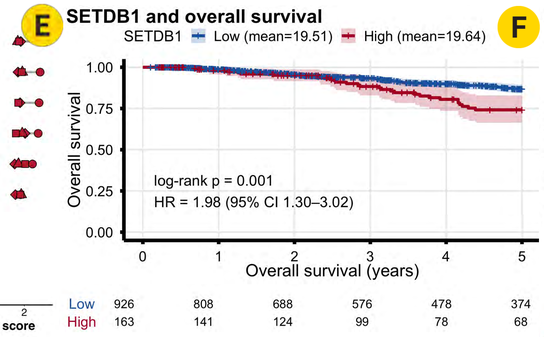
C. SETDB1 co-expression is associated with proliferative and immune-suppressive pathways in the TCGA EC cohort.



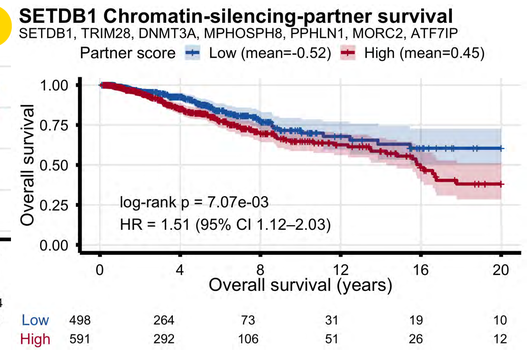
J. SETDB1 expression is inversely associated with inferred immune-cell abundance.



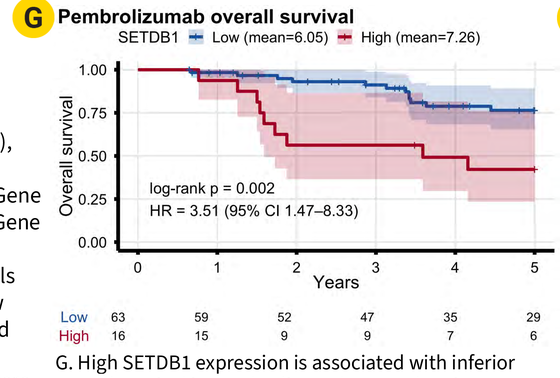
D. SETDB1-associated pathways are concordant across Yang, ORIEN and TCGA independent cohorts.



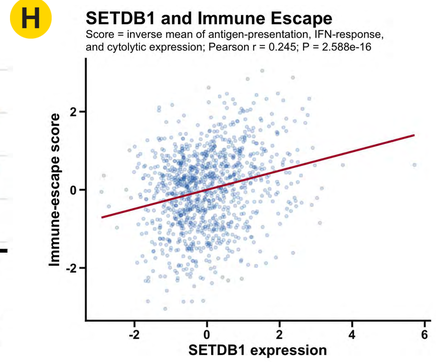
E. High SETDB1 expression is associated with inferior overall survival in endometrial cancer



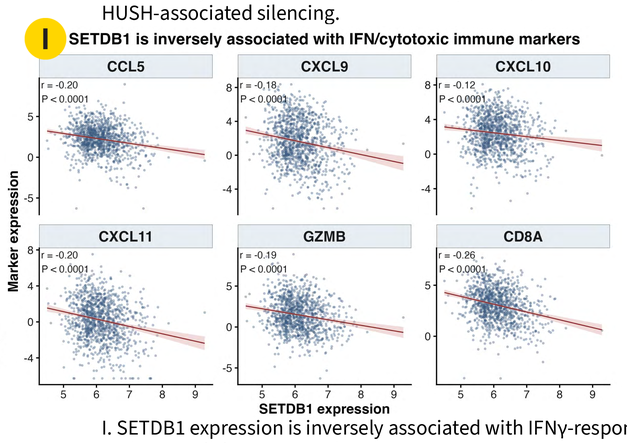
F. SETDB1 chromatin-silencing-partner score is associated with overall survival. Genes represent a chromatin-silencing partner panel: SETDB1-mediated H3K9 methylation, TRIM28/DNMT3A corepression, and HUSH-associated silencing.



G. High SETDB1 expression is associated with inferior overall survival in pembrolizumab-treated patients.



H. SETDB1 expression correlates with a composite immune-escape score including antigen presentation, cytolytic, and IFNγ-response programs.



I. SETDB1 expression is inversely associated with IFNγ-response and cytotoxic immune markers.

Conclusion

1. Oncogenic cell cycle and RNA-processing pathways are activated by SETDB1. [Figures A-D]
2. Immune pathways for antigens, leucocytes and lymphocytes are suppressed by SETDB1. [Figures A-D]
3. SETDB1-high and SETBD1-partner-high expression are associated with worsened survival over 20 years using optimal cutpoint. [Figures E-F]
4. SETDB1 associated with worsened prognosis after Pembrolizumab treatment, consistent with ”cold” tumors limiting PD-1 effectiveness. [Figure G]
5. SETDB1 inversely correlated IFNγ-response and cytotoxic immune markers. cytotoxic lymphocytes and CD8A ,CCL5, and CXCL11 genes had the greatest inverse correlation with SETDB1. [Figure H-J]

Future Direction

- Validate SETDB1 and partner survival in cohorts separated by age, stage, histology, tumor purity, and molecular subtype.
- Validate CD8 T cells, NK cells, antigen-presenting cells, and SETDB1 protein by immunohistochemistry, multiplex imaging, and flow cytometry.
- Further investigate the immune escape finding in EC cells, organoids, and mouse models, focusing on CCL5 and CD8A.

Acknowledgments

Thank you to Dr. Yang and Dr. Salari for your invaluable support, and mentorship. This project was supported by NIH R37-CA238274 (SY) and the Department of Pathology Start-Up Fund (SY).

IOWA HEALTH CARE | Holden Comprehensive Cancer Center

NCI Comprehensive Cancer Center
A Cancer Center Designated by the National Cancer Institute

References:

Adrian Chan
cheuklokadrian-chan@uiowa.edu
cchan2@exeter.edu
Dr. Shujie Yang Laboratory

Investigating the Metal-Binding Ability of Thiazole Orange and a Related Cyanine Dye

Ashley Chen[1], Tommy Branstad Phillips[2], Prof. Chris Pigge[2]

[1]The Bear Creek School (Redmond, WA), [2]Department of Chemistry, University of Iowa

Introduction

- **Cyanine dyes are conjugated organic molecules** that exhibit strong absorption in the visible to near-infrared region, making them useful in bioimaging, fluorescent sensing, and medical diagnostics.[1-3]
- **Noble metals**, such as Rhodium and Palladium, **form stable complexes** with many organic ligands.
- These complexes are widely used as **catalysts** in high value chemical and pharmaceutical synthesis.[4-5]
- However, **the ability of these specific cyanine dyes to bind metals has not been extensively investigated.**
- Examining which metals these dyes coordinate to can provide insight into **ligand-metal interactions** and guide the design of **new metal complexes** and **photocatalysts**.

Research Objective

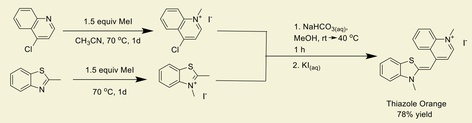
To determine **which noble metals**, if any, **form complexes** with Thiazole Orange and a structurally related derivative and to investigate **how the structural and electronic properties of both the dye and metal influence metal binding.**

Hypothesis- Thiazole Orange and its derivative will form metal complexes with noble metals that commonly coordinate to carbon-based ligands.

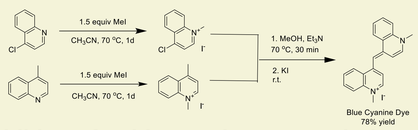
Methodology

1. Convergent synthesis of the cyanine dyes

Thiazole Orange ($C_{19}H_{17}IN_2S$):



Cyanine Blue ($C_{21}H_{19}IN_2$):



2. Addition of noble metal compounds (AuCl(tht), $PdCl_2$, $[RhCl(CO)_2]_2$) to attempt to make metal complexes

3. Characterization by ^{1}H NMR*, ^{13}C NMR and HRMS*

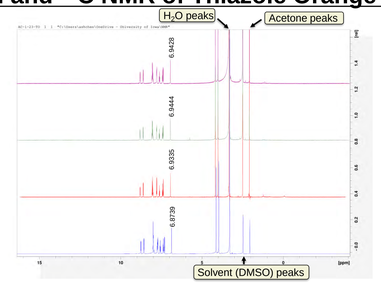


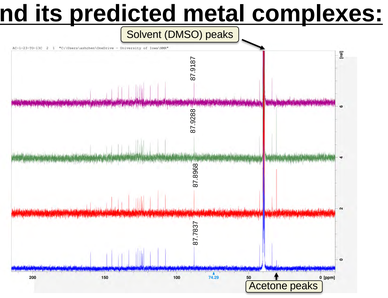


*Nuclear Magnetic Resonance, High Resolution Mass Spectrometry

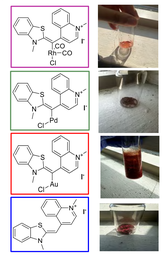
Results

^{1}H and ^{13}C NMR of Thiazole Orange and its predicted metal complexes:



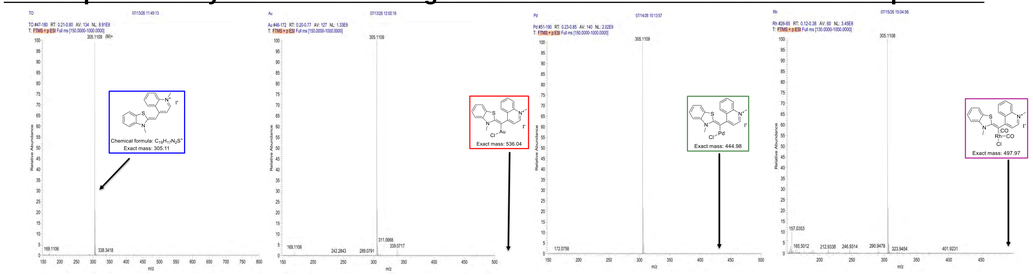


Structures and pictures of confirmed Thiazole Orange and its predicted metal complexes:



- Each ^{1}H NMR spectrum showed the expected integration (17 H) and peak pattern for Thiazole Orange.
- Each ^{13}C NMR spectrum contained 19 carbon signals, consistent with the structure of Thiazole Orange.
- NMR data for Thiazole Orange itself is also consistent with literature values.
- Addition of the metal compounds resulted in a uniform ~0.2 ppm shift in all ^{1}H and ^{13}C NMR peaks.

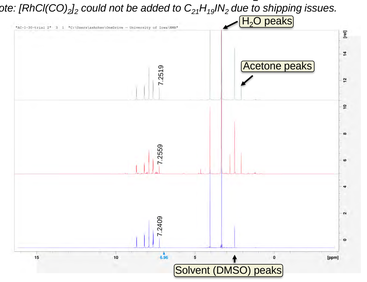
Mass spectrometry for Thiazole Orange before and after addition of metal compounds:



- The mass spectra of Thiazole Orange and the three metal-treated samples show nearly identical peak patterns, with the dominant peak at *m/z* ≈ 305.11.
- The mass spectra of the metal-treated samples do not show the theoretical masses of the predicted metal complexes.

^{1}H NMR of Cyanine Blue and its predicted metal complexes:

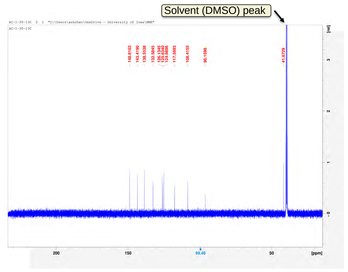
Note: $[RhCl(CO)_2]_2$ could not be added to $C_{21}H_{19}IN_2$ due to shipping issues.



Structures and pictures of confirmed cyanine blue and its predicted metal complexes:

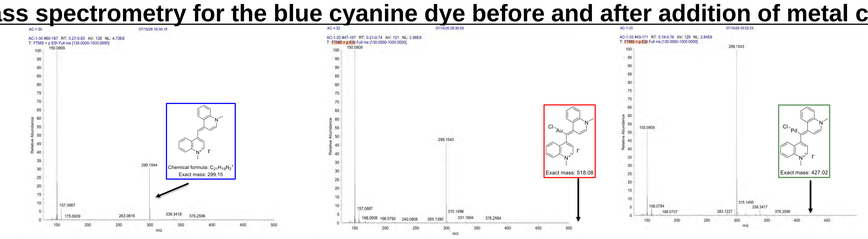


^{13}C NMR of Cyanine Blue:



- Each ^{1}H NMR spectrum showed the expected integration and peak pattern for Cyanine Blue.
- The ^{13}C NMR spectrum of the dye contained the expected carbon signals, confirming its structure.
- Addition of the metal compounds resulted in only a minimal ~0.01 ppm shift in all the ^{1}H NMR peaks.

Mass spectrometry for the blue cyanine dye before and after addition of metal compounds:



- The mass spectra of Cyanine Blue and the two metal-treated samples show similar peak patterns, with the major peak at *m/z* ≈ 299.15.
- The mass spectra of the metal-treated samples do not show the theoretical masses of the predicted metal complexes.

Conclusions

- Thiazole Orange and Cyanine Blue were **successfully synthesized in high yield (78%)** and **confirmed** by clean ^{1}H NMR, ^{13}C NMR, and HRMS.
- Addition of AuCl(tht), $PdCl_2$, and $[RhCl(CO)_2]_2$ **did not produce evidence of metal complex formation**, as NMR spectra showed only **minimal chemical shift changes** and HRMS detected only the **dyes themselves** rather than the predicted metal complexes.
- These results suggest that these cyanine dyes **do not readily coordinate** to these metals under these mild conditions.
- We hypothesize that the lack of coordination may result from **insufficient nucleophilicity** of the central binding carbon due to electron delocalization across the molecule, or from **structural rigidity** due to the double bond next to that central carbon limiting metal-ligand interactions.

Future Directions

- Obtain NMR and mass spectrometry data for cyanine blue after the addition of $[RhCl(CO)_2]_2$.
- Test **different reaction conditions** (e.g. metal-dye ratio, solvent, counterion, addition of a base or acid, etc.) and **metals** to promote metal complex formation.
- **Verify** metal complex formation using ^{1}H NMR, ^{13}C NMR, HRMS, and possibly X-ray crystallography.
- Investigate the **photophysical* properties** of the successful metal complexes using fluorescence spectroscopy.
- Evaluate the **catalytic* activity** of the complexes in different reactions.

*interaction with light, effectiveness as a catalyst

Acknowledgements

I would like to thank Prof. Chris Pigge and Tommy Branstad Phillips for providing me this opportunity to contribute to this project and guiding me through every step of the research process.

References

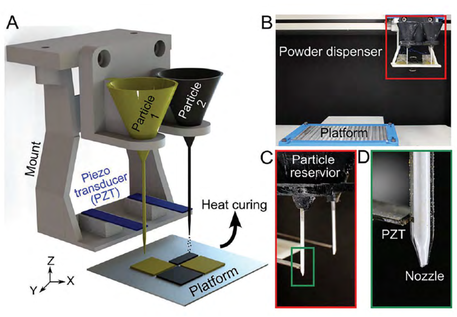
1. Gopika, G. S.; Prasad, P. M. H.; Lekshmi, A. G.; Lekshmypriya, S.; Sreesaila, S.; Arunima, C.; Kumar, M. S.; Anila, A.; Sreekumar, Z. P.; Pillai, P. S. Chemistry of Cyanine Dyes—A Review. *Mater. Today Proc.* **2021**, *46*, 3102–3108. https://doi.org/10.1016/j.matpr.2021.02.622.
2. Wang, B.-L.; Jiang, C. DNA G-Quadruplexes as a Template To Direct Cyanine Dyes To Form H-Aggregates and Application of the Self-Assembly Entity as a New G-Quadruplexes Ligands Screening Platform. *Anal. Chem.* **2019**, *91*(2), 1541-1547. https://doi.org/10.1021/acs.analchem.8b04677
3. Deligeorgiev, T. G.; Zaneva, D. A.; Kim, S. H.; Sabnis, R. W. Preparation of Monomethine Cyanine Dyes for Nucleic Acid Detection. *Dyes Pigm.* **1998**, *37* (3), 205–211. https://doi.org/10.1016/S0143-7208(97)80088-5
4. Watson, I. C.; Schumann, A.; Yu, H.; Davy, E. C.; McDonald, R.; Ferguson, M. J.; Hering-Junghans, C.; Rivard, E. *N*-Heterocyclic Olefin-Ligated Palladium(II) Complexes as Pre-Catalysts for Buchwald–Hartwig Aminations. *Chem. Eur. J.* **2019**, *25* (40), 9678–9690. https://doi.org/10.1002/chem.201901376.
5. König, S.; Jones, P. G.; Tamm, M. Preparation of 2-Alkylidene-Substituted 1,3,4,5- Tetramethylimidazolines and Their Reactivity Towards Rhodium(I) Complexes and B(C6F5)3. *Eur. J. Inorg. Chem.* **2013**, *2013* (14), 2301–2314. https://doi.org/10.1002/ejic.201201516.
6. Fürstner, A.; Alcarazo, M.; Goddard, R.; Lehmann, C. W. Coordination Chemistry of Ene-1,1-diamines and a Prototype "Carbodicarbene". *Angew. Chem., Int. Ed.* **2008**, *47* (17), 3210–3214. https://doi.org/10.1002/anie.200705798.
7. Körner, L.; Yang, L.; Bockfeld, D.; Tamm, M. 1,1-Enediamines as Highly Polarized Olefin Ligands. *J. Organomet. Chem.* **2023**, *984*, 122572. https://doi.org/10.1016/j.jorganchem.2022.122572.
8. Powers, K.; Hering-Junghans, C.; McDonald, R.; Ferguson, M. J.; Rivard, E. Improved Synthesis of *N*-Heterocyclic Olefins and Evaluation of Their Donor Strengths. *Polyhedron* **2016**, *108*, 8–14. https://doi.org/10.1016/j.poly.2015.07.070.
9. Sen, P. P.; Saha, N.; Roy, S. R. Investigating the Potency of a Phenalenyl-Based Photocatalyst under the Photoelectrochemical Condition for Intramolecular C–S Bond Formation. *ACS Catal.* **2024**, *14*, 907-920. https://doi.org/10.1021/acscatal.3c05500.
10. Fulmer, G. R.; Miller, A. J. M.; Sherden, N. H.; Gottlieb, H. E.; Nudelman, A.; Stoltz, B. M.; Bercaw, J. E.; Goldberg, K. I. NMR Chemical Shifts of Trace Impurities: Common Laboratory Solvents, Organics, and Gases in Deuterated Solvents Relevant to the Organometallic Chemist. *Organometallics* **2010**, *29* (9), 2176–2179. https://doi.org/10.1021/om100106e.

Aerodynamic Focusing of Powder Streams for Acoustic-Modulated Additive Manufacturing

Brad Chen, Yi Wei, Xuan Song PhD
Industrial Systems Engineering, University of Iowa

IOWA

Introduction



Scott, M. et al. (2023

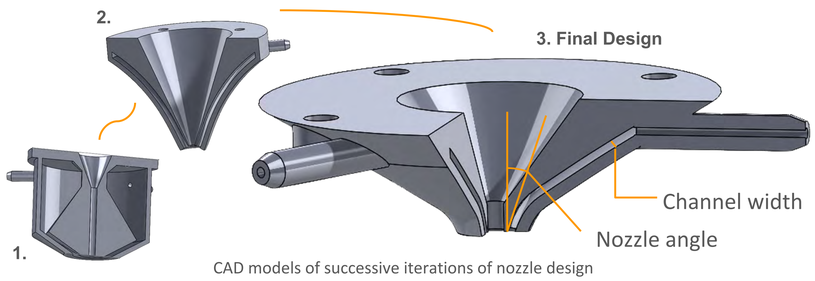
- Vibrations from the piezo transducer (PZT) hits the nozzle to dispense powder
- Acoustic modulated depositions is a novel and relatively cheap approach to powder deposition
- Sugar particles of were used as a substitute for polymer bonded explosive materials

Enables cheap customizable multi-material 3D printing for aerospace, biomedical, and electronics.

Problem
Current powder flow is not fine enough

Goal
Understand how air can be used to focus powder streams

Design Process

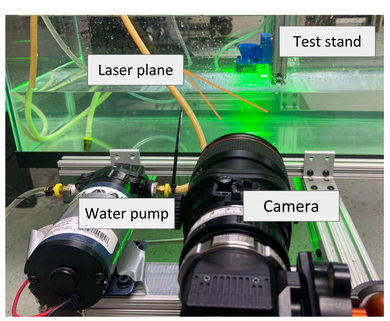


CAD models of successive iterations of nozzle design

Methodology

Liquid Testing (1)

- Submerge test stand in water filled with silver-coated glass microspheres
- Illuminate plane perpendicular to camera with a laser
- Attached test nozzle onto test stand
- Run water pump at different voltages
- Record a one second clip at 400 fps

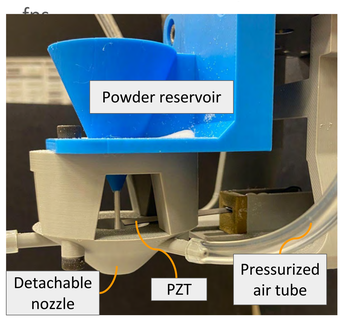


Liquid testing setup

In-air PZT Testing (2)

Flow behavior in fluid testing narrowed down parameters tested in in-air PZT testing.

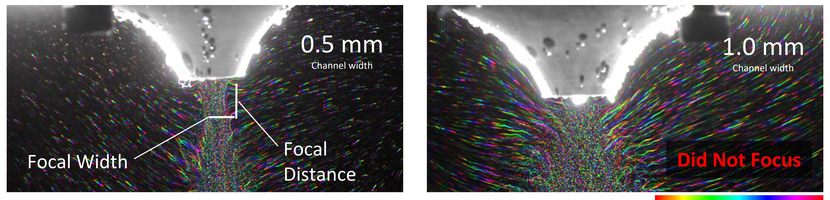
- Attached designed nozzle
- Blow air at different pressures
- Record a one second clip at 1000 fps



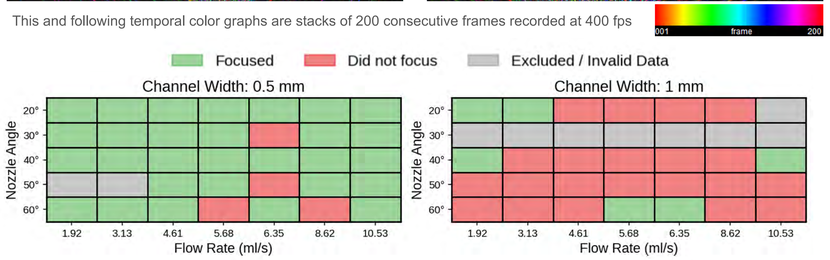
In-air PZT test stand

Results - Liquid Testing

20 degree nozzles at 1.92 ml/sec

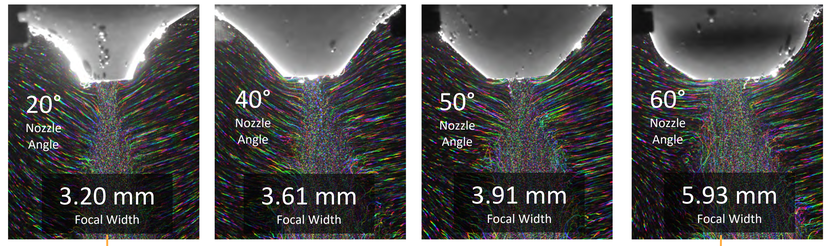


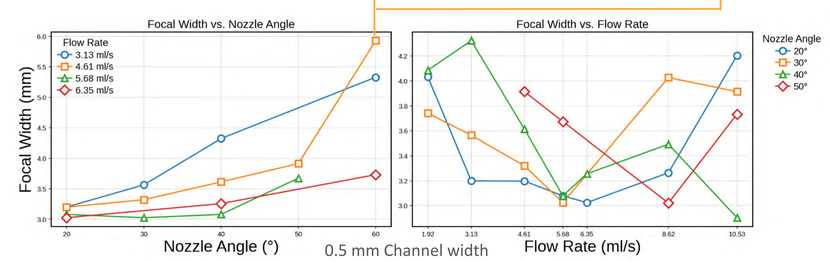
This and following temporal color graphs are stacks of 200 consecutive frames recorded at 400 fps



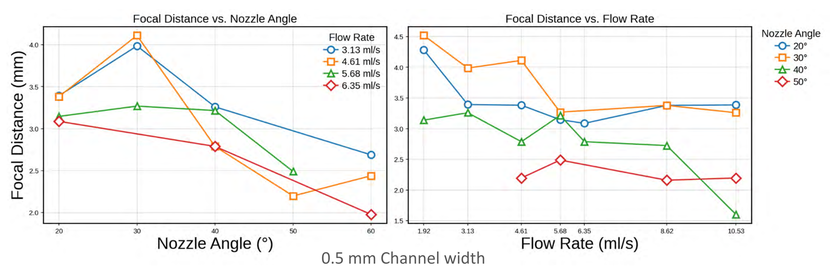
Smaller channel widths correlate with **stronger** focusing behavior

0.5 mm channel width nozzles at 4.61 ml/sec



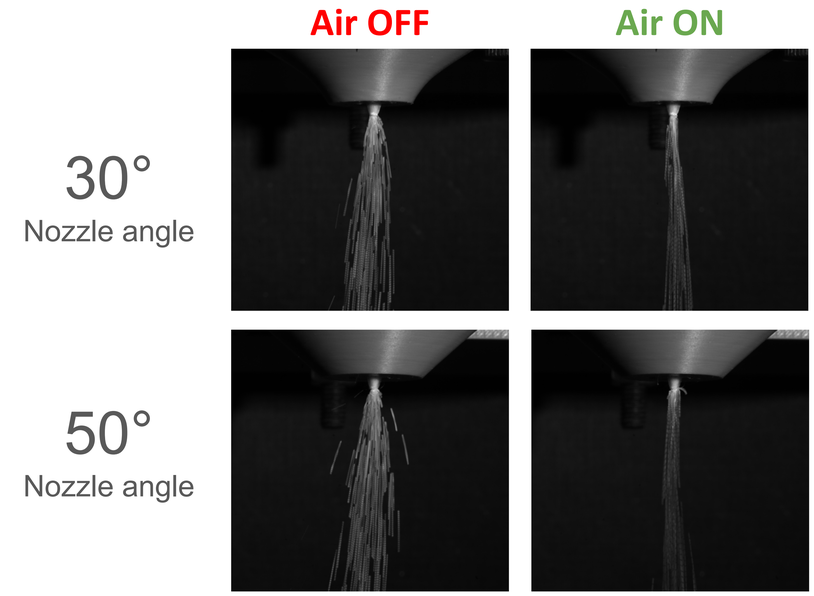


Smaller nozzle angles correlate with **smaller** focal widths



Larger nozzle angles correlate with **shorter** focal distances

Results - Air Testing



The 4 figures above are each composed of 20 consecutive frames stacked on top of each other recorded at 1000 fps

Preliminary tests of different nozzle angles at a 0.5 mm channel width at ~0.05 psi show that this solution has potential to focus powder. However, pressures required for focusing could not be accurately measured and should be revisited with more accurate equipment.

Conclusion

- A narrower annular air stream exit creates a narrower focused stream of fluid
- Factors that affect **focal width**
  - Nozzle angle and focal width has a positive correlation
  - Flow rate has no significant effect on focal width
- Factors that affect **focal distance**
  - Nozzle angle are negatively correlated with focal distance
  - Flow rate has no significant effects on focal distance
- Air stream focusing requires laminar flow

Future Work

- Design changes to reduce turbulence and further decrease focal width
- Test nozzles with smaller channel widths sizes
- Continue in air testing
- Characterize deposited powders with real test cases

Acknowledgements & References

We would like to acknowledge Yerlik Gabdulla, Arjun Shankar, Skinder Dar, Cong Wang, and the Belin Blank Center for their help in this research.

Scott, Michael, et al. "Acoustic-Modulated, Selective Particle Deposition for Muti-Material Additive Manufacturing." Advanced Materials Technologies, vol. 8, no. 19, 2023, article 2300424. Wiley Online Library, https://doi.org/10.1002/admt.202300424.
Svetlizky, David, et al. "Directed Energy Deposition (DED) Additive Manufacturing: Physical Characteristics, Defects, Challenges and Applications." Materials Today, vol. 49, 2021, pp. 271–95. ScienceDirect, https://doi.org/10.1016/j.mattod.2021.03.020.
Yi, Hao, et al. "Material and Process Integrated Innovations in Aerosol Jet Printing: A Review." Materials Today, 2025. ScienceDirect, www.sciencedirect.com/science/article/pii/S1369702125004596.

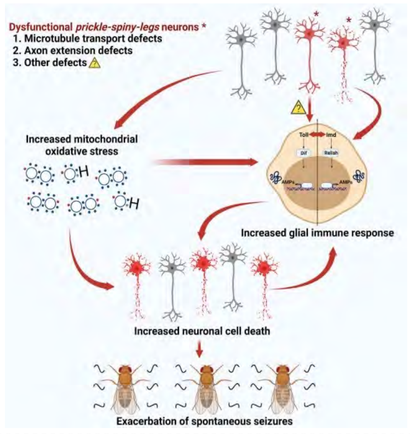
Comparing Antioxidants for Reducing Seizure Activity In A *Drosophila melanogaster* Model of Epilepsy

Letong Chen[1] ; Sophia Tian[2]; Brady Williquett[3]; J. Robert Manak, PhD[3,4]

[1]Westtown School, [2]Cinco Ranch High School, [3]Department of Biology, University of Iowa, [4]Department of Pediatrics, University of Iowa

Introduction

- Epilepsy is a neurological disorder affecting over 50 million people worldwide. [1]
- Approximately 1/3 of people with epilepsy continue to have seizures despite taking anti-seizure medications; 2 out of 3 patients experience adverse events from taking medications. [1,2]
- The *prickle-spiny-legs* (*pk^{sple}*) mutation causes spontaneous seizures and ataxia in *Drosophila melanogaster,* similar to what is observed in humans carrying *PRICKLE* mutations. Previous work in the Manak Lab demonstrated that elevated oxidative stress in *pk^{sple}* brains led to increased neuronal death and an increase in seizure frequency. [3]
- Antioxidants help remove excess reactive oxygen species (ROS) and may protect nerve cells from oxidative damage.[4,5]



Objective

- Compare the effects of 6 antioxidant drugs on seizure activity in a *Drosophila* model of epilepsy.
- Determine which antioxidant is the most effective at reducing spontaneous seizure activity.
- Explore the potential of antioxidant therapy as a future strategy for treating epilepsy.

Materials & Method

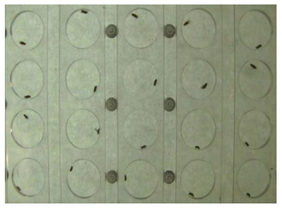
pk^{sple} flies were fed standard cornmeal molasses medium containing antioxidants from embryo up until 15 days post-eclosion. The drugs tested are shown below:

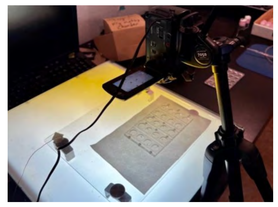
N-Acetylcysteine Amide (NACA), N-Acetylcysteine (NAC)
Trans-resveratrol, Curcumin, Genistein, Valdecoxib

Spontaneous Seizure Assay:

Individual flies were gently transferred into 20 wells using a mouth pipette

- Behaviors were recorded via cellphone video
- Videos were analyzed by eye to identify seizure events. Analysis was performed in a blinded manner to eliminate bias.





Results

1

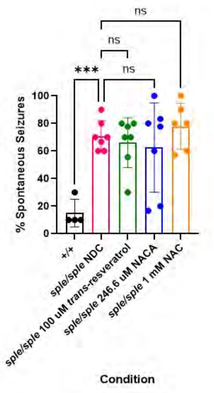


Figure 1. **NACA, NAC, and trans-resveratrol do not suppress seizures in *pk^{sple}* mutant flies.** Data shown are mean +/- SD. Brown-Forsythe and Welch ANOVA test with Dunnett's T3 multiple comparisons test, n >= 4 assays per condition, 5-10 flies per assay. ns = not significant, ** = p< 0.01, *** = p < 0.001

2

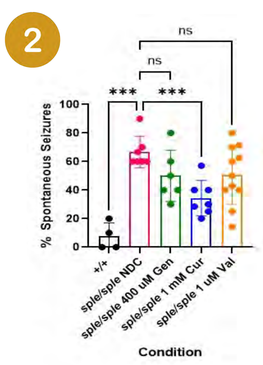


Figure 2. **Curcumin suppresses seizures in *pk^{sple}* mutant flies.** Data shown are mean +/- SD. Brown-Forsythe and Welch ANOVA test with Dunnett's T3 multiple comparisons test, n >= 4 assays per condition, 5-10 flies per assay. ns = not significant, ** = p< 0.01, *** = p < 0.001

3

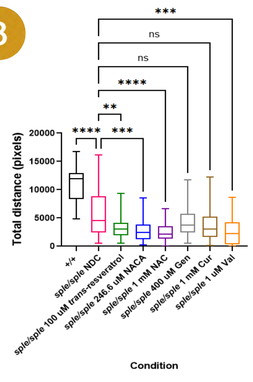


Figure 3. **Antioxidants reduce the activity level of *pk^{sple}* mutant flies.** Data shown are mean +/- SD. Brown-Forsythe and Welch ANOVA test with Dunnett's T3 multiple comparisons test, n >= 40 flies per condition. ns = not significant, * = p < 0.05, ** = p< 0.01, *** = p < 0.001, **** = p < 0.0001.

4

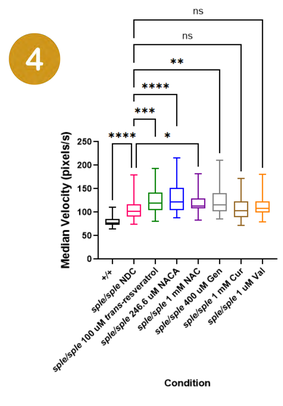


Figure 4. **Antioxidants increase the velocity of *pk^{sple}* mutant flies.** Data shown are mean +/- SD. Brown-Forsythe and Welch ANOVA test with Dunnett's T3 multiple comparisons test, n >= 40 flies per condition. ns = not significant, * = p < 0.05, ** = p< 0.01, *** = p < 0.001, **** = p < 0.0001.

Conclusion

Seizure Activity:
-NAC, NACA, trans-resveratrol were unable to suppress seizure activity in *pk^{sple}* mutants to a statistically significant extent
-Both genistein and valdecoxib showed some seizure suppressive activity, although not to a statistically significant extent.
-Curcumin robustly suppressed seizure activity to a significant extent ($p<0.001$) compared to *pk^{sple}* with no drug.

Total Distance & Median Velocity:
-Antioxidants lower the total distance traveled by *pk^{sple}* mutant flies, reducing the overall activity level.
-Antioxidants increase the median velocity of *pk^{sple}* mutant flies, indicating that all antioxidants improve the motor activity of *pk^{sple}* mutant flies.

Discussion

Our results show that only curcumin significantly suppressed seizure activity in *pk^{sple}* mutant flies, making it a promising treatment for epilepsy. Other antioxidant drugs (NAC, NACA, trans-resveratrol, genistein, and valdecoxib) did not provide statistically significant suppression of seizure activity, although both genistein and valdecoxib showed some reduction in seizure penetrance, suggesting that statistical significance may be reached by increasing the number of flies screened. Several antioxidants exhibited high variability in seizure responses, implying that different individuals may respond differently to these drugs, or that the behavior of some flies may have been affected due to experimental manipulations.

The results also suggest that antioxidants may improve motor activity even if they are incapable of suppressing seizures, thus allowing flies to walk at a faster rate. However, most antioxidants reduced the total distance traveled which may be due to the relatively high drug concentration used, thus producing a deadening effect on overall activity.

Future studies could evaluate the effects of combinations of antioxidants as well as validate the findings in mammalian seizure models.

Acknowledgments

We would like to thank Dr. Manak, Brady Williquett, and the Manak Lab for their invaluable guidance and mentorship. We thank the Manak Lab, University of Iowa, and Belin-Blank Center for providing us with this opportunity.

References

1. Kanner AM, Bicchi MM. Antiseizure medications for adults with epilepsy: a review. *JAMA*.2022;327(13):1269-1281. doi:10.1001/jama.2022.3880
2. Asadi-Pooya AA, Brigo F, Lattanzi S, Blümcke I. Adult epilepsy. *Lancet*. 2023;402(10399):412-424.doi:10.1016/S0140-6736(23)01048-6
3. Nukala KM, Lilienthal AJ, Lye SH, Bassuk AG, Chtarbanova S, Manak JR. Downregulation of oxidative stress-mediated glial innate immune response suppresses seizures in a fly epilepsy model. *Cell Rep*.2023;42(1):112004. doi:10.1016/j.celrep.2023.112004
4. Aguiar CC, Almeida AB, Araújo PV, et al. Oxidative stress and epilepsy: literature review. *Oxid Med Cell Longev*. 2012;2012:795259. doi:10.1155/2012/795259
5. Lüthy K, Mei D, Fischer B, et al. TBC1D24-TLDc-related epilepsy exercise-induced dystonia: rescue by antioxidants in a disease model. *Brain*. 2019;142(8):2319-2335. doi:10.1093/brain/awz175

Investigating Nest-Building Behavior in a Mouse Model of Houge-Janssens Syndrome 1: Insights from Cell-Type-Specific E420K Mutants

Manasvi DeviReddy[1], Tehreem Haider[2], Chian Ju Jong[2], Ph.D, Ruiqi Lyu[2], Ph.D, Stefan Strack[2], Ph.D

[1]Linn Mar High School, Marion, Iowa, [2]Department of Neuroscience and Pharmacology, Carver College of Medicine, University of Iowa

Introduction

- PP2A/PPP2 is a heterotrimeric Ser/Thr phosphatase composed of scaffolding A, catalytic C and one of 12 regulatory B subunits (Figure 1).
- Houge-Janssens Syndrome 1 (HJS1) is a rare neurodevelopmental disorder caused by de novo mutations in the PPP2R5D gene (Figure 1) (Shang et al., 2016).
- Both E198K and E420K mutations are the most severe form of mutation, while E200K mutation has a milder phenotype (Shang et al., 2016).
- Symptoms include macrocephaly, hypotonia, autism spectrum disorder (ASD) and developmental and cognitive delays (Levine et al., 2023) .

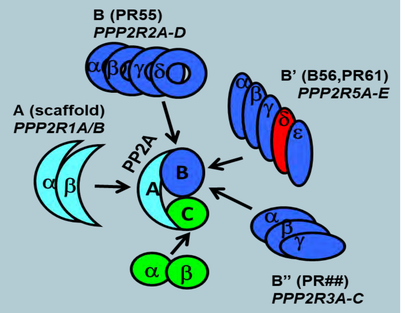


Figure 1. PP2A enzyme structure

- Restricted interests is one of the common autistic features (Lung et al., 2024).
- Nestlet shredding/nest-building is used as an indirect measure of repetitive, compulsive-like behavior in mouse models of ASD (Angoa-Pérez et al., 2013).
- Parvalbumin (PV)-expressing inhibitory interneurons help regulate cortical excitatory/inhibitory balance, and PV interneuron dysfunction has been increasingly implicated as a common contributor to neurodevelopmental disorders including autism spectrum disorder (Contractor et al., 2021).
- Our preliminary data show restricted interests in nestlet shredding/nest building behaviors in the E420K mice. We studied whether Parvalbumin inhibitory interneurons (PV cre) could cause the restricted interests in the E420K mice.

Methodology

•Nestlet Shredding/Building Protocol:

• WT and E420K mice (germline, Gad2 cre- and PV Cre-conditional) were habituated in corncob bedding for 30 minutes.

• A pre-weighed nestlet, food, and water were placed in the cage, and mice were left undisturbed overnight.

• The next morning, mice were removed and three independent, blinded raters scored the quality of each nest (0–5 scale; Figure 2).

- The remaining intact nestlet was weighed to calculate the percent of nestlet material shredded.

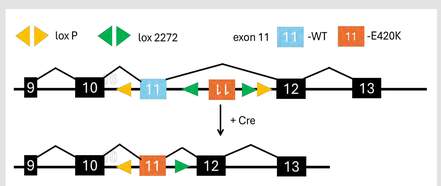


Figure 3. The conditional E420K knock-in mouse model of HJS1 was generated at University of Iowa Genome Editing Core Facility using the FLEx technique to introduce the E420K mutation into the murine Ppp2r5d locus. When crossed with a PV-cre mouse, the E420K mutation will be turned on in the parvalbumin-specific interneurons.

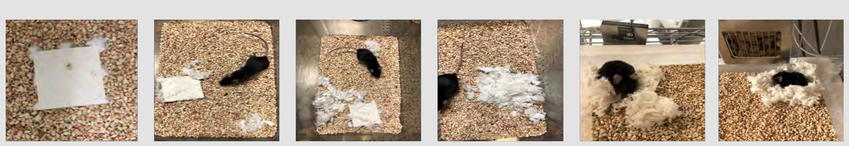


Figure 2. Nestlet scoring rubric. Score 0 = material untouched; Score 5 = nest has fully-formed walls with a prominent indentation.

Results

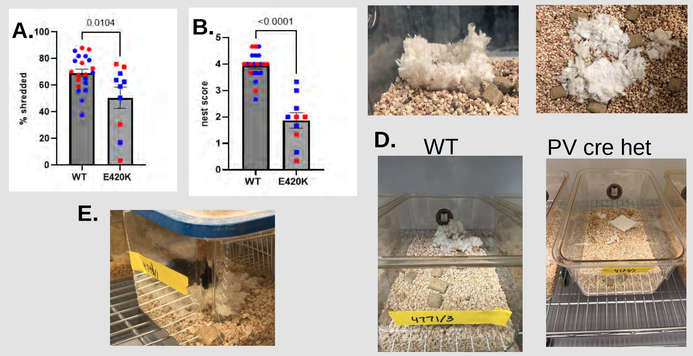


Figure 5. (A) E420K mice shredded significantly less nestlet material than WT mice (p=0.0104) and (B)built significantly lower-scoring nests (p<0.0001),indicating reduced nest-building behavior in germline E420K mice. (C) Representative nest built by a WT mouse (left) and a E420K mouse (right). (D) Representative nest built by a WT mouse (left) and a PV cre het E420K mouse (right). (E) Mouse in nestlet built during assay.

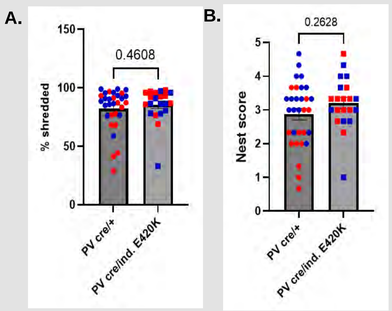


Figure 6. Nestlet shredding/building in PV Cre het E420K mice observed in both sexes. No significant difference was observed from PV cre/+ controls in % shredded (p=0.46) or nest score (p=0.26).

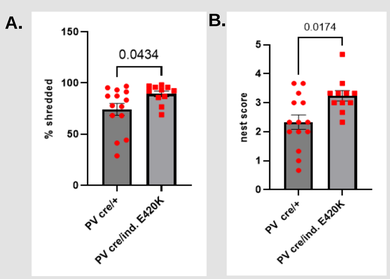


Figure 7. In females, PV Cre het E420K mice shredded significantly more nestlet (p=0.043) and built higher-scoring nests (p=0.017) than PV cre/+ controls — the opposite direction from the germline E420K phenotype.

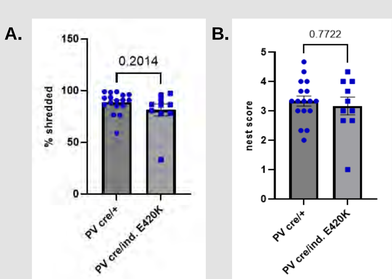


Figure 8. In males, no significant differences were seen between PV Cre het E420K and PV cre/+ controls in % shredded (p=0.20) or nest score (p=0.77).

Conclusion and Discussion

- Germline E420K mice showed significantly reduced nestlet shredding (p=0.0104) and significantly lower nest-building scores (p<0.0001) compared to WT mice, indicating impaired nest-building/repetitive behavior in the constitutive knock-in model.
- Targeting the E420K mutation specifically to PV interneurons (PV Cre/ind. E420K) did not reduce nestlet shredding or nest score overall compared to PV cre/+ controls (p=0.46, p=0.26).
- When split by sex, female PV Cre/ind. E420K mice unexpectedly shredded significantly more nestlet material (p=0.043) and built higher-scoring nests (p=0.017) than female controls — opposite in direction to the germline phenotype. Male PV Cre het mice showed no significant differences (p=0.20, p=0.77).
- Together, these results suggest that PV interneuron dysfunction alone is not sufficient to reproduce the reduced nest-building phenotype seen in germline E420K mice. Other cell types, or broader developmental/network effects present only in the germline model, likely drive that reduced-shredding phenotype. The female-specific reversal further suggests PV circuits may play a sex-dependent role in nest-building behavior.

Future Directions: (1) We would like to test additional interneuron-specific Cre lines (e.g., Gad2-Cre, which also showed no significant effect on nestlet shredding) to map which cell types contribute to the repetitive-behavior phenotype. (2) We would like to pair nestlet shredding with open field activity testing to control for baseline locomotor differences. (3) We would like to extend nestlet shredding testing to the E198K and E200K lines for comparison with their marble-burying phenotypes.

Acknowledgements

I would like to thank the Strack lab for all their help this summer. We would like to thank William Paradee of Genome Editing Core for generating the mouse models of HJS1.

Fundings

PPP2R5D support by State of California/JGA (#A19-3376-S004)
PPP2R5D support by State of California/JGA
PPP2R5D support by Simons Foundation Autism Research Initiative (#877875)

References

Angoa-Pérez, M., Kane, M. J., Briggs, D. I., Francescutti, D. M., & Kuhn, D. M. (2013). Marble burying and nestlet shredding as tests of repetitive, compulsive-like behaviors in mice. Journal of Visualized Experiments, (82), 50978. https://doi.org/10.3791/50978

Contractor, A., Ethell, I. M., & Portera-Cailliau, C. (2021). Cortical interneurons in autism. Nature Neuroscience, 24(12), 1648–1659. https://doi.org/10.1038/s41593-021-00967-6

Deciphering Developmental Disorders Study. (2017). Prevalence and architecture of de novo mutations in developmental disorders. Nature, 542(7642), 433–438. https://doi.org/10.1038/nature21062

Gurney, M. E., Cogram, P., Deacon, R. M., Rex, C., & Tranfaglia, M. (2017). Multiple behavior phenotypes of the fragile-X syndrome mouse model respond to chronic inhibition of phosphodiesterase-4D (PDE4D). Scientific Reports, 7, 14653. https://doi.org/10.1038/s41598-017-15028-x

Gurney, M. E., Nugent, R. A., Mo, X., Sindac, J. A., Hagen, T. J., Fox, D., O'Donnell, J. M., Zhang, C., Xu, Y., Zhang, H.-T., Groppi, V. E., Bailie, M., White, R. E., Romero, D. L., Vellekoop, A. S., Walker, J. R., Surman, M. D., Zhu, L., & Campbell, R. F. (2019). Design and synthesis of selective phosphodiesterase 4D (PDE4D) allosteric inhibitors for the treatment of fragile X syndrome and other brain disorders. Journal of Medicinal Chemistry, 62(10), 4884–4901. https://doi.org/10.1021/acs.jmedchem.9b00193

Hamilton, J. (2024, September 23). Fragile X held him back. An experimental drug is helping him break free. NPR. https://www.npr.org/sections/shots-health-news/2024/09/22/nx-s1-5076913/fragile-x-experimental-drug-helping-autism-adhd-intellectual-disability

Janssens, V., & Goris, J. (2001). Protein phosphatase 2A: A highly regulated family of serine/threonine phosphatases implicated in cell growth and signalling. Biochemical Journal, 353(2), 417–439. https://doi.org/10.1042/bj3530417

Levine, A. D., & Chung, W. K. (2023). Clinical features of PPP2 syndrome type R5D (Jordan's syndrome) to support standardization of care. Cold Spring Harbor Molecular Case Studies, 9(3), a006285. https://doi.org/10.1101/mcs.a006285

Lung, S. L. M., Picard, E., Soulieres, I., & Bertone, A. (2024). Identifying the functions of restricted and repetitive behaviors and interests in autism: A scoping review. Research in Autism Spectrum Disorders, 117, 102458. https://doi.org/10.1016/j.rasd.2024.102458

Pelkey, K. A., Chittajallu, R., Craig, M. T., Tricoire, L., Wester, J. C., & McBain, C. J. (2017). Hippocampal GABAergic inhibitory interneurons. Physiological Reviews, 97(4), 1619–1747. https://doi.org/10.1152/physrev.00007.2017

Qin, Y., Du, Y., Chen, L., Liu, Y., Xu, W., Liu, Y., Li, Y., Leng, J., Wang, Y., Zhang, X. Y., Feng, J., Zhang, F., Jin, L., Qiu, Z., Gong, X., & Wang, H. (2022). A recurrent SHANK1 mutation implicated in autism spectrum disorder causes autistic-like core behaviors in mice via downregulation of mGluR1-IP3R1-calcium signaling. Molecular Psychiatry, 27(7), 2985–2998. https://doi.org/10.1038/s41380-022-01539-1

Shang, L., Henderson, L. B., Cho, M. T., Petrey, D. S., Fong, C.-T., Haude, K. M., Shur, N., Lundberg, J., Hauser, N., Carmichael, J., Innis, J., Schuette, J., Wu, Y. W., Asaikar, S., Pearson, M., Folk, L., Retterer, K., Monaghan, K. G., & Chung, W. K. (2016). De novo missense variants in PPP2R5D are associated with intellectual disability, macrocephaly, hypotonia, and autism. Neurogenetics, 17(1), 43–49. https://doi.org/10.1007/s10048-015-0466-9

Shionogi Provides Updates on Zatolmilast, an Investigational Drug for Fragile X Syndrome, Including Recent Changes to Study Protocol to Increase Access for Participants and Families. (2024, July 18). Shionogi. https://www.shionogi.com/us/en/news/2024/07/shionogi-provides-updates-on-zatolmilast-an-investigational-drug-for-fragile-x-syndrome-including-recent-changes-to-study-protocol-to-increase-access-for-participants-and-families.html

Sonzogni, M., Wallaard, I., Santos, S. S., Kingma, J., du Mee, D., van Woerden, G. M., & Elgersma, Y. (2018). A behavioral test battery for mouse models of Angelman syndrome: a powerful tool for testing drugs and novel Ube3a mutants. Molecular Autism, 9, 47. https://doi.org/10.1186/s13229-018-0231-7

Task-switching costs reflect action-effects encoded in task representation

Grace Guang[1]; Kaylani Datta[2]; Eliot Hazeltine, Ph.D.[2]

[1]St. Paul's School, Concord, NH; [2]University of Iowa, Dept. of Psychological and Brain Sciences, Iowa City, IA

Introduction

Event-file binding: theory that the brain binds perceptual, contextual, and motor features in stimulus and response.

Switch-costs: difference in reaction time when shifting tasks

Action-effect (AE): the anticipated sensory consequences that a voluntary movement produces

Response-repetition: repeats the exact same action, word, or motor response to a recurring stimulus



Figure 1. Pressing a switch produces an anticipated consequence: light on/off

Previous neuroimaging studies of task-switching have interpreted changes in neural activation during switch trials → changes working memory (Qiao et al., 2017), as indicative of the stimulus-response model

- Existing findings: (1) performance is worse when the task on the previous trial is different (Schacherer & Hazeltine, 2022), (2) partial repetition causes an even stronger decline in performance, potentially due to event-file interference (Hommel, 2004), (3) response-repetitions were performed more quickly only when the task was repeated (Rogers & Monsell, 1995).

The present study aims to study the stimulus-response paradigm to examine how the anticipated consequences may be part of the representation of action.

Objectives

Research Questions

(1) Do task-switching costs result from changes in the representation of an action, rather than from the stimulus-response reconfiguration?

(2) When a response is repeated across a task switch, does the resulting cost (or benefit) in performance depend on whether that repeated response is tied to the same action-effect?

Hypothesis

- Changes in the representation of action (action-effects) are a source of switch costs and response-repetition costs
- Stimulus-response mappings have smaller influence

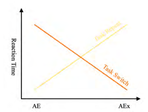


Figure 2. Hypothesized impact of action-effects in task repeats/switches

Methods

29 (Experiment 1) + 43 (Experiment 2) participants were instructed to select the stimulus (ingredients) producing the meal outcome (action-effect) that best fulfills the current cue (bowl, plate, breakfast, lunch).

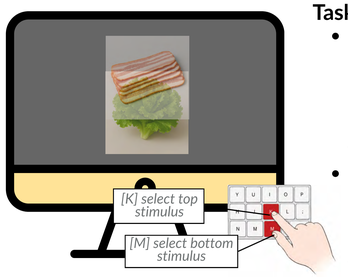


Figure 3. Following the cue, the stimuli will be presented in such a fashion as to eliminate spatial effects on switch costs.

Task

- In Experiment 1, cues (Lunch, Breakfast, Plate, Bowl) were associated with meals (Burger, Salad, Eggs-bacon, or Scramble) composed of ingredients (e.g., lettuce, patty, bacon). Critically, some stimuli in Experiment 1 were associated with either one or two action-effects.
- In Experiment 2, the same cue hierarchy (Lunch/Breakfast → Plate/Bowl) yielded a different stimulus set (BLT, Chicken Salad, Omelet, Scramble). every stimulus was associated with exactly two action-effects
- During the task, each target stimulus appeared alongside an overlapping distractor.

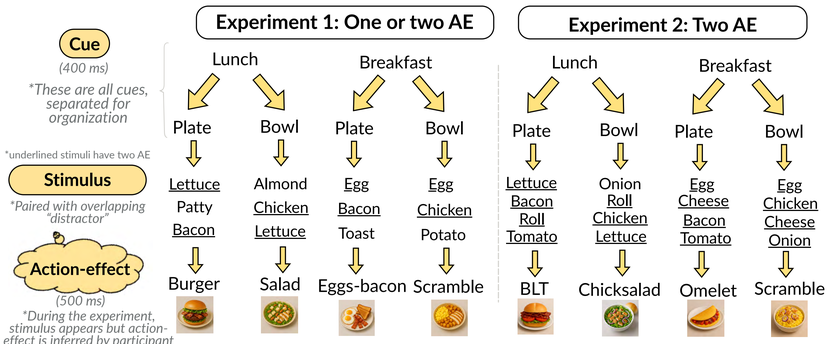


Figure 4. The cues associated with its corresponding stimulus (ingredients) and action-effects (meal).

Discussion

Table 1. Repeated-Measures ANOVA statistics for switch type, action-effect repetition, response-repetition, and target-to-target (T2T) effects, Diner 1 vs. Diner 2 (Type 2 stimuli only).

Experiment	Effect	F	p	η^{p2}	Sig.
Diner 1	Switch Type × Repeated Action-Effect	3.22	.084	.103	ns
	Switch Type × Repeated Action-Effect (T2T trials removed)	3.61	.068	.114	trend
	Response Type (main effect) — repeat: 1,176 ms; switch: 1,114 ms	13.05	.001	.034	*
	Switch Type × Target-to-Target (T2T)	27.95	< .001	.528	*
	Switch Type × T2T × Response-Repetition	22.97	< .001	.766	*
	Switch Type × T2T × Response-Repetition (Type 2 stimuli only)	9.06	.006	.266	*
Diner 2 (Type 2 AE only)	Switch Type × Repeated Action-Effect	3.68	.065	.109	trend
	Response Type (main effect) — repeat: 1,309 ms; switch: 1,284 ms	6.861	.014	.186	*
	Switch Type × Target-to-Target (T2T)	11.37	.002	.275	*
	Switch Type × T2T × Response-Repetition	13.39	< .001	.308	*

Experiment 1

- There is a clear effect with response-repetition and target repetition, but the effect of repetition of action effects was smaller than expected
- Switch Type × repeated AE crossover had the same trend *magnified when T2T eliminated → splicing trials with stimuli with different action-effect was insignficant

Experiment 2

- Response-repetitions were slower, not faster (Fig. 7) → partial-repetition cost, consistent with event-file theory
- Switch Type × repeated AE crossover had the same trend (close to significant)

Experiment 1

Action-effect helps when the task switches (trend)

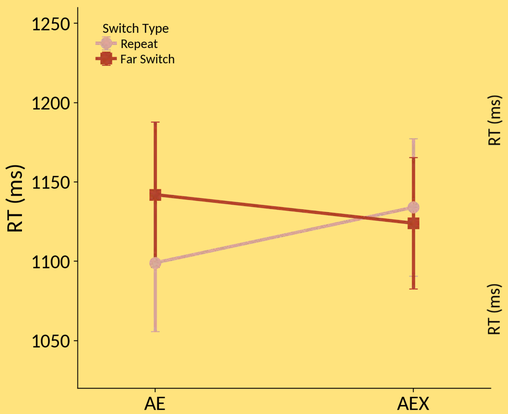


Figure 5. Repeating action effects help when task switches but not when the task repeats: F(2, 28) = 3.611, p = .068 (ns), ηp^2 = .1141, expected crossover under the conditions that T2T does not happen

Target repetitions are hard for near switches, especially when the response repeats

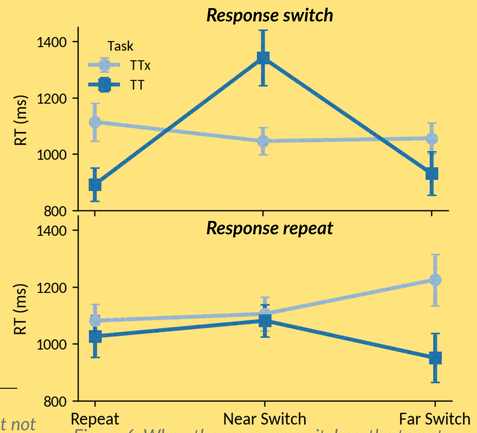


Figure 6. When the response switches, the target repetition interaction disappears compared to when the response repeats. F(3, 26) = 22.97, p < .001, ηp^2 = .7664

Experiment 2

When action-effect repeats, there is advantage when task repeats too

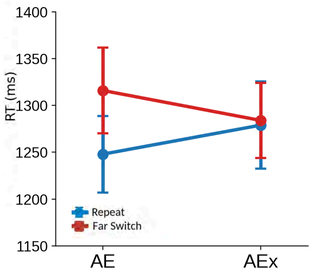


Figure 7. Repeating action effects help when task switches but not when the task repeats: F(2, 30) = 3.676, p = .065, ηp^2 = .1092

Target repetition trends differ from experiment 1

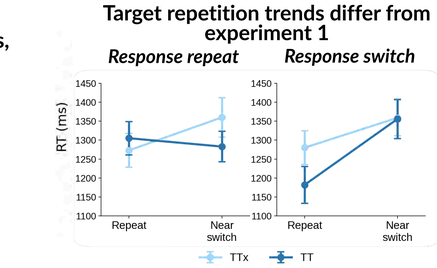
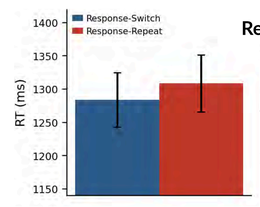


Figure 8. When the response repeats, the target repetition benefits during a switch. F(3, 26) = 13.39, p < .001, ηp^2 = .3084



Response-repetition increases switch costs compared to response-switch

Figure 9. Repeating the motor response has increased switch costs; signs of partial-repetition costs in the event-file model: F(1, 30) = 6.861, p = .014, ηp^2 = .1861

Conclusion & Future Direction

Combined Outcomes

- Stimulus and response had more effect on switch costs; people might be representing the action based on stimulus-response>goals
- Stimulus associated with one versus two action-effects led to an inherent bias in the experimental design, task was too complicated for participants to use action-effects
- Continue with simpler tasks that emphasize goal-directed action in task-switching experiments to learn more about executive function (Logan, 2003)

Acknowledgements

I would like to thank Dr. Hazeltine and Kalyani Datta for their extensive guidance and inspiring passion throughout this project; Olivia Richards and Gunner Myers for data collection; and the Belin-Blank Center for arranging the SSTP program. It has been an amazing opportunity full of experiences I will bring to my future aspirations.

References

Optimizing Anti-MAP2 Antibody Penetration in Mouse Tissue

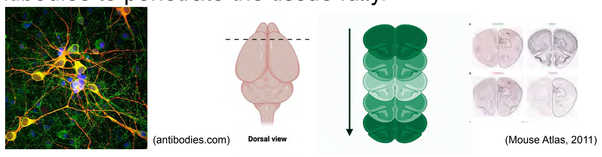
Divya Jayam, Sura Smadi, Georgina Aldridge

The Wheatley School, Aldridge Lab, Department of Neurology, University of Iowa, Iowa City, Iowa

Introduction

Lewy Body Dementia (LBD) is a neurodegenerative disease characterized by the aggregation of α-synuclein into called Lewy bodies, which spread and disrupt normal cellular function. Introducing Lewy body pathology impacts cells, so reconstructing them requires a good marker. We use MAP2 to visualize the cells affected by Lewy bodies.

Immunohistochemical staining (IHC) is used to detect antibody-specific antigens in tissues. The results depend on the ability of the primary antibody to bind to the secondary antibody. Thus, the results depend on the ability of the antibodies to penetrate the tissue fully.

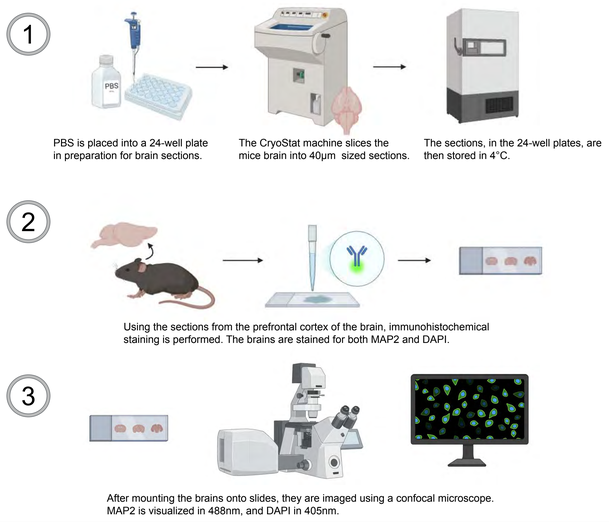


Microtubule associated protein 2, or MAP2, is an abundant microtubule protein that participates in the outgrowth of neuronal processes and synaptic plasticity. It is localized primarily within cell bodies and cell dendrites.

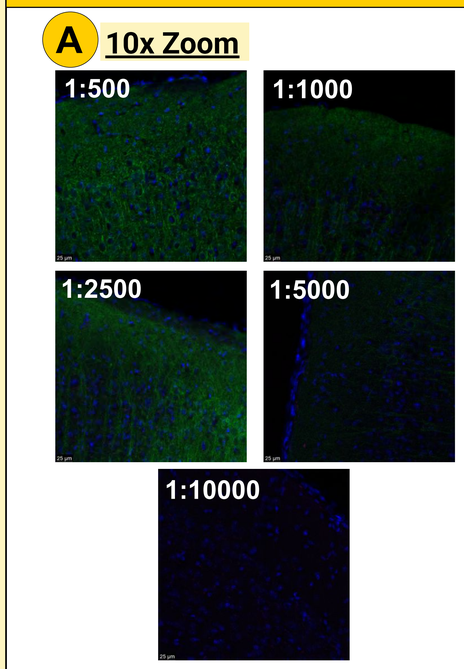
Hypothesis

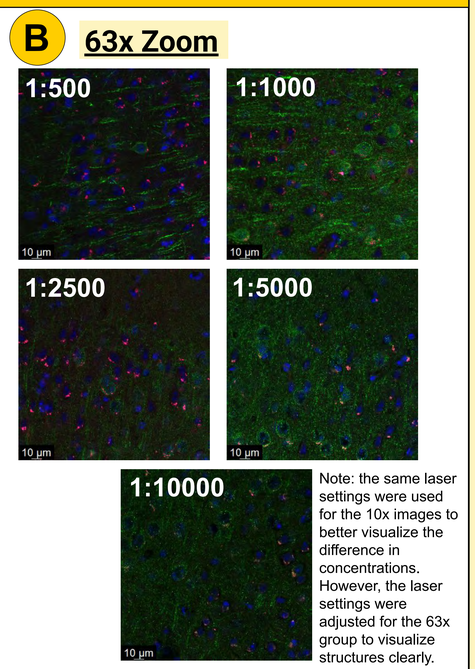
We hypothesize that as the concentration of the MAP2 decreases, the ability of the antibody to wholly penetrate the mice tissue will increase.

Methods

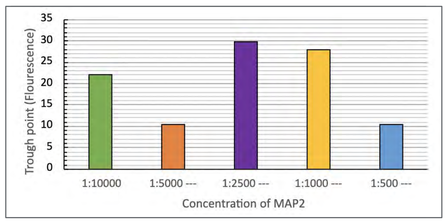


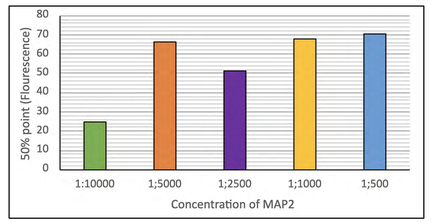
Results

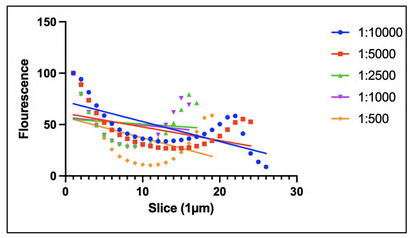


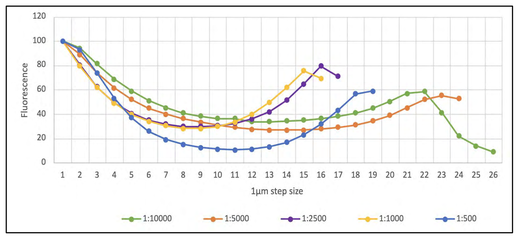


Note: the same laser settings were used for the 10x images to better visualize the difference in concentrations. However, the laser settings were adjusted for the 63x group to visualize structures clearly.









Discussion



(Mages et al, 2021)

To qualitatively analyze, the 1:500 images produced within Mages et al.'s study showcased a slight difference in visibility (dimness) of the 1:500 concentration staining of MAP2. However, laser settings, secondary antibodies, and imaging platforms were not matched, which could affect analysis.

Conclusions

1:10000 performs the best. As the antibody was diluted more, the signal takes longer to drop to half its peak. This supports the idea that (highly concentrated) antibodies bind to available targets near the tissue surface before it has time to diffuse deeper, which leaves little leftover to label the interior tissue. Variability in cryostat sectioning could introduce inconsistencies independent of antibody dilution, since section thickness fluctuations, tissue compression, or micro tears during cutting may alter the antibody's penetration. Additionally, photobleaching at the confocal microscope could reduce signal and affect the fluorescence results because deeper slices are imaged after more cumulative laser passes through the sample.

Future Directions

To further optimize the visualization of MAP2, future experiments could involve fixing the tissue at 1:10000 and using longer incubation time (48-72 hours).. Using even more dilute concentrations like 1:20000 and 1:50000 could help determine if this trend continues or plateaus.

Acknowledgements

I would like to thank Sura Smadi and Dr. Georgina Aldridge for their guidance and for providing me with the opportunity to create this project.

References

Sokratian, A., Zhou, Y., Tatli, M., Burbidge, K. J., Xu, E., Viverette, E., Donzelli, S., Duda, A. M., Yuan, Y., Li, H., Strader, S., Patel, N., Shiell, L., Malankhanova, T., Chen, O., Mazzulli, J. R., Perera, L., Stahlberg, H., Borgnia, M., Bartesaghi, A., West, A. B. (2024). Mouse α-synuclein fibrils are structurally and functionally distinct from human fibrils associated with Lewy body diseases. Science advances, 10(44), eadq3539. https://doi.org/10.1126/sciadv.adq3539

Pirhaghi, M., Mamashli, F., Davaeil, B., Mohammad-Zaheri, M., Mousavi-Jarrahi, Z., Tatzelt, J., & Saboury, A. A. (2025). Hidden faces of alpha-synuclein: Cryo-EM revelation of fibril polymorphs driven by disease, mutations, and PTMs. BBA advances, 9, 100179. https://doi.org/10.1016/j.bbadva.2025.100179

Lau, D., Tang, Y., Kenche, V., Copie, T., Kempe, D., Jary, E., Graves, N. J., Biro, M., Masters, C. L., Dzamko, N., Gambin, Y., & Sierecki, E. (2024). Single-Molecule Fingerprinting Reveals Different Growth Mechanisms in Seed Amplification Assays for Different Polymorphs of α-Synuclein Fibrils. ACS chemical neuroscience, 15(18), 3270–3285. https://doi.org/10.1021/acschemneuro.4c00185Li, B., Ge, P., Murray, K. A., Sheth, P., Zhang, M., Nair, G., Sawaya, M. R., Shin, W. S., Boyer, D. R., Ye, S., Eisenberg, D. S., Zhou, Z. H., & Jiang, L. (2018). Cryo-EM of full-length α-synuclein reveals fibril polymorphs with a common structural kernel. Nature communications, 9(1), 3609. https://doi.org/10.1038/s41467-018-05971-2

Zhang, S., Dauer, K., Strohäker, T., Tatenhorst, L., Caldi Gomes, L., Mayer, S., Jung, B. C., Kim, W. S., Lee, S. J., Becker, S., Liesche-Starnecker, F., Zweckstetter, M., & Lingor, P. (2023). Alpha-synuclein fibrils amplified from multiple system atrophy and Parkinson's disease patient brain spread after intracerebral injection into mouse brain. Brain pathology (Zurich, Switzerland), 33(5), e13196. https://doi.org/10.1111/bpa.13196

Sequential Response Variability in Pigeons Following Guided Trials

Olivia Jones[1], Odysseus Orr[2], Edward Wasserman[2]

[1]Geffen Academy at UCLA, [2]Department of Psychological and Brain Sciences, The University of Iowa

Introduction

- Research has established that rewarded behaviors are more likely to recur. Continuous reinforcement also reduces response variability across sessions [1].
- However, few studies have examined whether this reduction in variability occurs within sessions [2].
- The mechanisms underlying response variability also remain unclear. To assess whether response variability is sensitive to recent exposure, we guided subjects through all possible response sequences before allowing free choice to occur.

We investigated two key questions:

1. **How will pigeons' response sequences vary within training sessions?**
2. **When pigeons are guided to perform all sequences, will they become more variable during free-choice trials?**

Method

Training: Eight pigeons completed at least 250 daily sessions, each containing 120 trials. The pigeons pecked a start stimulus, followed by four distinct stimuli, with each peck removing the corresponding stimulus. Pecking all four in any order yielded food.

Guided Trials: After training, a guided trial procedure was added on alternate days, in which only one stimulus was presented at a time, removing any choice in which stimulus to peck. Each pigeon completed all 24 possible sequences before free-choice trials began.

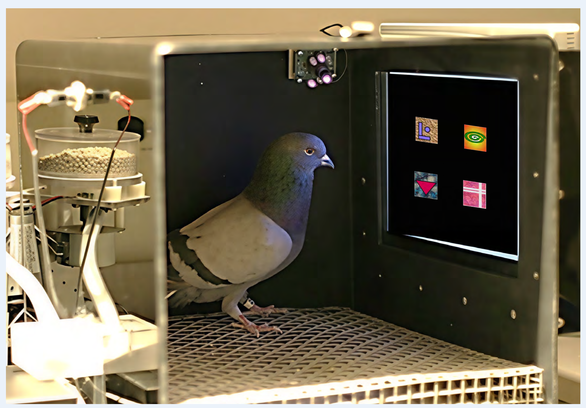


Figure 1. Pigeon subject in Skinner box with four stimuli shown.

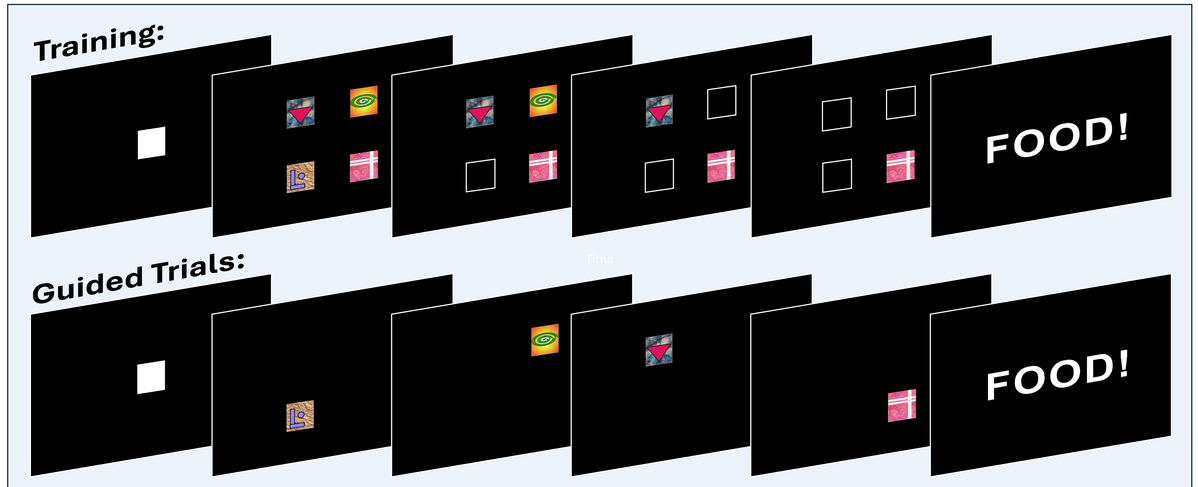


Figure 2. Trial sequence during training and guided trials; reinforcement is given only after all four stimuli have been pecked.

Results

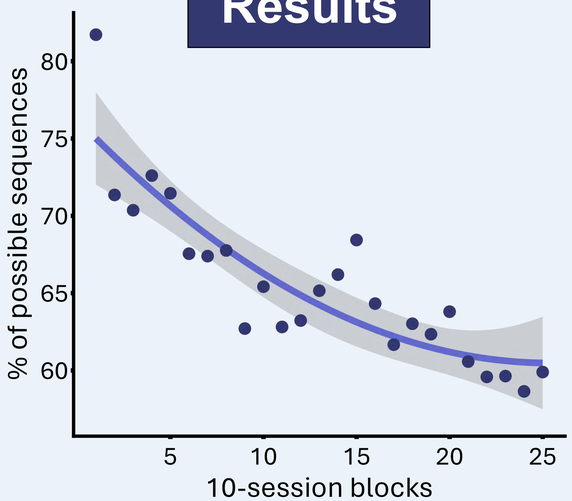


Figure 3. Mean percentage of possible sequences performed each session, averaged across 10-session blocks.

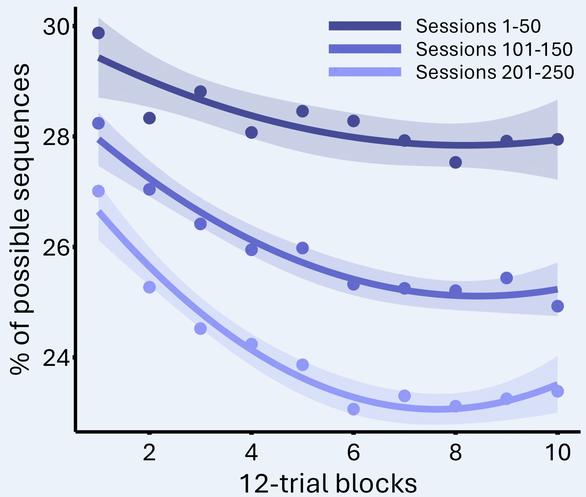


Figure 4. Mean percentage of possible sequences performed every 12 trials during early, middle, and late training.

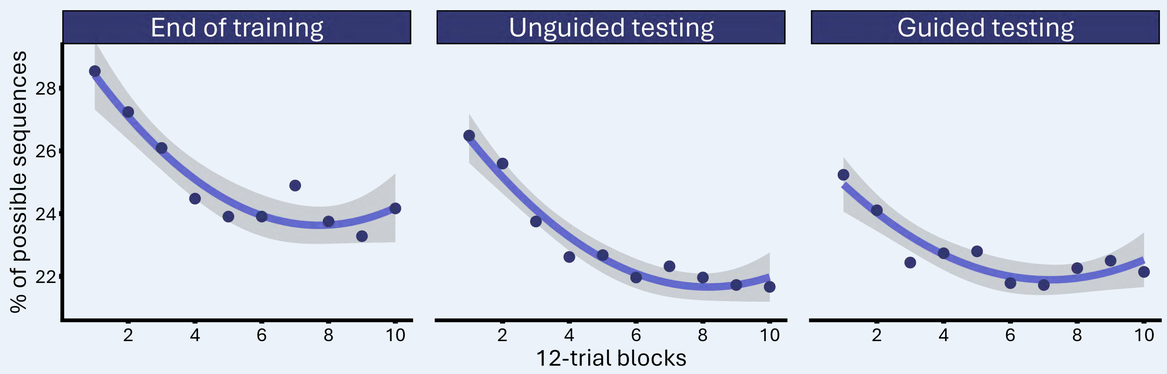


Figure 5. Mean percentage of possible sequences performed every 12 trials, with end of training, unguided testing, guided testing.

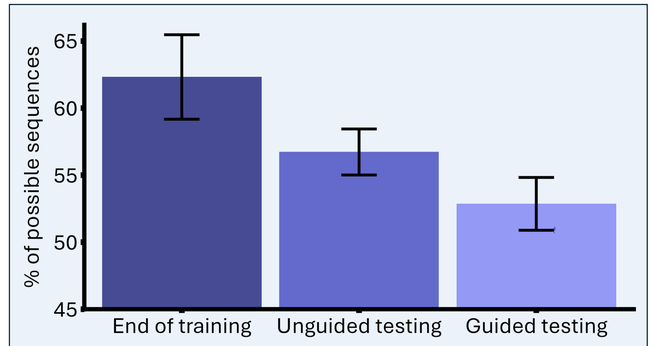


Figure 6. Mean percentage of possible sequences performed each session during end of training, unguided testing, and guided testing.

Conclusions

- **Variability within training sessions decreased.**
- Instead of increasing variability, guided testing elicited the **lowest variability of the three conditions.**
- **The reduction may indicate a lower drive to explore the reward environment after forced exploration.**
- Further research will examine whether variability returns to baseline levels after testing.
- These results speak to the question of when to keep exploring versus settle on a known reward, a problem shared by animals, humans, and even AI models.
- Understanding this balance could shed light on how organisms learn, create, and make decisions.

Acknowledgments

I would like to profusely thank Dr. Wasserman and Odysseus Orr, as well as the Comparative Cognition Lab, for their mentorship and support. I would also like to acknowledge the Belin-Blank Center and the Secondary Student Training Program for organizing this year's summer research program.

References

1. Wasserman, E. A., Orr, O. R. P., & Li, S. (2026). Variability, stability, and the law of effect. *Journal of Experimental Psychology: Animal Learning and Cognition, 52*(3), 129–138. https://doi.org/10.1037/xan0000427
2. Antonitis, J. J. (1951). Response variability in the white rat during conditioning, extinction, and reconditioning. *Journal of Experimental Psychology*, *42*(4), 273–281. https://doi.org/10.1037/h0060407

Semantic and Structural Similarities of Global Mythology: A Geo-Social Network Analysis

Yaejoon Jung[1]; Caglar Koylu[2]

Phillips Academy Andover, Andover, MA[1] ; School of Earth, Environment, and Sustainability, University of Iowa, Iowa City, IA[2]

Background Information

Myths in Human History

- Human history is beautifully complex; it is shaped by migration, cultural exchange, shared ancestry, and different environments
- Myths preserve human culture by recording how societies understand nature, identity, morality, the unknown, and reality
- It serves as a unique and valuable lens in which the intangible cultural heritage of societies can be accurately observed and understood
- Therefore, exploring myths is exploring the intricate history, thought, and relationship people had with their community and surroundings

Importance of Myth Today

- **Intangible Cultural Heritage:** Preserve collection memory and identity that may otherwise disappear across generations
- **Indigenous Knowledge:** Contain knowledge that is increasingly endangered by language loss and cultural displacement
- **AI and Information Homogenization:** Algorithms amplify dominant narratives; studying myths helps preserve diverse ways of understanding the world around us



(Source: Russell, ca. 1893-1895)

Previous Research

- European folktale variations reflect both geographic proximity and ethnolinguistic population history, suggesting the stories preserve traces of cultural movements around the world
- However, anthropological field suggests the Galton's Problem, which indicates that folktales and culture is simultaneously influenced by migration, cross-cultural contact, ancestry, and the environment
- Large-scale, global analysis of myths have been successful recently with the advent of digitized cross-cultural folklore databases and computational methods
- Topic modeling have shown to be able to identify broader semantic relationships among folklore motifs, but abstract and hierarchical themes remain difficult to computationally represent

Research Question

Question 01: How does the network structure, similarity representation, and cultural understandings derived from the networks different when the global mythology is analyzed using the binary motif matrix and unsupervised topic modeling network?

Question 02: How does the representation of myths affect our ability to accurately determine whether cross-cultural similarities reflect migration, cultural exchange, shared ancestry, or common environments?

Objective

To better understand how the stories of human history are represented, remembered, and transmitted today, this research specifically focuses on these three objectives for this research:

- **Binary Motif Network:** Identify motif similarities between traditions and communities of myths
- **Topic-Modeling Motif Network:** Identify broader thematic relationships beyond the catalogue using topic modeling
- **Comparison Analysis:** Where and why the networks coverage and diverge and what insights can be derived?

Data and Methodology

1) Binary Motif Network Construction

Berezkin Catalogue (926 traditions x 2,138 motifs)

	Motif A	Motif B	Motif C	. . . . .
Tradition 1	1	0	1	
Tradition 2	0	1	0	
Tradition 3	1	1	0	
⋮				

→ **Jaccard Similarity** — Using binary matrix and network edge weights

↓

Leiden Community Detection — Clustering based on optimized modularity

↓

Node Attribute Extraction — Analyze the composition of each community

2) Topic Modeling Motif Network Construction

<Text Processing of Berezkin Catalogue>

Motif Title	Motif Description
The old sun	Another sun, usually less benevolent and/or powerful, existed before the present one

1. Text Normalization: Convert "Motif Title; Motif Description" into combined text
2. Tokenization: Filter the text with English stopword list and include terms relevant to mythology
3. Unigram & Bigram Construction: Create title_local and description_local Bigrams for analysis

Finalized Unigram/Bigram for Topic Modeling

old sun old_sun sun usually benevolent powerful existed before present one sun_usually usually_benevolent benevolent_powerful powerful_existed existed_before before_present present_one

<Document Frequency Filtering>
Filter the text with English stopword list and include terms relevant to mythology (df_min = 2.00, df_max = 0.80)

<TF-IDF Algorithm>
Filter the text with English stopword list and include terms relevant to mythology

<Topic Modeling> Non-Negative Matrix Factorization (NMF), k=15

5,172 Unigrams/Bigrams (2,138 motifs) ≈ 15 Topics (2,138 motifs) × 5,172 Unigrams/Bigrams (15 Topics)

<Network Construction>

1. Cosine Similarity computed for each tradition pair
2. Union kNN similarity network using k = 12
3. Leiden Community Detection, resolution gamma = 0.75

Jaccard Distance

$$J(A,B) = \frac{A \cap B}{A \cup B}$$

Cosine Distance

$$Sim(A,B) = \cos\theta$$

3) Comparison Analysis

<Community Overlap>
Compare the motifs sorted into the binary and topic modeling Leiden communities to find the distribution of motifs across communities and identify overlapping communities

In-Depth Analysis on Topic Modeling Community T2 & T4

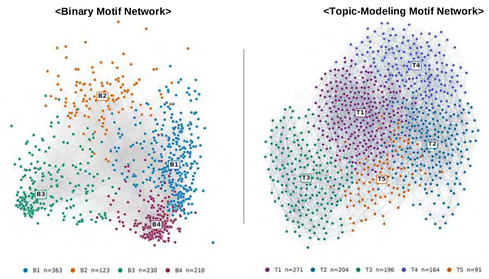
<Topic Prevalence + Distribution>
Identify the prevalence of each of the 15 NMF factors for both T2 and T4 to observe how much of each NMF factor were accounted for in the two distinct communities. Further, overlay the prevalence of these factors with the geographical region to derive which regions were highly concentrated with the factors present in T2 and T4.

<Climate Analysis>
<Precipitation Rate>
Investigate what environment/climate each of the binary and topic-modeling network communities influenced the creation, spread, or dispersion of specific stories.
<Longitude Level>
Investigate where each of the 4 binary and 5 topic-modeling network community are located on the latitude and identifying the insights obtained from the topic-modeling approach that cannot be derived from the binary matrix

Results

Leiden Community Detection

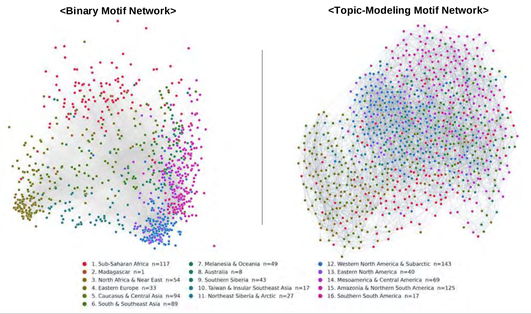
<Binary Motif Network> <Topic-Modeling Motif Network>



Binary and Topic-Modeling Network with each node representing each tradition and edge representing the weighted similarity between traditions: 1) each Leiden cluster labeled in different color; 2) geographical region labeled with region code color

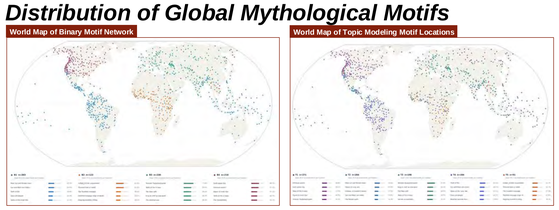
Leiden Community and Geographical Location

<Binary Motif Network> <Topic-Modeling Motif Network>



Distribution of Global Mythological Motifs

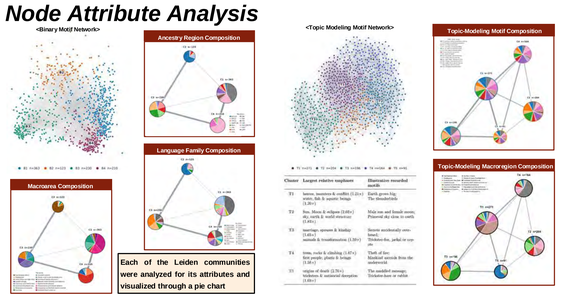
World Map of Binary Motif Network | World Map of Topic Modeling Motif Locations



Binary Motif Network and Topic-Modeling Motif Network were mapped geographically in the Equal Earth Map; the prevalent motifs in the traditions in each cluster are displayed below the map

Node Attribute Analysis

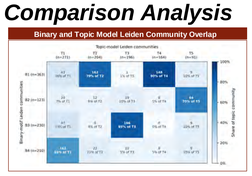
<Binary Motif Network> <Topic Modeling Motif Network>



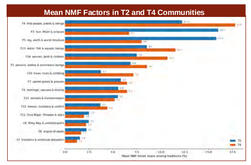
Each of the Leiden communities were analyzed for its attributes and visualized through a pie chart

Comparison Analysis

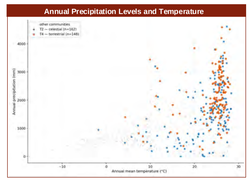
Binary and Topic Model Leiden Community Overlap



Mean NMF Factors in T2 and T4 Communities

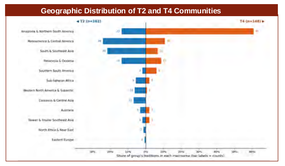


Annual Precipitation Levels and Temperature

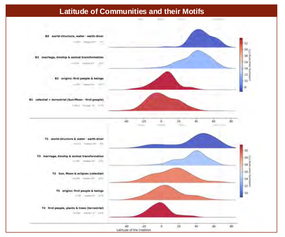


<In-Depth Analysis of Communities: T2 and T4>
Binary community B1 is subdivided by topic-modeling community T2 and T4. Each of the tradition show a distinct geographical pattern in terms of region, climate, and latitude. The topics are also distributed differently for T2 and T4 topic-modeling Leiden communities.

Geographic Distribution of T2 and T4 Communities



Latitude of Communities and their Motifs



Discussion

Analysis

<Leiden Community Detection Comparison>

- The Binary Motif Leiden community detection created 4 communities while Topic-Modeling Leiden community detection created 5 distinct communities. When mapped onto global map, most of points corresponded with each other, but variations existed in the Topic-Modeling network
- Supporting the geographic distribution, most traditions corresponded (B4 → T1, B3 → T3, B2 → T5), except B1 community mapping to 2 distinct topic communities, T2 and T4

Case Study of T2 and T2 Leiden Communities

	T2 Community	T4 Community
Theme	Celestial, Cosmology	Terrestrial
Geography	Global	Northern South America
Ancestry	Across unrelated languages	Amazonian language family
Climate	No significant correlation	Warm, humid climate

<T2 Community> Unsupervised Leiden algorithm detects a common celestial phenomenon that can be observed from many places around the world

<T4 Community> Unsupervised Leiden algorithm detects a specific theme from a region of the world; this is further supported by the language family and climate

The comparison analysis of the two different network algorithm revealed drastic differences in the communities it captured. With in the same B1 community, the T2 community highlight global, celestial themes and the T4 community highlights the region-specific, terrestrial themes.

One Catalogue, Two Stories

Berezkin Catalogue (926 traditions x 2,138 motifs)

Binary Recorded Motif Network

- Detects terrestrial-narrative profiles concentrated Amazonia and Northern South America
- Sensitive to rare, geographically restricted traditions
- Able to identify region-specific variants of myths and also precisely identify unique stories

→ The binary matrix approach to mythology allows precise, specific observations of motifs and culture around the world

Topic-Modeling Semantic Motif Network

- Forms communities by shared meaning and stories
- Enables identification of underlying, common mythological structure in human societies
- Reveals more subtle semantic trends that are not captured/overlooked by the binary motif matrix

→ The topic-modeling approach to mythology allows observations of common human tendency, instinct, and imagination

In order for more accurate and complete understanding of human history, a combination of binary motif matrix and the topic-modeling approach should both use in tandem. The binary motif matrix highlights the specific overlapping motifs in traditions; the topic-modeling provides insight into the universal human thought and imagination, especially in phenomena that was observed all around the world. Hence, this shows that viewing the world and understanding myths in the context of human history requires a nuanced combination of both approaches.

Limitations and Future Directions

<Limitations>

Catalogue Bias: Uneven documentation, translation, and author perspective may influence recorded traditions and myths

Reduction of Complex Narratives: Binary matrix and topic-modeling cannot capture the narratives and complete nuances of myths various cultures

Lack of causal inference: Analysis of mythological similarities does not indicate a casual relationship

<Future Directions>

Additional Representations: Since binary motif and topic-modeling yielded different results, testing different networks can reveal insights

Integrating Historical Evidence: Combine networks with ancient trade roots, phylogenies, and languages to identify similarities and differences in networks

Expert Validation Work with historians and archaeologists to receive advice and explore mythologies and human history more accurately

Conclusion

This research shows that representations of myth produce distinct yet complementary networks of human culture. Exact motifs pre-designated by the Berezkin Catalogue reveals specific, geographically localized stories, while topic modeling identifies broader thematic connections across regions. Together, they demonstrate that global mythological similarity reflects both cultural specificity and shared patterns of human instinct and imagination.

Throughout human history, myth has always been present to pass on the knowledge, advice, observations, warning, and messages through space and time. Yet, as modern technology advances and the primarily Western narrative dominates the world of "information", this computational geo-social network analysis to global mythology aims to highlight the value of mythology in understanding human imagination, thought, and sense of self in this world. Ultimately, this research provides a framework for analyzing mythology and preserving the intangible cultural heritage at a global scale.

Acknowledgements

I want to extend my greatest gratitude to Professor Koylu for guiding me through the rigorous research process and providing feedback that made helped me grow both as a researcher and a student. I also want to thank the Geo-Social Lab and its members for supporting my journey this summer at SSTP. Finally, I would like to express my heartfelt thanks to Rushil, Joshua, and Sriaditya for being wonderful fellow SSTP colleagues throughout this experience. Thank you for making this experience unforgettable.

Citations

Compound Parabolic Concentrator Cross-Sections and 3D-Printed Designs for Solar Thermophotovoltaic Systems

Mihika Kamat[1], Jayden Leung[2], Matteo Yu[3], Molly McLaughlin[4], Dr. Fatima Toor[4]

[1]Los Altos High School, Los Altos, CA, [2]Noble and Greenough School, Dedham, MA, [3]Georgetown Preparatory School, North Bethesda, MD, [4]Department of Electrical and Computer Engineering, University of Iowa, Iowa City, Iowa

Background

Shockley-Queisser limit. Single-junction silicon solar cells are limited to ~31% efficiency due to spectral mismatch. [1].

Solar Thermophotovoltaic systems STPVs use an absorber and emitter to convert sunlight into thermal radiation better matched to a PV cell, with theoretical efficiencies up to 85%. With this efficiency, arn area the size of New Jersey, could power Earth's entire population and industries. Recent STPV systems have achieved as much as 42% efficiency through the utilization of Class III-V PV cells, and selective emitters, however these systems can be impractical and expensive due to low availability of materials.

Methods

Understanding the system. A solar thermophotovoltaic (STPV) system converts sunlight into heat and re-emits it as infrared radiation matched to the PV cell bandgap. Concentrated sunlight is absorbed as heat, then emitted toward the PV cell.

Concentrator. Focuses sunlight on to the absorber. This work studies Compound Parabolic Concentrators (CPCs).

Absorber. Converts concentrated sunlight into heat.

Emitter. Radiates thermal energy towards PV cell at wavelengths close to bandgap.

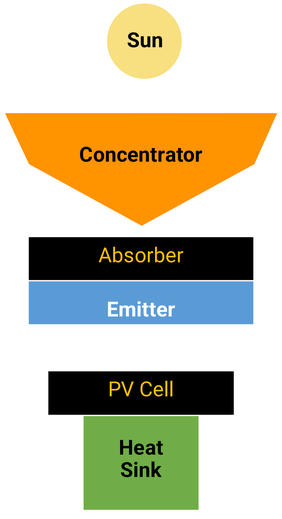


Figure 1. Components of an STPV System.

PV Cell. Semiconductors that absorb photons above their bandgap to convert to energy into electricity.

Heat Sink. Dissipates heat from PV cell to maintain efficiency.

Concentrator Sweep. We conducted a parameter sweep over the shape of the concentrator cross-section: circle, ellipse, rectangle; acceptance angle; and relevant dimensions. Introducing split, a new dimension that allows the concentrator to be lengthened.

Build

Absorber / Emitter Combination:

Figure 2. Absorber /Emitters Tested

Silicon Carbide (SiC / Ceramic) 3 x 3 in

Black Silicon Carbide (SiC / Ceramic) 3 x 3 in

Silicon Carbide (SiC / Ceramic) 1 x 1 cm

Absorber painted black; Silicon Carbide (SiC / Ceramic) 1 x 1 cm

One side black finish Aluminum 1 x 1 cm

Assembly Rig: CAD with Autodesk Fusion

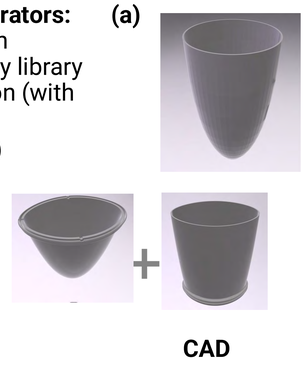


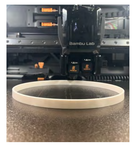
Figure 3. Variable heights of Assembly Rigs, shown in CAD

Concentrators: CAD with Cadquery library on python (with Claude)

(a)

(b)





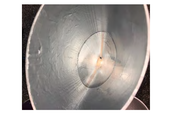


Print

CAD



Paint

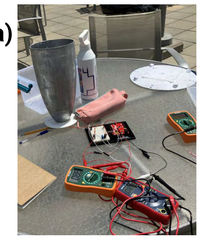




Results

Figure 4. (a) Control; Circular cross-section CPC. (b) Elliptical cross-section CPC, designed as two-part with intermediate connector.

(a)



(b)



Figure 5. (a) Outdoor Testing Setup. (b) Indoor Testing setup

Outdoor Testing

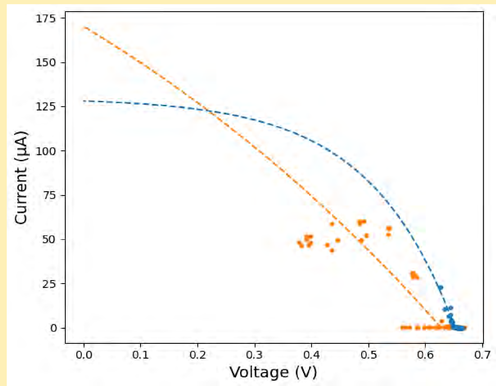
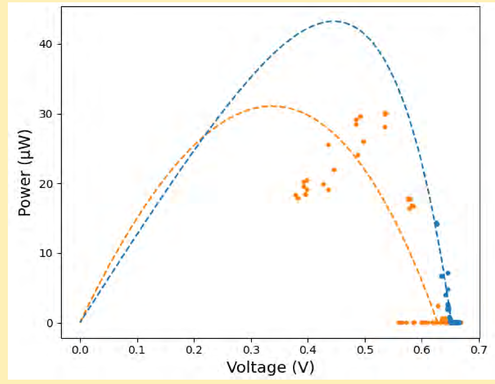


Figure 8. Current and Power comparison for circular and elliptical-split CPC designs.



Under optimized resistance the elliptical CPC could achieve an efficiency as high as 2.1% compared to 0.36% for the circular CPC, and a maximum power output of 43.25 mW compared to 31.1 mW

Indoors Testing

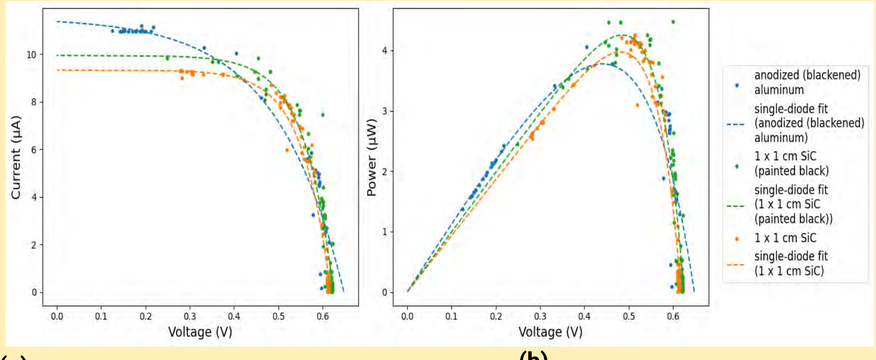
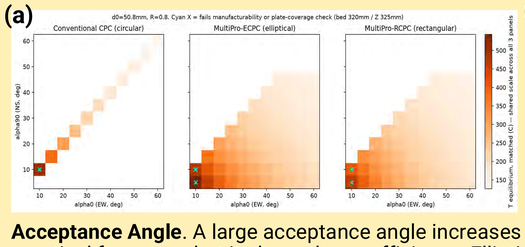


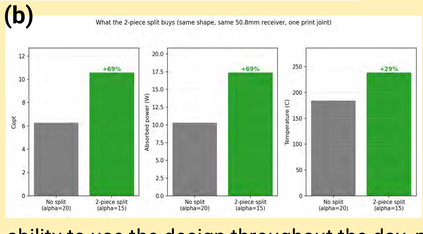
Figure 6. All 1 x 1 cm cut materials exhibited comparable performance from 3.5 to 4% efficiency, with a maximum power output of about 4 mW. The larger sheets (76.2 x 76.2 mm) outputted no voltage and no currents due to difficulty heating them.

Figure 7. Sweeps run on different cross-sectional shape designs for Solar concentrators. (a) Analyzing Temperature as a function of acceptance angle. (b) Effect of Split design on efficiency

(a)



(b)



Split. For both circular and elliptical CPCs, a 2-piece split print was predicted to increase system efficiency by 69%.

Acceptance Angle. A large acceptance angle increases ability to use the design throughout the day, making it more practical for usage, but it also reduces efficiency. Elliptical designs, able to maintain a wide East-West angle alongside a narrow North-South angle, showed more resistance to this change.

Discussion

Novelty. Previous 3D-printed CPCs were limited to circular cross-sections. The usage of a male-female interlocking geometry enables printing a longer elliptical CPC shown to achieve a theoretical efficiency of 2.1% under optimized resistance for a silicon PV cell-anodized aluminum absorber/emitter system.

Limitations. The system used a silicon PV cell instead of the higher-efficiency InGa cells typically used in STPV systems due to cost constraint. In addition, the emitter–PV cell spacing was not optimized, reducing radiative coupling efficiency. Finally, the chrome spray coating (~50% reflectivity) lowered concentrator optical efficiency.

Acknowledgements

Thank you to Schaffer Finney, Maryam Vaghefi Esfidani, and Zhengyang Li for your help with cutting SiC and 3D Printing.

References

Scan this QR code for references.

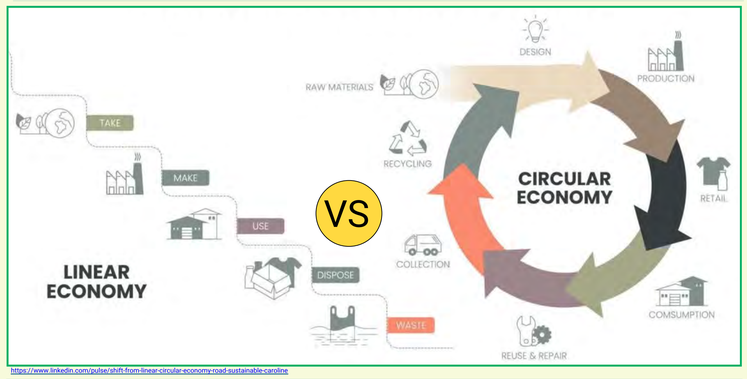
Making Use of Waste: Engineering *Escherichia coli (E. coli)* to Produce Polyhydroxybutyrate (PHB) Bioplastic From Xylose

Annabel Kim[a], Ji Woo Han[b], Nadia Bawa Fio Bekoe[b], Hyeongmin Seo, PhD[b]

a. New Trier High School, Winnetka, IL
b. Department of Chemical and Biochemical Engineering, University of Iowa

Introduction

- Most fast fashion is composed of **polyester**
- Polyester —> made from **non-biodegradable** petroleum-based plastic polyethylene terephthalate (PET)
- Clothing waste dumped into secondhand countries, releases harmful gases, harms humans, water, and soil



https://www.linkedin.com/pulse/shift-from-linear-circular-economy-road-sustainable-caroline

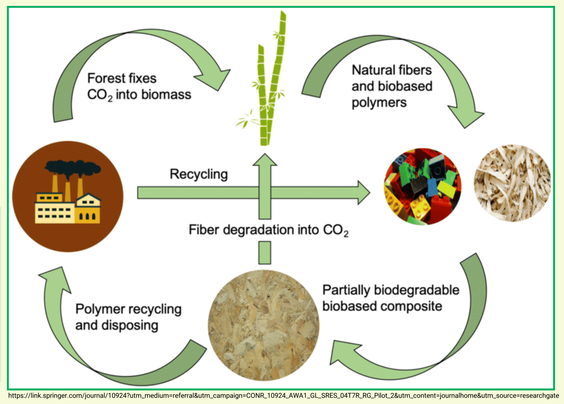
- **Linear economy** is unsustainable
- Polyhydroxybutyrate (**PHB**): biodegradable plastic, potential alternative to PET
- **Xylose:** 2nd most abundant sugar, our chosen carbon source
  - Derived from plant waste (cheap) and supports the **circular economy**
- **Goal:** make bioplastic production more economically viable to replace PET.

PH

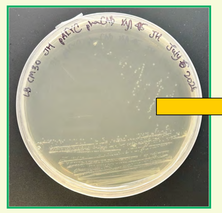


https://circularmaterialslibrary.org/material/phb-polyhydroxyalkanoate/

IPTG: induces expression of genes that produce PHB (Faust et al., 2015)



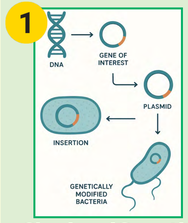
https://link.springer.com/journal/10924?utm_medium=referral&utm_campaign=CONR_10924_AWA1_GL_SRES_04T7R_RG_Pilot_2&utm_content=journalhome&utm_source=researchgate



Genetically modified *E. coli*: produces PHB, prefers to consume xylose over glucose

Strain: *E. coli* HSEC0415xyl harboring pACYC::phaCAB (Seo et al., 2024)

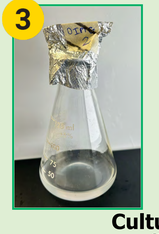
Methodology



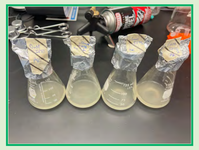
Cloning (Genetic Modification)



Pre-culture



IPTG concentrations: 0 and .1 mM





Culture + OD Measurement (IPTG added at time 0)



Rinse, Centrifuge, and Freeze



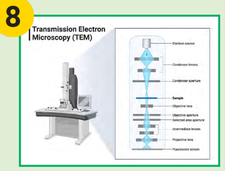
Lyophilization



FAME Reaction



GC-MS



Transmission Electron Microscopy (TEM)

Results

Without	With

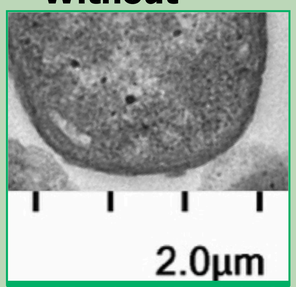


Fig. 1 Imaging of *E. coli* with 0 mM IPTG from TEM (10x)

- Larger cells on average
- No PHB granules present

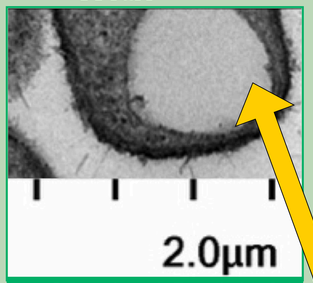


Fig. 2 Imaging of *E. coli* with 0.1 mM IPTG from TEM (10x)

- Smaller cells on average
- Some PHB granules visible

GC-MS

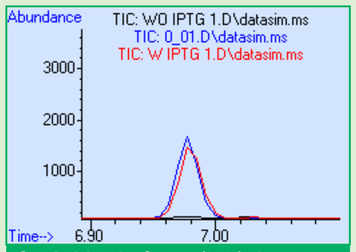


Fig. 3 GC-MS of *E. coli* with 0 mM IPTG (black), *E. coli* .1 mM IPTG (red), and .01 g/L PHB standard (blue)

- *E. coli* with IPTG produced .01 g/L PHB
- *E. coli* without IPTG did not produce PHB

Absorption of *E. coli* Culture with IPTG Concentrations 0 and .1 mM

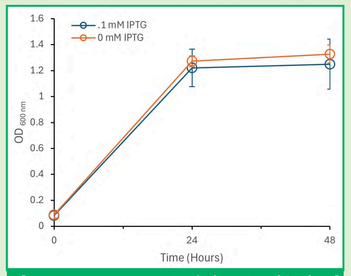
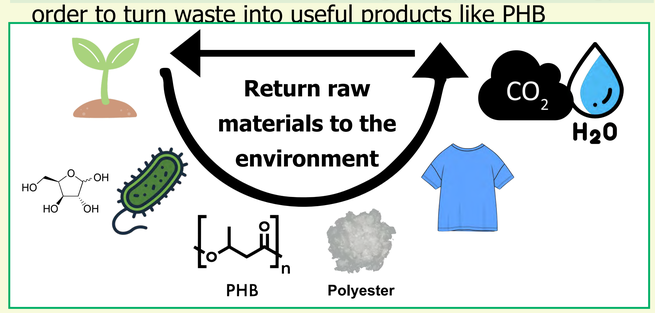


Fig. 4 Average optical density (OD) of *E. coli* cultures with and without IPTG at 0, 24, and 48 hours. The error bars represent standard deviation.

Conclusion

- *E. coli* grew faster on average with no IPTG than with IPTG, according to ODs, suggesting energy was diverted from multiplication in cells with IPTG and toward PHB production
- *E. coli* with IPTG produced PHB, whereas *E. coli* without IPTG did not, providing evidence that IPTG induced phaCAB gene expression
- Optimization of PHB production can make it viable for industrial scale production and support circular economy
- We can continue to take advantage of synthetic biology in order to turn waste into useful products like PHB



Future Directions

- Optimize PHB production conditions
- Develop industrial scale PHB production at a bioreactor
- Utilize unrefined xylose from sources such corn stalks

Acknowledgments

I would like to thank Ji Woo, Nadia, and Dr. Seo for their guidance and sincere support throughout this project. I am also grateful for the rest of the Biosynthesis Lab members for making the lab a fun and educational community.

References

Agus, J., Kahar, P., Abe, H., Doi, Y., & Tsuge, T. (2006). Altered expression of polyhydroxyalkanoate synthase gene and its effect on poly[(R)-3-hydroxybutyrate] synthesis in recombinant Escherichia coli. Polymer Degradation and Stability, 91(8), 1645-1650. https://doi.org/10.1016/j.polymdegradstab.2005.12.011

Faust, G., Stand, A. and Weuster-Botz, D. (2015), IPTG can replace lactose in auto-induction media to enhance protein expression in batch-cultured Escherichia coli. Eng. Life Sci., 15: 824-829. https://doi.org/10.1002/elsc.201500011

Kelwick, R., Ricci, L., Chee, S. M., Bell, D., Webb, A. J., & Freemont, P. S. (2018). Cell-free prototyping strategies for enhancing the sustainable production of polyhydroxyalkanoates bioplastics. Synthetic biology (Oxford, England), 3(1), ysy016. https://doi.org/10.1093/synbio/ysy016

Nawab, S., Keerio, H. A., Li, X., Chen, Y., Wu, C., Zhang, H., Han, R., Wang, H., & Liu, Y. (2026). Engineering Escherichia coli for high-level poly(3-hydroxybutyrate) production: Recent advances and future perspective. Biotechnology advances, 89, 108858. https://doi.org/10.1016/j.biotechadv.2026.108858

Seo, H., Castro, G., & Trinh, C. T. (2024). Engineering a Synthetic Escherichia coli Coculture for Compartmentalized de novo Biosynthesis of Isobutyl Butyrate from Mixed Sugars. ACS synthetic biology, 13(1), 259-268. https://doi.org/10.1021/acssynbio.3c00493

IOWA



Design of Dual-Stage Parabolic Concentrator for Power Optimization in a Solar Thermophotovoltaic System

Jayden Leung[1], Mihika Kamat,[2] Matteo Yu,[3] Molly McLaughlin,[4] Fatima Toor[4]

[1]Noble and Greenough School, Dedham, MA, [2]Los Altos High School, Los Altos, CA, [3]Georgetown Preparatory School, North Bethesda, MD, [4]Department of Electrical and Computer Engineering, University of Iowa, Iowa City, IA

Introduction

- Solar thermophotovoltaics (STPV) bypass the Shockley-Queisser limit (31%) of traditional solar/photovoltaic (PV) cell efficiency to ~85% [1].
- STPV include intermediate materials that absorb solar radiation and emit photons matching the solar cell material's bandgap [1].
- Experimental efficiency record is 8.6%. [2]
- STPV literature focuses on a single concentrator; secondary concentrators not well explored.

Issue: Reflected image is larger than absorber, causing some light to not land on the absorber.

Solution: Use a secondary non-imaging concentrator to focus the incoming light onto the absorber.

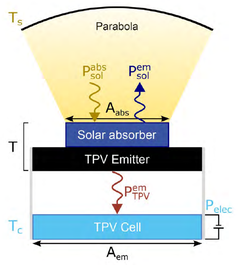


Fig. 1. Diagram of a typical STPV system, adapted from [3].

STPV Efficiency (η_{STPV}) Simulation

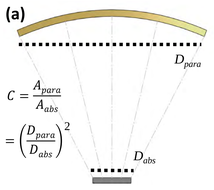
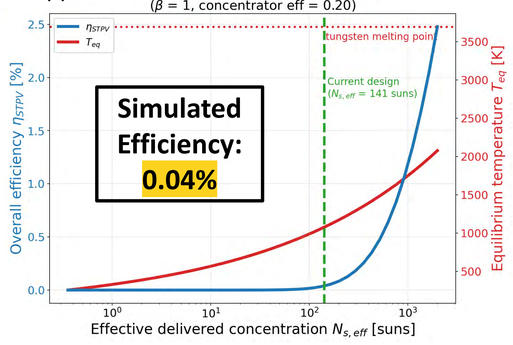
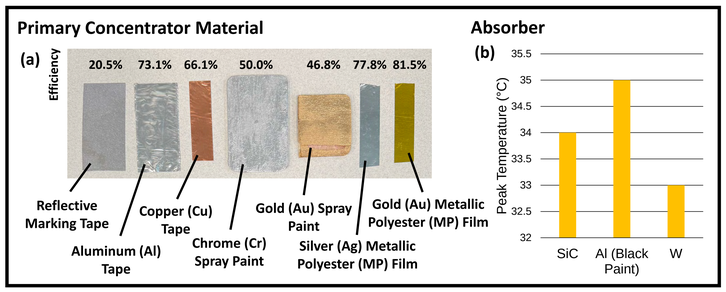
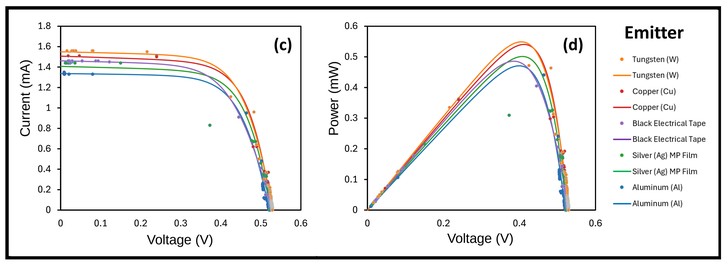


Fig. 2. (a) Concentration schematic and equation. (b) System efficiency vs. concentration sweep for STPV system with silicon carbide (SiC) absorber/emitter.



Component Design





Limitations: Silicon solar cell, blackbody absorber/emitter, no spectral management.

Fig. 3. (a) Tapes, coatings, and films considered for concentrator. (b) Absorber peak temperature (°C) under 1 sun (1 kW/m²) for 3 minutes. (c) IV and (d) PV curves of emitters.

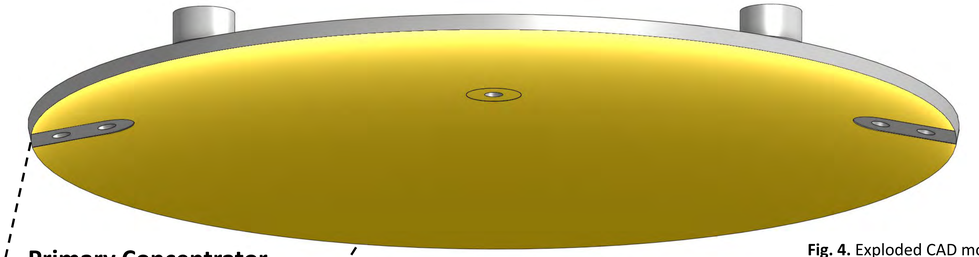


Fig. 4. Exploded CAD model of our STPV system rig and its individual components.

Primary Concentrator
Coated Parabolic Dish

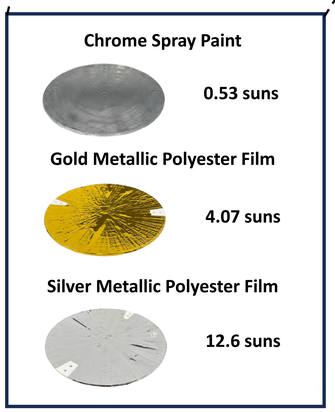
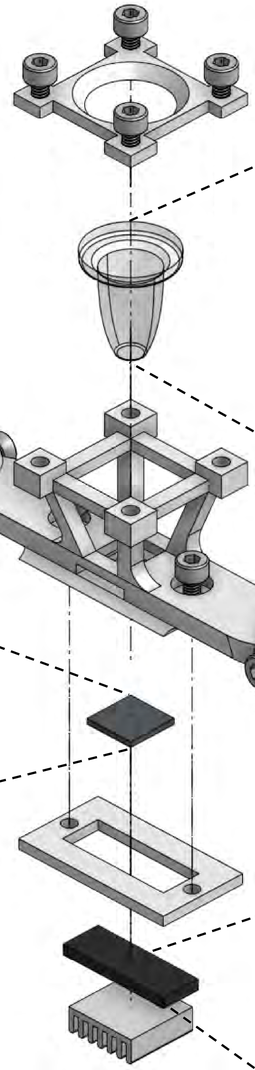


Fig. 5. Films and coatings tested directly on the parabolic reflector under the sun.



Secondary Concentrator
Compound Parabolic Concentrator

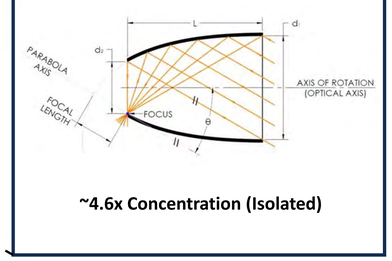


Fig. 6. Diagram of working CPC model. Theoretical concentration noted for our CPC. Adapted from [4].

Absorber and Emitter
Tested Materials

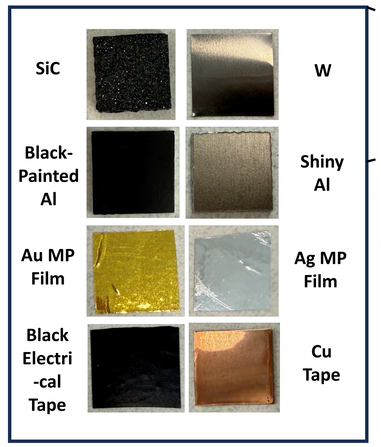


Fig. 7. Materials considered for absorber, emitter, or both.

Solar Cell
Measured IV/PV Curve

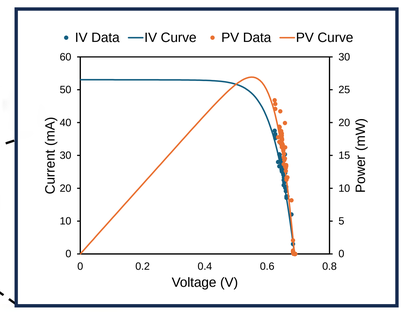


Fig. 8. Experimental IV and PV curve for our solar cell under 1 sun from indoor lamp simulator.

Methods

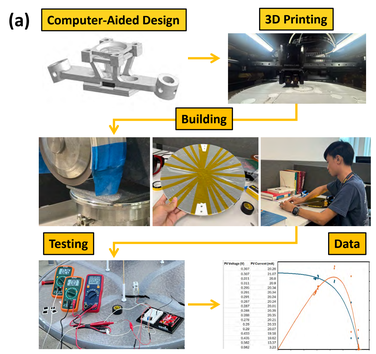
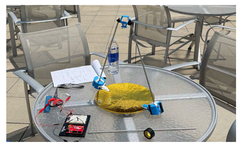


Fig. 9. (a) Flow diagram of how the full STPV system was fabricated and tested. (b) Flow diagram of how we parsed our data, occurring in between Testing and Data stages in (a).

Results



System Efficiency

Without CPC: 0.0213%
With CPC: 0.0121%



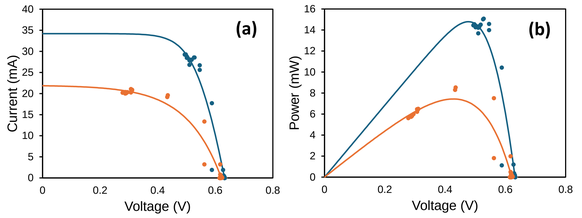


Fig. 10. (a) IV and (b) PV curves of STPV system with and without CPC.

Conclusion

Secondary concentrators need to be further explored and developed.

Primary FOR **Collecting**

Secondary FOR **Focusing**

Improvements:
- Larger CPC
- Deeper dish
- Better power efficiency

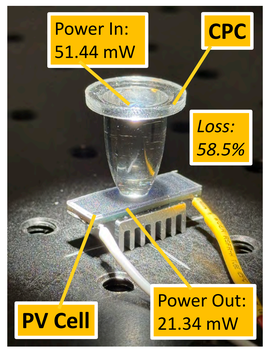


Fig. 11. Experimental power efficiency of our CPC.

Acknowledgements & References

Acknowledgements

This work was supported by the Toor Lab at the University of Iowa. We thank Maryam Vaghefi for the referral to the Materials Analysis, Testing, and Fabrication (MATFab) Facility, and Hossein Zandipour and Schaffer Finney at MATFab for assistance in dicing the SiC sheet.

References

Repeated Exposure to CO_2 Reduced Acute Arousal Response in Mice

Aaron Li[1,2], Lauren Smith[3,4], Jensen Lin[5,6], Rui Li[3,4], Gordon F. Buchanan[3,4]

[1]Camas High School; WA, [2]Secondary Student Training Program; [3]Department of Neurology, [4]Iowa Neuroscience Institute, Carver College of Medicine, University of Iowa,IA; [5]West High School, IA; [6]Kirkwood Community College Workplace Learning Connection, IA

Introduction

- One in 26 people will be diagnosed with epilepsy over their lifetime.
- One third of those people develop refractory epilepsy, which means their seizures are uncontrolled by medicine[1].
- Refractory epilepsy is associated with having multiple seizures within a short timespan[2] and increased risk of sudden unexpected death in epilepsy (SUDEP)[3].
- In a genetic mouse model of epilepsy, increased seizure frequency is found before death[4].
- Seizures can lead to hypercapnia[5], or excess CO_2 levels in body. Therefore, multiple seizures in succession can lead to repeated CO_2 exposure.
- CO_2 arousal latency is increased in animals with epilepsy.
- Serotonin is implicated in seizure regulation and CO_2 induced arousal[6].

Hypothesis: Repeated CO_2 exposure worsens the CO_2 induced arousal response and disturbs normal sleep-wake structure.

Methods



Surgery

- Surgical implantation of EEG/EMG headmount



Model of Epilepsy

- Pilocarpine injections for status epilepticus, survivors have spontaneous seizures



Recording

- Closed loop system for autosleep detection, changes in CO_2 level, breathing, EEG/EMG



Analysis

- Sleep scoring using Sirenia Sleep, Matlab and Jasp for arousal latency analysis

Results

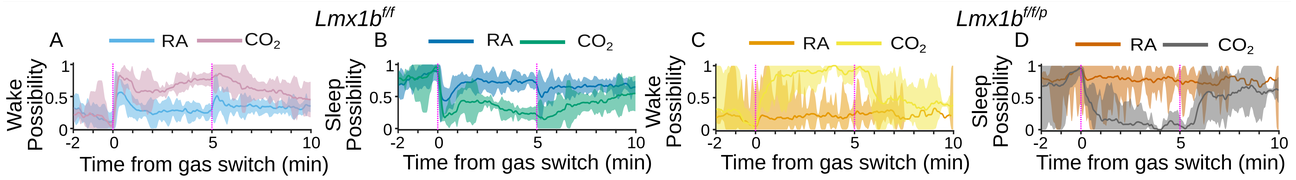


Figure 1. Vigilance state possibility. (A) Wake Possibility for *Lmx1b*$^{f/f}$ mice under RA (sky blue) and CO_2 (soft pink) conditions. (B) Sleep possibility for *Lmx1b*$^{f/f}$ mice under RA (dark blue) and CO_2 (teal green). (C) Wake Possibility for Lmx1b$^{f/f/p}$ mice under RA (bright orange) and CO_2 (yellow) conditions. (D) Sleep possibility for *Lmx1b*$^{f/f/p}$ mice under RA (burnt orange) and CO_2 (dark gray). Vertical mangeta lines indicate the onset and offset of gas change. Shaded areas indicate 95% confident interval.

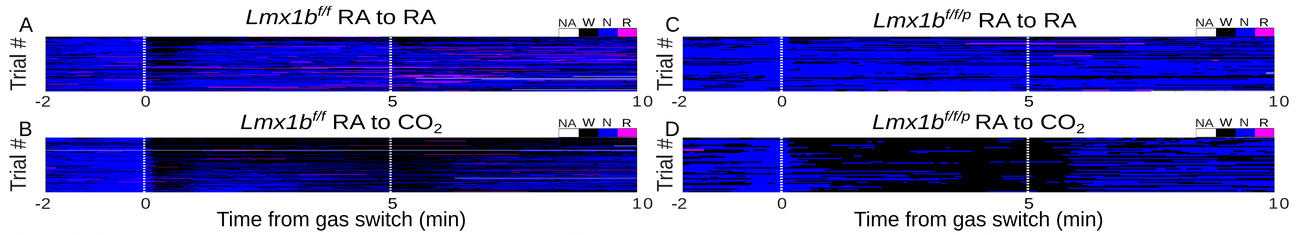


Figure 2. Sequential trial hypnograms during hypercapnia challenge. Repeated trial hypnograms stacked chronologically from top to bottom across experimental conditions: *Lmx1b*$^{f/f}$ mice exposed to RA (A) and to 7% CO_2 (B), and *Lmx1b*$^{f/f/p}$ mice exposed to RA (C) and to 7% CO_2 (D). Each trial comprises a 12-minute window: 2 minutes baseline, 5 minutes gas exposure, and 5 minutes post-exposure recovery. Sleep-wake structure is scored using 2-sec epochs. States: Wake (black), NREM sleep (blue), REM sleep (magenta), and not available (white). Vertical white lines indicate onset and offset of gas change.

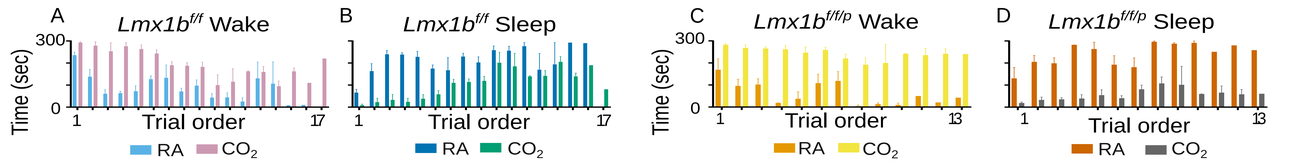


Figure 3. Chronological changes in wake and sleep time during gas exposure. Time spent in wake (A) and sleep (B) in *Lmx1b*$^{f/f}$ mice during RA or CO_2 exposure. Time spent in wake (C) and sleep (D) in *Lmx1b*$^{f/f/p}$ mice during RA or CO_2 exposure. Mixed-effects analysis was used to test the main effects of gas type and trial order on time spent in wake and sleep. Data were presented in mean ± SEM.

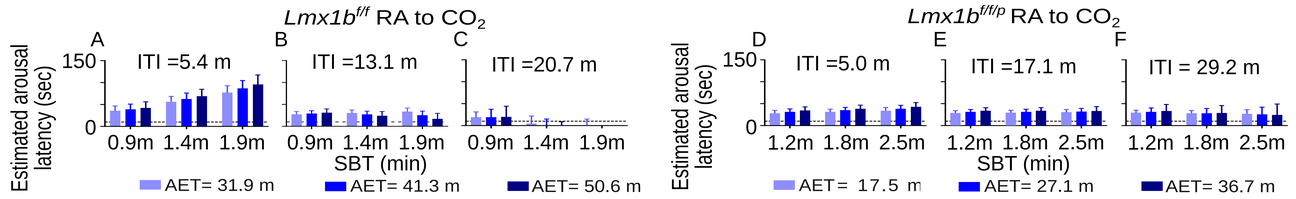


Figure 4. Dynamic CO_2 habituation in *Lmx1b*$^{f/f}$ mice but not in *Lmx1b*$^{f/f/p}$ mice. (A-C) *Lmx1b*$^{f/f}$ mice display dynamic CO_2 habituation, characterized by synergistic effect of accumulated CO_2 exposure time (AET) and sleep time before trigger (SBT) on arousal latency when trial intervals (ITI) are low. (D-E) *Lmx1b*$^{f/f/p}$ mice showed flat arousal latency across different ITI, AET, and SBT conditions. Data presented as linear mixed model estimated marginal means

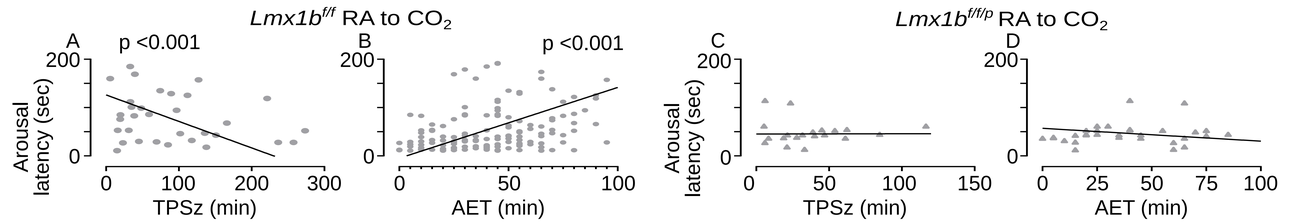


Figure 5. Dual independent control of CO_2-induced arousal after a seizure in *Lmx1b*$^{f/f}$ mice but not in *Lmx1b*$^{f/f/p}$ mice. (A-B) CO_2 induced arousal latency after a seizure is dynamically controlled by both time from previous seizure (A; TPSz) and accumulated CO_2 exposure time (B; AET) in *Lmx1b*$^{f/f}$ mice. (C-D) No significant relationship between arousal latency and either TPSz (C) or AET (D) in *Lmx1b*$^{f/f/p}$ mice. Each dot or triangle indicates a trial. Solid lines indicate fitted OLS regression slopes.

Conclusion

- CO_2 increased possibility of wake and decreased possibility of sleep in both *Lmx1b*$^{f/f}$ and *Lmx1b*$^{f/f/p}$ mice.
- *Lmx1b*$^{f/f}$ mice exhibited a progressive, trial order dependent reduction in wakefulness amount and increase in sleep amount during CO_2 gas exposure, whereas *Lmx1b*$^{f/f/p}$ mice did not.
- CO_2 arousal latency in *Lmx1b*$^{f/f}$ mice was increased by both accumulated CO_2 exposure time and sleep time before trigger, with long inter trial intervals acting as a reset. This dynamic was largely absent in *Lmx1b*$^{f/f/p}$ mice
- In *Lmx1b*$^{f/f}$ mice, post-ictal CO_2-induced arousal latency was dual independently controlled by both time from previous seizure and accumulated CO_2 exposure time, while sleep time before trigger did not interact with either. *Lmx1b*$^{f/f/p}$ mice did not show any interaction.
- These results suggested that 5-HT plays an important role in control arousal and sleep-wake structure under repeated CO_2 exposure in both seizure naive and epileptic animals.

Acknowledgments

I would like to thank the Buchanan Lab and my mentors for their guidance in this project, and this work is supported by NIH/NINDS R01NS129722 (GFB), Beth L. Tross Epilepsy Professorship (GFB). I would also like to thank the Secondary Student Training Program and the Belin-Blank Center for their support. Graphical illustrations were made using BioRender. Analysis completed using Graphpad.

Reference

1. Thurman, D. J., Hesdorffer, D. C., & French, J. A. (2014). Sudden unexpected death in epilepsy: assessing the public health burden. Epilepsia, 55(10), 1479–1485.
2. Jafarpour, S., Stredny, C. M., Piantino, J., & Chapman, K. E. (2019). Baseline and outcome assessment in pediatric status epilepticus. Seizure, 68, 52-61.
3.Ryvlin, P., Nashef, L., Lhatoo, S. D., Bateman, L. M., Bird, J., Bleasel, A., Boon, P., Crespel, A., Dworetzky, B. A., Høgenhaven, H., Lerche, H., Maillard, L., Malter, M. P., Marchal, C., Murthy, J. M., Nitsche, M., Pataraia, E., Rabben, T., Rheims, S., . . . Tomson, T. (2013). Incidence and mechanisms of cardiorespiratory arrests in epilepsy monitoring units (MORTEMUS): A retrospective study. The Lancet Neurology, 12(10), 966-977.
4. Iyer, S. H., Matthews, S. A., Hallgren, J., Netzel, L., Simeone, T. A., & Simeone, K. A. (2026). A Longitudinal Study of the Effects of Ketogenic Diet on Seizures, Cardiorespiration, Sleep Architecture and Mortality in the Kv1.1 Knockout Mouse Model of Sudden Unexpected Death in Epilepsy (SUDEP). Nutrients, 18(5), 809.
5. Sainju, R. K., Dragon, D. N., Winnike, H. B., Nashelsky, M. B., Granner, M. A., Gehlbach, B. K., & Richerson, G. B. (2019). Ventilatory response to CO2 in patients with epilepsy. Epilepsia, 60(3), 508–517.
6. Petrucci, A. N., Joyal, K. G., Purnell, B. S., & Buchanan, G. F. (2020). Serotonin and sudden unexpected death in epilepsy. Experimental neurology, 325, 113145.

The effects of excessive neonatal testosterone during a critical period on the social and developmental behaviors of wild-type mice

Alicia Li[1], Pravda Quiñones-Labernik[2,3], Emily Hagan[2,4] , Anthony Lange[3,4], Sarah Ferri[3,4]

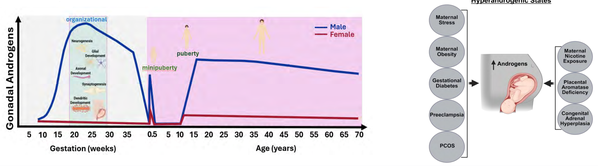
[1]Troy High School, Troy, MI
[2]Department of Neuroscience and Pharmacology, Carver College of Medicine, IA
[3]Iowa Neuroscience Institute, University of Iowa, IA
[4]Stead Family Department of Pediatrics, Carver College of Medicine, IA

An Introduction to ASD

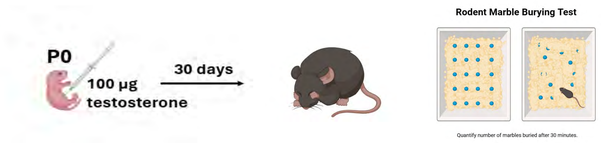
- Neurodevelopmental disorders are extremely common nationwide.
- Males are disproportionately affected by Autism Spectrum Disorder, an NDD, compared to females.
- ASD is broadly defined as having social deficits and repetitive behaviors.
- In males, an increase in testosterone levels occurs in both humans and mice during a critical period following birth, which permanently organizes the brain and induces sex-specific changes.
- However, males who are injected with excessive testosterone during this period develop symptoms like in autism, but for females the impact of it is not as large.
- How do specific hormones such as testosterone affect the behaviors of a mouse and contribute to repetitive behaviors, a symptom of autism?

Androgen Dysregulation Effects

- Common pregnancy complications such as preeclampsia, gestational diabetes, and PCOS can result in heightened levels of androgen in the mother.
- These complications are associated with an increased risk of NDD's for both humans and mice.
- Maternal stress, obesity, or nicotine exposure can also increase androgen levels, and increase the risk for NDD's as well.

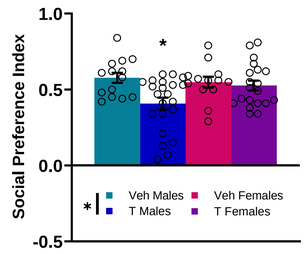


Methodology



- Mice from seven different litters (both testosterone-treated mice and control mice) were each placed in housing environments containing 12 marbles and a bed of crushed corn cob.
- Mice were then given 30 minutes to wander around the environment.
- The frequency of grooming for the mice, which is considered a repetitive behavior and therefore a symptom of ASD, was measured.
- The percentage of marbles buried was also measured.
- Social behavior was also evaluated in a free interaction test in which two mice were allowed to interact freely in a gated arena for 10 minutes.
  - Incidents of social behaviors were recorded using the EthoVision XT software.

Excess Neonatal Testosterone in Male Mice Causes Social Deficits

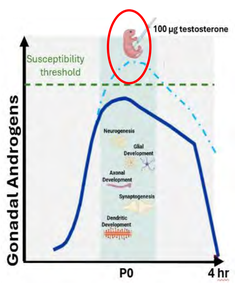


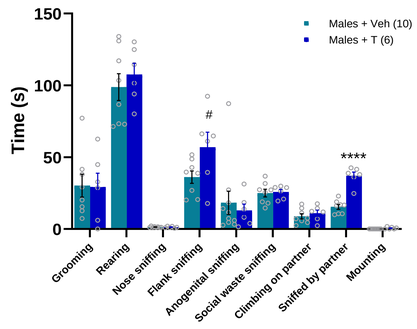
Quiñones-Labernik et al, 2025

- At P0 (a critical period for mice), male and female mice were injected with either testosterone propionate (T) or vehicle control (sesame oil).
- 30 days later (P30) in a 3-chambered gated arena, a social preference test was performed. Both the T-treated mice and control mice were given 10 minutes for habituation, and 10 minutes to choose between a novel toy or another mouse.
- Male mice injected with excessive testosterone had reduced social preference indexes.
- Excess testosterone had no significant effect on females.



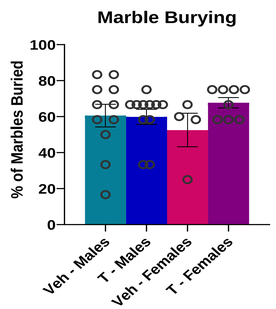
Excess Testosterone in Males Results in Increased Sniffing

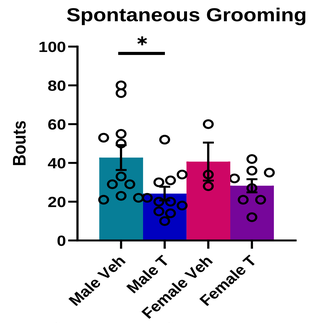




- In P0, excess testosterone was given to males during a critical period after birth, in which development is crucial.
- Two mice (one with testosterone and the other without) were allowed to socialize for 10 minutes to further evaluate social behavior.
- Social behaviors, such as sniffing the other, were recorded.
- T-treated males had a higher likelihood of sniffing the other.
- However, T-treated males were sniffed more by their partner.
- Rearing (when a mouse stands on its hind legs or on another mouse) is a potential dominance display for mice and occurred more frequently for T-treated males.

Excess Testosterone Affects Grooming in Both Sexes and Marble Burying in Females





- Excess testosterone in both males and females decreased the frequency of grooming behaviors.
- Females with excess testosterone buried a higher percentage of marbles compared to the vehicle females.
- There was no significant difference of the percentage buried between the T-treated males and the vehicle males.

Conclusions

- Mice injected with testosterone groomed less, indicating less repetitive behavior. This suggests that while excess testosterone can induce other ASD-related symptoms, the frequency of repetitive behaviors is reduced.
- Compared to females, testosterone had a greater difference in grooming frequency for males, suggesting that testosterone may have a greater effect on males.
- T-treated females had a higher number of grooming incidents compared to T-treated males.

Consequences

- By understanding gonadal hormone dysregulation in mice, it can help us better understand autism/other neurodevelopmental disorders in humans.
- This research could allow us to consider the maternal environment and how it may also contribute to NDD's.
- This research can also help us view autism/other neurodevelopmental disorders differently and find ways to alleviate the social and memory deficits related to them.

Further Directions

- Further understand why mice with excess testosterone do not display repetitive behaviors but do display other symptoms related to ASD.
- Continue investigating the effects of testosterone.
- Determine other factors that may contribute to the differing frequencies of repetitive behaviors and why.
- Examine if other gonadal hormones can either negatively or positively affect the frequency of repetitive behaviors.

Acknowledgements

Secondary Student Training Program, Belin-Blank Center
Iowa Neuroscience Institute

References

1. Pravda Quiñones-Labernik, Blocklinger, K. L., Bruce, M. R., Hagan, E., Preuschl, D., Tesar, C., & Ferri, S. L. (2025). Excess Neonatal Testosterone Causes Male-Specific Social and Fear Memory Deficits in Wild-Type Mice. *ENeuro*, 12(8), ENEURO.0020-25.2025. https://doi.org/10.1523/eneuro.0020-25.2025
2. Mong, J. A., & McCarthy, M. M. (2012). Brain sexual differentiation: Clues toward the understanding of neural dysfunctions. *Reviews in Endocrine and Metabolic Disorders*, 13(3), 149–149. https://doi.org/10.1007/s11154-012-9222-8
3. Bell, M. R. (2018). Comparing Postnatal Development of Gonadal Hormones and Associated Social Behaviors in Rats, Mice, and Humans. *Endocrinology*,159(7), 2596–2613. https://doi.org/10.1210/en.2018-00220
4. Porcelli, S., Van Der Wee, N., van der Werff, S., Aghajani, M., Glennon, J. C., van Heukelum, S., Mogavero, F., Lobo, A., Olivera, F. J., Lobo, E., Posadas, M., Dukart, J., Kozak, R., Arce, E., Ikram, A., Vorstman, J., Bilderbeck, A., Saris, I., Kas, M. J., & Serretti, A. (2019). Social brain, social dysfunction and social withdrawal. *Neuroscience & Biobehavioral Reviews*, 97(97), 10–33. https://doi.org/10.1016/j.neubiorev.2018.09.012
5. Santos, S., Ferreira, H., Martins, J., Gonçalves, J., & Castelo-Branco, M. (2022). Male sex bias in early and late onset neurodevelopmental disorders: Shared aspects and differences in Autism Spectrum Disorder, Attention Deficit/hyperactivity Disorder, and Schizophrenia. *Neuroscience & Biobehavioral Reviews*, 135,104577.https://doi.org/10.1016/j.neubiorev.2022.104577

Friendship or Fixation? Exploring Mental Health Impacts and Cognitive Distortions in Reddit Discussions of AI Companions

Sarah Li[1], Haixia He[2], Weiguo Fan[2]

[1]McLean High School; [2]Department of Business Analytics, University of Iowa

Background

- AI companionship (AIC) is gaining popularity; Replika has **40 million+** users (Replika, 2026)
- High-profile suicide cases and lack of safety guardrails for bot conversations (Sanford, 2025)
- Accessible therapy and comfort vs. overdependency and social isolation

Objectives

Purpose: To understand the impacts of AIC on mental health and create models that **screen for impacts**

RQ1: What **mental health themes and cognitive distortions** are discussed in AIC-related Reddit texts?

RQ2: Can machine learning models **detect and classify** mental health impacts & cognitive distortions from AIC-related Reddit texts, and how?

Methodology

Dataset of Reddit Texts — **3,953 Reddit posts and comments** related to AI companionship, labeled for mental health (Yes or No; κ=0.73), attitude (Positive/Negative/Mixed; κ=0.71), and cognitive distortions

Topic Analysis
- Identify dominant discussion and attitudes
- Analyze high-density topics and themes using BERTopic

Embedding Generation
- MentalBERT, SBERT, and TF-IDF to convert Reddit texts to **numerical representations**
- MentalBERT: best performance; SBERT: semantics; TF-IDF: explainability

Grid Search

7 embedding combinations (MB, SB, TF, MB+SB, MB+TF, SB+TF, MB+SB+TF) and **5 models** (LR, SVM, KNN, RF, XGB) for the optimal pipeline to predict:

Evaluation: F1 score, accuracy, AUC, precision recall. Focus on F1

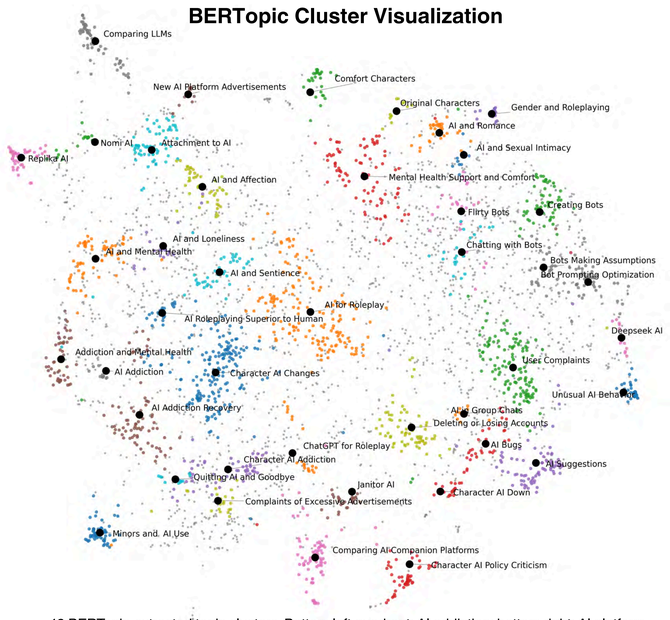
Mental Health Impacts
Detect: Yes, No
Classify: +, –, Mixed

Cognitive Distortions
Detect: Yes, No
Classify: Yes, No on 10 labels

Feature Analysis
- Extract words from TF-IDF using LR weights
- Identify influential words for each category

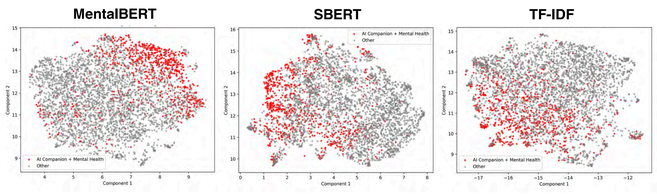
Results

Exploratory Topic Analysis



42 BERTopic-extracted topic clusters. Bottom left quadrant: AI addiction; bottom right: AI platform feedback; top left: AI platform comparisons and attachment; top right: AI, relationships, and roleplaying.

Mental Health Embedding Clusters



UMAP-reduced embeddings from MentalBERT, SBERT, and TF-IDF; mental health texts highlighted in red. MentalBERT shows the best separation between mental health texts and the rest of the corpus.

Model-Extracted Mental Health Features



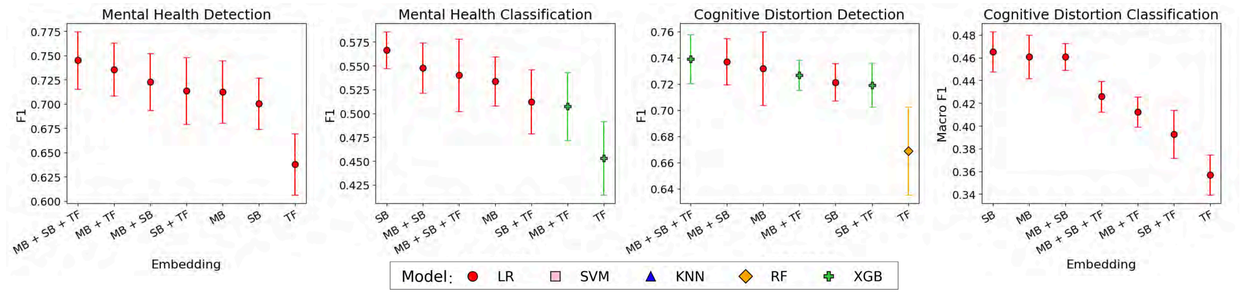
Mental Health Prediction

Task	Best Embedding	Best Model	F1	Interpretation
Detect	MB+SB+TF	LR	0.745	Combining embeddings works best for binary classification tasks
Classify	SB	LR	0.566	

Cognitive Distortion Prediction

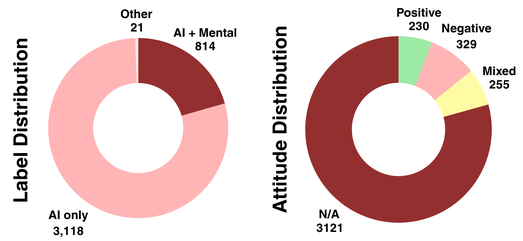
Task	Best Embedding	Best Model	F1	Interpretation
Detect	MB+SB+TF	XGB	0.739	XGBoost appears for detection, but logistic regression is best across tasks
Classify	SB	LR	0.465	

Model Performance Comparison Across Embedding Combinations



LR consistently performs best out of the five models, followed by XGB and RF. TF is consistently the worst embedding method, but can help in combined embeddings for binary detection.

Supplementary Information



Abbreviations: logistic regression (LR), LinearSVM (SVM), k-nearest neighbors (KNN), random forest (RF), XGBoost (XGB), MentalBERT (MB), SBERT (SB), TF-IDF (TF)

Conclusion and Next Steps

RQ1: Analysis
- Minority of texts showed mental health impacts
- 40% of mental health impacts were negative
- Texts focused on **AI platforms, suggestions, addiction, and roleplay**.

RQ2: Model Development
- Best was **F1=0.75** for mental health detection
- **Combining embeddings** improves performance for binary, but not multilabel classification.
- **Lexicon of features** that serve as markers to indicate mental health impacts.

Future directions:
- Analysis of users' posts over time
- Prediction using the lexicon extracted from TF-IDF

Acknowledgments

- Secondary Student Training Program (SSTP) - facilitated the amazing opportunity to conduct this research
- Dr. Haixia He and Dr. Weiguo Fan at the Tippie College of Business - provided invaluable mentorship and resources
- Kai Seifan - helped annotate and compare the data labels
- Elizabeth Wang and James Cao - served as emotional support

Appendix

References

Full Paper Here!

Contact At:
sarah.yingqi.li@gmail.com

Understanding the Role of Mixed Ligands in Metal-Organic Framework Flexibility

Abigale Liu[1], Thumini Dias[2], Alexei Tivanski, Ph.D.[2]

[1]Farragut High School, [2]University of Iowa, Department of Chemistry

Introduction

- **Metal-organic frameworks** (MOFs) are highly porous materials made of metal ions and organic linkers
- **Zeolitic imidazolate frameworks** (ZIFs) are a subclass of MOFs known for their pore tunability, thermal stability, flexibility and in some cases, switchable behavior
- **Mixed-ligand MOFs**, a combination of two or more ligands within a single framework, are a new approach that allow for the structural modulation of MOFs, and potentially the modulation of mechanical properties and gas adsorption

Figure 1. Explanation of Mixed Ligand MOFs



- **Atomic force microscopy** (AFM) is a non-destructive imaging method that uses probes with sharp tips to generate high resolution nanoscale images as well as collect Force vs. indentation distance data

Research Question

How do mixed ligands modulate the mechanical properties of metal-organic frameworks?

Hypothesis: Mixed-ligand ZIFs will have different flexibilities from their parent ZIFs.

Methodology

Materials Synthesis

Figure 2. ZIF-7, ZIF-8, and ZIF-7-8 Structures

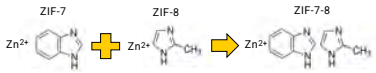
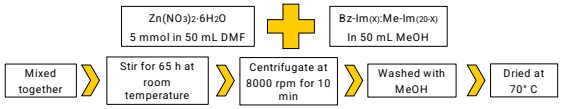


Figure 3. Table of ZIF-7 and ZIF-8 characteristics

	ZIF-7	ZIF-8
Topology	SOD	SOD
Symmetry	Rhombohedral	Cubic
Space group	R3	I-43m
Pore diameter (Å)	4.31	11.60
Theoretical density, ρ, (gcm^{-3})	1.24	0.95

Figure 4. Synthesis of ZIF-7-8 hybrids



Note: DMF is Dimethylformamide and MeOH is Methanol

Characterization

Figure 5. ^{1}H nuclear magnetic resonance (NMR) spectra of ZIF-7, ZIF-8, and ZIF-7-8 dissolved in deuterated acetic acid

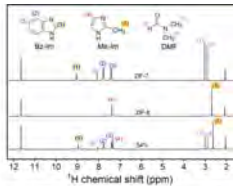
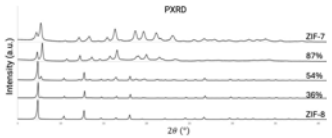


Figure 6. Powder X-ray diffraction (PXRD) graphs of synthesized ZIF-7, ZIF-8, and ZIF-7-8

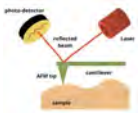


Note: The peaks confirmed the crystallinity of the synthesized ZIF-7-8

Note: After analyzing and comparing the areas of the peaks, the sample used in the experiment was determined to be ZIF-7$_{54\%}$-8$_{46\%}$

1. A crystal suspension in MeOH was made and drop-casted on a mica substrate
2. AFM is used to collect images of individual crystals
   - Size (area-equivalent diameter) range of nanocrystals: 900 nm – 1300 nm
3. AFM nanoindentation is used to collect force vs. indentation plots
4. Johnson-Kendall-Roberts (JKR) model is used to analyze data and produce the Young's Modulus

Figure 7. Schematic of AFM Imaging[3]



Note: AC (tapping) mode and contact mode were used to image the crystals and collect force vs indentation data, respectively

$$F_{JKR} = F + 3\pi W R^* + \sqrt{6\pi W R^* + 9\pi^2 W^2 R^{*2}}$$

$$a_{JKR}^3 = \frac{3RF_{JKR}}{4E^*} \qquad h = \frac{a_{JKR}^2}{R} - \sqrt{\frac{2\pi W a_{JKR}}{E^*}}$$

$$\frac{1}{E^*} = \frac{1-\nu_{tip}^2}{E_{tip}} + \frac{1-\nu_{sample}^2}{E_{sample}}$$

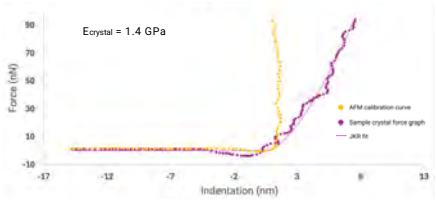
E* – Effective Young's Modulus
R – Tip radius of curvature
F_{JKR} – Load between tip and sphere
h – Indentation/deformation of sphere
a_{JKR} – Contact area radius between tip and sphere
F – Loading force
W – Work adhesion
V – Poisson's ratio
E – Young's Modulus



Figure 8. AFM amplitude image showing where the data in Figure 9 was collected

Note: Purple represents more flexible crystal, while yellow is the rigid mica substrate.

Figure 9. Sample Force vs. Indentation plot



Results

Figure 10. AFM 3D height image of a ZIF-7$_{54\%}$-8$_{46\%}$ crystal

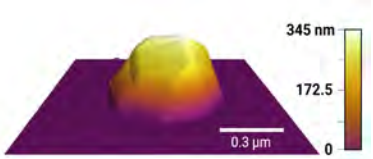


Figure 11. Force vs. Indentation plot of a ZIF-7$_{54\%}$-8$_{46\%}$ crystal

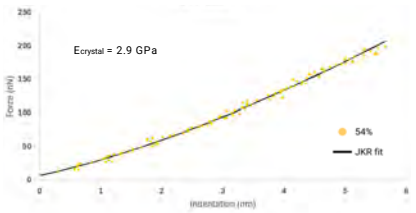
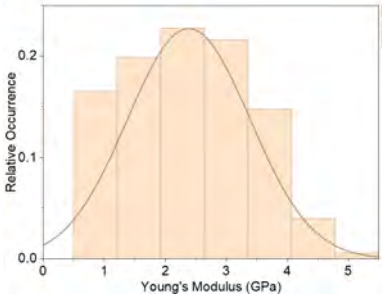


Figure 12. Histogram of Young's Modulus values for the ZIF-7-8 54%



Most probable Young's Modulus value for ZIF-7$_{54\%}$-8$_{46\%}$: 2.4 ± 1 GPa (this work)

For comparison, ZIF-7 and ZIF-8 Young's Moduli were taken from previous studies:[4,5]

ZIF-7: 0.9 GPa ± 0.4 GPa

ZIF-8: 3.2 ± 0.2 GPa

Conclusions

- Mixed-ligand ZIF-7$_{54\%}$-8$_{46\%}$ has Young's Modulus value of 2.4 ± 1 GPa, which is different than that reported in the literature for parent ZIF-7 (~0.9 GPa) and ZIF-8 (~3.2 GPa)
- The extent of Young's modulus variability for ZIF-7$_{54\%}$-8$_{46\%}$ (1 GPa standard deviation) likely suggests that while the average fraction is 54%, on an individual crystal basis we likely have some crystal-to-crystal fraction variability (confirmed by Thumini Dias's measurements using single crystal IR spectroscopy)

Future Directions

- Finish the experiment with parent ZIF-7 and ZIF-8 individual crystals of similar size range of ~900–1300 nm
- Similarly extend the measurements to other ZIF-7-8 hybrids with various fractions (e.g., 30%, 70%, 80%)
- Explore other types of MOFs (different metals and/or ligands)

Acknowledgments

I would like to thank the Tivanski group for their help and guidance as well as Thumini for her invaluable mentorship

References

1. Thompson, J. A.; Blad, C. R.; Brunelli, N. A.; Lydon, M. E.; Lively, R. P.; Jones, C. W.; Nair, S. Hybrid Zeolitic Imidazolate Frameworks: Controlling Framework Porosity and Functionality by Mixed-Linker Synthesis. *Chemistry of Materials*. **2012**, *24* (10), 1930-1936.

2. Åhlén, M.; Jaworski, A.; Strømme, M.; Cheung, O. Selective Adsorption of CO_2 and SF_6 on Mixed-linker ZIF-7–8s: The Effect of Linker Substitution on Uptake Capacity and Kinetics. *Chemical Engineering Journal*. **2021**, 422, 120117.

3. Sivarajah, I. Atomic Force Microscopy: General Principles and Applications. *Azo Optics*. Dec 8, **2021**.

4. Ekanayake, A. B.; Tiba, A. A.; MacGillivray, L. R.; Tivanski, A. V. Crystal Size-dependent Framework Flexibility of a Prototypical Metal Organic Framework is Related to Metal Content: Zeolitic Imidazolate Framework-7. *Mater. Adv.* **2024**, 5 (22), 9055-9060.

5. Tan, J. C.; Bennett, T. D.; Cheetham, A. K. Chemical Structure, Network Topology, and Porosity Effects on the Mechanical Properties of Zeolitic Imidazolate Frameworks. *Proc Natl Acad Sci USA*. **2010,** 107 (22), 9938-9943.

IOWA

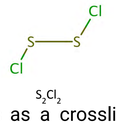
Effects of Disulfide and Monosulfide Bonds on Selectivity in Polydicyclopentadiene (pDCPD) Membranes

Allen Ma[1], Patrick Zhang[2], Jett Tjaden[3], BS, Saurav Katuwal[3], MS, Ned B. Bowden[3], PhD

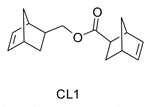
[1]Princeton International School of Mathematics and Science, NJ, [2]Head-Royce School, CA, [3]Department of Chemistry, University of Iowa, IA

Introduction

- Fatty acid separation is essential in biofuel and vegetable oil production
- Traditional separation methods such as distillation and recrystallization consume large amounts of energy or are restricted to specific molecules[1]
- Membranes can separate molecules at room temperature, are cheap to produce, and can be engineered to separate specific chemicals
- Dicyclopentadiene (DCPD) is an organic molecule that undergoes ring opening metathesis polymerization (ROMP) to form polydicyclopentadiene (pDCPD)
- pDCPD is durable and can be swelled by Dichloromethane (DCM) without sustaining permanent damage
- pDCPD acts as a good starting material to insert cross-linking agents such as S_2Cl_2 and crosslinker 1 (CL1)



S_2Cl_2



CL1

S_2Cl_2 acts as a crosslinker by inserting disulfide bonds into existing pDCPD linkages. CL1 undergoes a similar ROMP mechanism as DCPD, providing a higher degree of cross-linking.

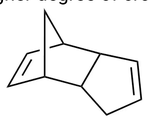


Figure 1. DCPD
Source: Sigma-Aldrich

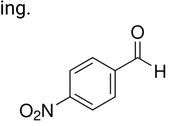


Figure 2. PNB
Source: PubChem

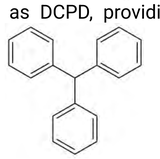


Figure 3. TPM
Source: Wikipedia

Research Question

What effect does crosslinking a pDCPD membrane with di- and monosulfur bonds have on its separation of Paranitrobenzaldehyde from triphenylmethane?

Methods

pDCPD membranes were synthesized by combining DCPD monomer and catalyst in a 5000:1 ratio and pressed between two glass plates. Selected membranes were measured to be approximately 50 – 80 µm thick.

pDCPD membranes cross-linked with CL1 were swelled in DCM for 30 minutes before S_2Cl_2 was added with 20 mL DCM and stirred on an orbital shaker for 30 minutes.

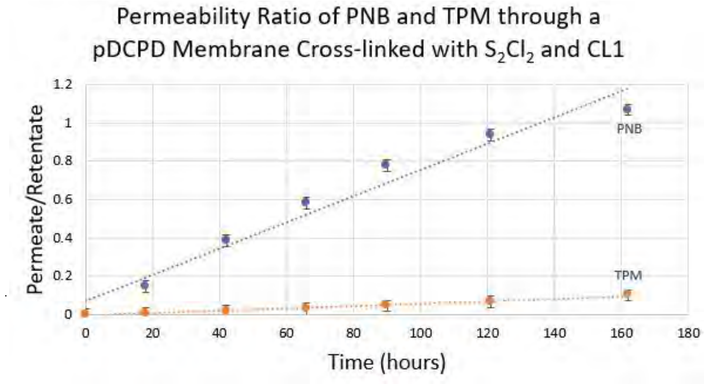
An alternate experiment was conducted with a similar procedure in which S_2Cl_2 in 19 mL of DCM and 1 mL of DMF was added to a pDCPD membrane.

Two bulbs were affixed together by two O-rings and a clamp, with the membrane placed in between the rings. The retentate, a 1:1 ratio of PNB and TPM dissolved in 30 mL of DCM, was added to one bulb, while 30 mL of DCM was added to the other bulb as the permeate.

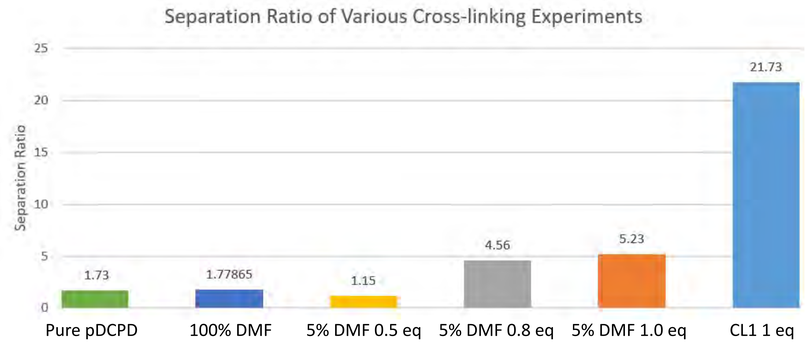
1 mL aliquots were extracted from each side every 24 hours and were analyzed using ^{1}H NMR Spectroscopy with C18 methyl stearate standard.



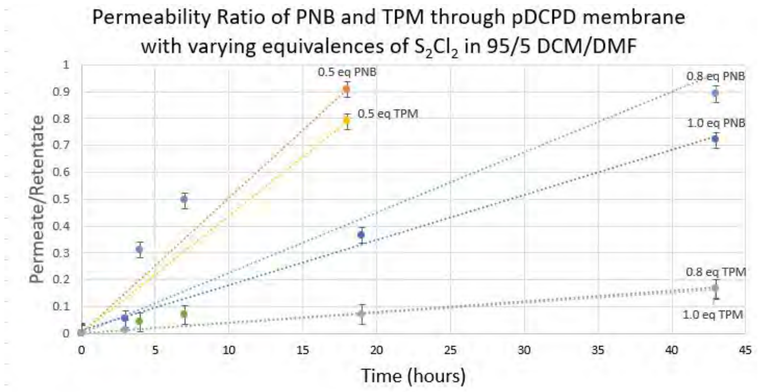
Results & Discussion



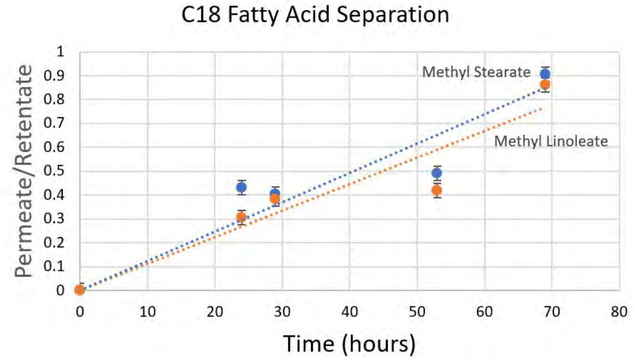
- pDCPD membrane cross-linked with S_2Cl_2 and CL1 achieved maximum separation ratio of **21.7**
- Flux of PNB slowed down once its P/R ratio surpassed 0.5
- Separation ratio reduced over time



- pDCPD membrane crosslinked with 0.5 eq S_2Cl_2 in 5% DMF achieved the worst separation
- pDCPD membrane crosslinked with CL1 and S_2Cl_2 in DCM achieved the best separation
- Excessive DMF or too little S_2Cl_2 resulted in poor separation ratios



- pDCPD membrane cross-linked with S_2Cl_2 in 5% DMF achieved maximum separation ratio of **5.23**
- 0.5 eq was significantly worse than 0.8 eq and 1.0 eq S_2Cl_2



- C18 methyl stearate and C18 Omega-6 methyl linoleate separation was attempted
- pDCPD membrane cross-linked with S_2Cl_2 and CL1 achieved maximum separation ratio of 1.4 times
- The molecules were too similar in size to be separated

Conclusion

pDCPD membranes cross-linked with CL1 and S_2Cl_2 were able to separate PNB and TPM at a maximum separation of 21.7 times. Membranes cross-linked with S_2Cl_2 in 19 mL of DCM and 1 mL of DMF separated PNB and TPM by a maximum ratio of 5.23. TPM has a larger surface area than PNB, and thus permeated through the membrane at a slower rate. The cross-linked pDCPD membranes were not able to separate fatty acids effectively.

Future Works

Investigate the degree of cross-linking in synthesized pDCPD membranes, and determine whether S_2Cl_2 and CL1 coexist or one dominates the other in cross-linking. Design 10 µm thick pDCPD polymer membranes cross-linked with monosulfur bonds and CL1 for pressure application to increase flux.

Acknowledgements

Thank you to Jett Tjaden, Patrick Zhang, Saurav Katuwal, the Bowden Lab, and Professor Bowden for your valuable support and guidance throughout my time here. Thank you to SSTP for providing me an opportunity to conduct this research.

References

(1) Gilmer, C. M., & Bowden, N. B. (2018). Reactive epoxy nanofiltration membranes with disulfide bonds for the separation of multicomponent chemical mixtures. *ACS Omega*, *3*(8), 10216–10224. https://doi.org/10.1021/acsomega.8b00931

(2) Gilmer, C. M., Zvokel, C., Vick, A., & Bowden, N. B. (2017). Separation of saturated fatty acids and fatty acid methyl esters with epoxy nanofiltration membranes. *RSC Advances*, *7*(88), 55626–55632. https://doi.org/10.1039/C7RA11326F

(3) Long, T. R., Gupta, A., Miller, A. L., Rethwisch, D. G., & Bowden, N. B. (2011). Selective flux of organic liquids and solids using nanoporous membranes of polydicyclopentadiene. *Journal of Materials Chemistry*, *21*(37), 14265–14276. https://doi.org/10.1039/C1JM11929G

(4) Marchetti, P., Jimenez Solomon, M. F., Szekely, G., & Livingston, A. G. (2014). Molecular separation with organic solvent nanofiltration: A critical review. *Chemical Reviews*, *114*(21), 10735–10806. https://doi.org/10.1021/cr5001616

(5) Marchetti, P., Peeva, L. G., & Livingston, A. G. (2017). The selectivity challenge in organic solvent nanofiltration: Membrane and process solutions. *Annual Review of Chemical and Biomolecular Engineering*, *8*(1), 473–497. https://doi.org/10.1146/annurev-chembioeng-060816-101344

The Phonetic Fingerprints of Dysarthria

Yashas Patil[1], Ethan Kutlu[2], Shawn Goodman[2], and Mili Kuruvilla-Dugdale[2]
[1]Washington High School, [2]Department of Communication Sciences and Disorders

Belin-Blank Center, College of Education

IOWA | Communication Sciences and Disorders

INTRODUCTION

- Neurodegenerative diseases often cause dysarthria, a speech movement disorder that affects all the speech subsystems (e.g., articulation).
- Dysarthria diagnosis mostly relies on a clinician's perception of speech changes, often delaying diagnosis and intervention (Muller et al., 2026)
- There are known limitations in auditory perception (Liberman et al., 1957), particularly in detecting mild dysarthria and subtle speech changes that occur with disease progression (**Figure 1**).
- An objective metric like Goodness of Pronunciation (GoP; Yeo et al., 2023) can augment listener perception by detecting subtle articulatory changes and capturing how closely a spoken phoneme matches an ideal pronunciation.
- As dysarthria worsens, patients are expected to receive higher GoP scores, particularly for phonemes requiring precise and/or complex movements.
- Analyzing GoP might be one way to expedite the diagnosis of dysarthria.

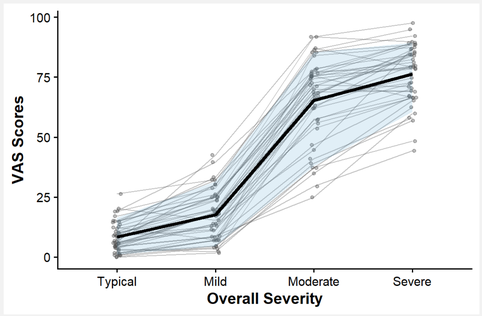


Figure 1. The shallow slope from typical to mild and moderate to severe indicates that listeners perceived little difference between these severity levels.

OBJECTIVE

Using GoP, identify phonemes that are challenging for patients with progressive dysarthria to produce to develop better diagnostic tools and models to detect milder forms of dysarthria.

METHODS

Healthy

Collected word-level speech samples of healthy and dysarthric speakers

Dysarthric

Extracted probabilities for the likelihood of the correct production for each phoneme in the word

A: Healthy Phoneme /r/ probabilities

[0.66 /r/, 0.24 /a/, 0.10 /o/]

/r/ /a/ /o/

B: Unhealthy Phoneme /r/ probabilities

[0.50 /r/, 0.26 /a/, 0.24 /o/]

Phoneme recognizer

Plotted the probability vectors at the phoneme level

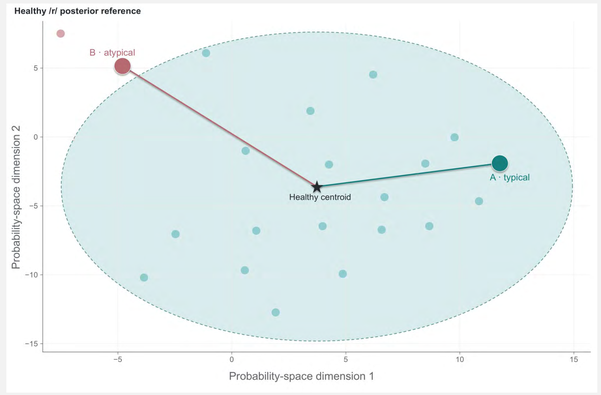


Figure 2. Healthy controls were used to define a reference range for $D_{/r/}$ rather than an ideal pronunciation, accounting for natural variation in classifying dysarthria severity by distance from that range.

Computed the healthy reference score (HRS)

Final score = mean ($D_{/r/}$, $D_{/p/}$, $D_{/b/}$, ...)

RESULTS

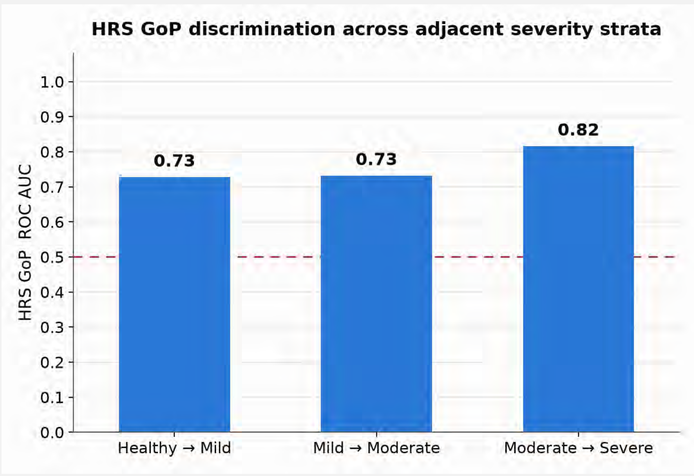


Figure 3. HRS GoP showed strong separation across all dysarthria severity levels, including mild vs. typical speech.

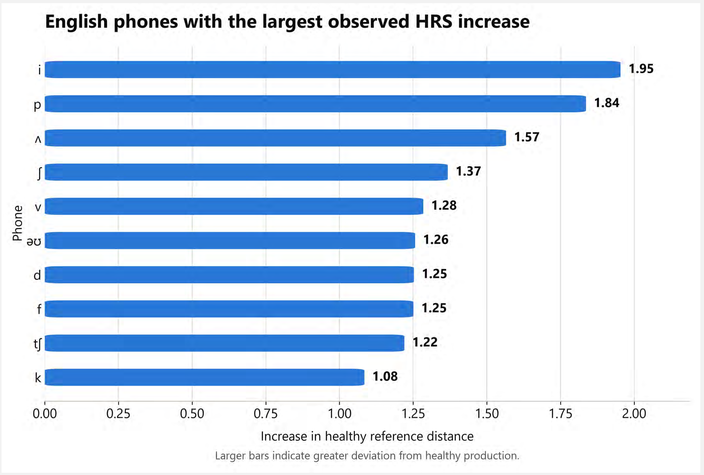


Figure 4. In our dataset, these phonemes led to the greatest increases in the HRS GoP score, indicating they are more challenging for dysarthric speakers to pronounce.

CONCLUSION

- HRS-GoP provided a framework of distance to separate healthy, mildly impaired, moderately impaired, and severely impaired speakers and potentially diagnose dysarthria using objective methods in conjunction with subjective clinical evaluation.
- The /i/ and /p/ phonemes were the hardest phonemes to produce for dysarthric speakers in our dataset.
- Linguistic differences also determine phoneme difficulty. /d/ was the most challenging in Italian

Future Directions

- Determine why some phonemes are harder than others.
- Use GoP and other related metrics to improve dysarthria test stimuli based on production difficulty.
- Compare HRS-GoP to a clinician's judgement.

ACKNOWLEDGMENTS

Thank you to everyone in the Communication Sciences and Disorders department who mentored me, especially Dr. Kuruvilla-Dugdale, Dr. Kutlu, and Dr. Goodman. I've grown a lot and learned so much thanks to all of you! Special thanks to Kayden Broking, Deepthi Crasta, Aubrey Haney, Katie Hennesy, and Piper Steburg from the SPeaK Lab for supporting me throughout these 5 weeks. Lastly, thank you to the Belin-Blank Center and all the RAs and mentors at SSTP.

Dysarthria can be detected by **measuring** how far a speaker's **phoneme patterns** deviate from the **healthy range**, even when their speech is perceived as typical.

REFERENCES

How Heat Influences Human Mobility: A Comparative Analysis of Alternative Heat-Stress and Mobility Indices

Sriaditya Pendyala[1], Caglar Koylu, PhD[2]

[1]The Quarry Lane School, Dublin, CA; [2]School of Earth, Environment, and Sustainability, University of Iowa, Iowa City, IA

Introduction

- Due to climate change, higher temperatures are becoming more common across densely populated metropolitan statistical areas (MSAs) in the United States[7].
- Extreme heat changes the spatial pattern of human movement[1,8]; these changes in mobility are broadly measured via flows, activity spaces, entropy, and spatial clustering[7,5,4].
- "Feels like" temperature is captured through several such heat-stress indices such as the Heat Index (HI), Wet-Bulb-Globe-Temperature (WBGT), and Universal Thermal Climate Index (UTCI)[7].
- Current literature is split on the type of heat-stress index to use; the United States uses HI, Europe uses UTCI[7], and militaries & government agencies use WBGT.
- Due to the disparities between these indices and their usage[2], it is important to understand how they differ with respect to measuring mobility.

Objectives

- Assess how extreme heat restructures the types of flows between tracts using mobility metrics.
- Examine the magnitude and direction of change in mobility based on the choice of heat stress index.
- Understand the extent to which different heat indices are qualitatively and quantitatively similar.

Data Collection

- Data was spatially and temporally bound to May 1 - Sep 30 of 2019 (153 days) and Maricopa County (895 census tracts)
- Aggregated Safegraph mobility data at the daily census tract level was collected[8]
  - All flows where the origin or destination is Maricopa County were included
  - Metrics are calculated on each tract-day
- Heat-stress index data was collected at the hourly census tract level[7]
  - Data was processed into a daily max for each tract-day
  - Heat-stress indices that produced unattainable temperatures were adjusted to the 95th percentile of the respective index.

Method A: Mapping Heat Stress Indices

- The chosen heat stress indices correlate very strongly with each other due to the similarity in which they represent "feels like" temperature, and the geographical location Phoenix, Arizona.

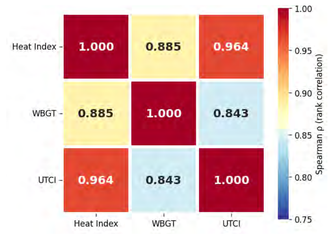


Fig 1. Spearman p for heat indices on daily-max from May –Sep 30 2019

- The distribution shows us monthly variations in heat.
- Fig 3: Strong spatial clustering between maps.

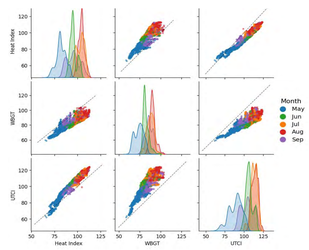


Fig 2. Scattermplot matrix of heat stress indices on each tract-day and their corresponding distributions. Heat depicted temporally.

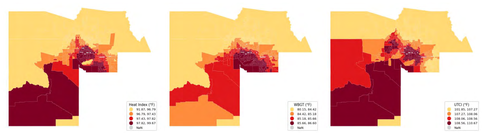


Fig 3. Choropleth maps of Maricopa County at tract level; left to right: HI, WBGT, UTCI; 153 day period-median quartiles. Heat depicted spatially.

Method B: Measuring Mobility Metrics

- Mobility can be visualized via traces of flows between tracts.

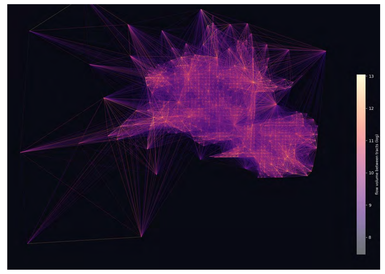


Fig 4. Top 20% Flows by Volume in Maricopa County. Edges Represent Flows log-scaled. Nodes Represent Centroids of Tracts

- Metrics that capture spatial nuances can be calculated with flow data; some key metrics we will observe are:
  - *Weighted Clustering Coefficient (WCC)*: gives the strength and cohesion of neighboring nodes

$$\mathrm{WCC}_i^w = \frac{1}{s_i(k_i-1)} \sum_{j,h} \frac{(w_{ij}+w_{ih})}{2} a_{ij}a_{ih}a_{jh}$$

  - *In-degree & Out-degree:* gives the number of connected tracts based on inflow and outflow.

$$Degree_i = \sum_{j \neq i} a_{ij}$$

  - *Inflow, Outflow, Within-flow:* gives the volume of flows into, out of, and within a tract

$$Inflow_i = \sum_{j \neq i}^{n} flow_{ji} \qquad Outflow_i = \sum_{j \neq i}^{n} flow_{ij} \qquad Withinflow_i = flow_{ii}$$

  - Outflow Weighted Radius of Gyration (OWRg): is the typical travel radius weighted for the volume of flows.

$$OWR_g(i) = \sqrt{\frac{\sum_{j=1}^{n} (d_j - l_{wc})^2}{n}}$$

Method C: Fixed Effects Model

$$y_{it} = \beta \cdot (heat\ index)_i + \alpha_i + \varepsilon_{it} + \gamma_{dow(t)}$$

- y is some metric on tract *i* on day *t*
- β is how much some metric (adjusted to a % of metric's typical value in Fig 5.) changes per 1 SD (adjusted to per 10°F) of change in some index.
- α is the intercept for tract *i*
- ε is the error on tract *i* on day *t*
- γ is the day-of-the-week pattern that can be controlled

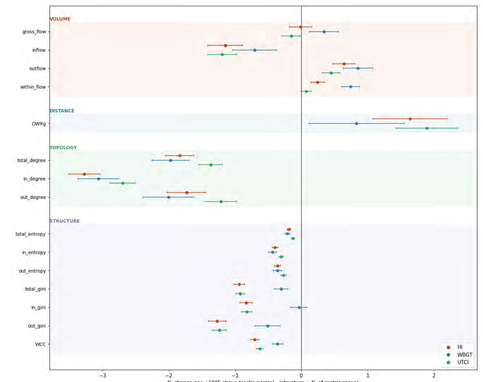


Fig 5. The % change from a tract's typical value for every +10°F on an index captured in a 95% CI for β where tract and day-of-week are Fixed Effects. Phoenix MSA 2019 May 1 to Sep 30.

- We use a fixed effects model to account for implicit variability within the tract and index.
- We aggregate the demeaned data for average y and average heat-index and run regressions for each tract-metric pair.
- The regression produces a 95% CI for β for each tract metric pair.
- The error epsilon is negligible

Spatial & Temporal Analyses of Divergences in Heat Indices

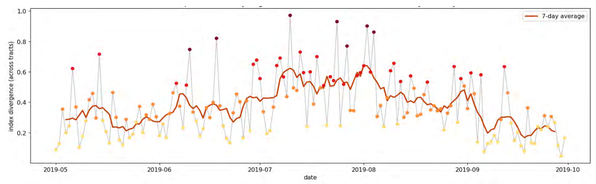


Fig 7. Divergence vs Time; Smoothed 7 Day Line Graph in Red

- The divergence increases most during the monsoon season in Phoenix due to greater variability in meteorological conditions
- Divergence is calculated using an average of Spearman's p pairs

$$Divergence = 1 - \frac{\rho^{HI,WBGT} + \rho^{HI,UTCI} + \rho^{UTCI,WBGT}}{3}$$

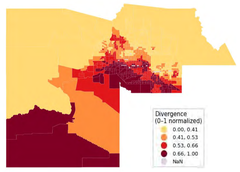


Fig 6. Index Divergence Per Tract; Min-Max Normalized and Split into Quartiles

- Divergence is greatest in urban tracts due to high aridity and lower elevation.

Results & Conclusion

- Studies that use UTCI will have consistently smaller magnitude changes in mobility compared to studies that use HI; European studies would measure smaller changes in mobility compared to American studies.
- Distance traveled from home increases due to a decreasing volume of shorter inter-tract and within-tract flows
- Communities will become less tightly knit; flows will concentrate between fewer denser urban areas due to decreasing flows between outer tracts.
- Due to how similar the 3 indices are, they perform nearly identically on each metric with a few exceptions.
  - Indices perform the same for measuring the volume of flows
  - Index choice matters most for measuring short distance flows and the directional-frequency of flows
- WBGT consistently separates itself from UTCI and HI which shows that it is the least similar to UTCI and HI; metrics calculated with WBGT would produce noticeably different results compared to HI & UTCI.

Future Works

- Observe how index-choice matters over other MSAs that aren't under constant heat-stress
- Assess how distinct meteorological factors (dry air-temperature, humidity, wind, etc...) individually contribute to variations in human mobility.

Selected References

1. Batur, Alhassan, V. O., Chester, M. V., Polzin, S. E., Chen, C., Bhat, C. R., & Pendyala, R. M. (2024). Understanding how extreme heat impacts human activity-mobility and time-use patterns. *Transportation Research Part D Transport and Environment*, *136*, 104431 104431. https://doi.org/10.1016/j.trd.2024.104431
2. Kwon, H., & Koylu, C. (2026). How we measure mobility matters: Comparing mobility change metrics and their associations with social vulnerability during the covid-19 pandemic. *Annals of the American Association of Geographers*, *116*(3), 697–719. https://doi.org/10.1080/24694452.2025.2580207
3. L. Liu, J. Wang, Y. Zhang, F. Chen. (2024). Recent advances in green synthesis of bioactive flavonoids from renewable sources. *Current Opinion in Green and Sustainable Chemistry*, *41*, 100681. https://doi.org/10.1016/j.cogsc.2024.100681
4. Mobility responses to snowfall in the greater Toronto area. (n.d.-a). *Findings*. Retrieved July 20, 2026, from https://findingspress.org/article/162965-mobility-responses-to-snowfall-in-the-greater-toronto-area
5. Moro, E., Calacci, D., Dong, X., & Pentland, A. (2021). Mobility patterns are associated with experienced income segregation in large US cities. *Nature Communications*, *12*(1). https://doi.org/10.1038/s41467-021-24819-8
6. Rahal, R., Kong, Q., & Dogan, T. (2026). Heat stress metrics for US census tracts 1998–2020. *Sci Data*, *13*, 515. https://doi.org/10.1038/s41597-026-06909-w
7. Renninger, A., & Cabrera, C. (2026). Extreme heat reduces and reshapes urban mobility. *PNAS Nexus*, *5*(4). https://academic.oup.com/pnasnexus/article/5/4/pgag078/8621395
8. Kang, Y., Gao, S., Liang, Y., Li, M., Rao, J., & Kruse, J. (2020). Multiscale dynamic human mobility flow dataset in the U.S. during the covid-19 epidemic. *Scientific Data*, *7*(1). https://doi.org/10.1038/s41597-020-00734-5

The University of Iowa | Belin-Blank Center

NSD2 Expression in B Cells and Human Bone Marrow Cells

Helen Peng[1], Guiru Ma MD[2], Michelle Buckman PhD[2], Anastasiia Vasileva MD[2], Melissa L. Bates, PhD, MBA, FAPS [2, 3, 4], Michael H. Tomasson MD[2,3,5]

[1]Cedar Falls High School, Cedar Falls, IA; [2]Department of Internal Medicine, [3]Division of Hematology, Oncology, and Bone Marrow Transplantation, [4]Department of Pediatrics, [5]Health and Human Physiology, University of Iowa, Iowa City, Iowa, USA

Introduction

- Multiple myeloma (MM) is a cancer of plasma cells in the bone marrow. 15-20% of MM patient have the t(4;14) (p15;q32.3) chromosomal translocation.[1]
- This translocation causes ectopic NSD2 (also known as WHSC1 or MMSET) expression by placing it under the control of the IgH promoter.[1] NSD2 is a histone methyltransferase (HMT), which catalyzes H3K36me2. [2]
- Within t(4;14) patients, breakpoints within the NSD2 gene are associated with higher risk for MM patients.[3] Of the NSD2Δ3 and NSD2^{WT} breakpoints, NSD2Δ3 breakpoint is within the NSD2 gene.[4]
- NSD2Δ3 is truncated and does not contain the N-terminus or PWWP domain[4]
- A large majority of previous studies analyze the effects of NSD2 in cell lines, not primary cells.
- Clinical trials regarding NSD2 in multiple myeloma are already occurring,[5] making the expression of NSD2 in primary cells extremely important.

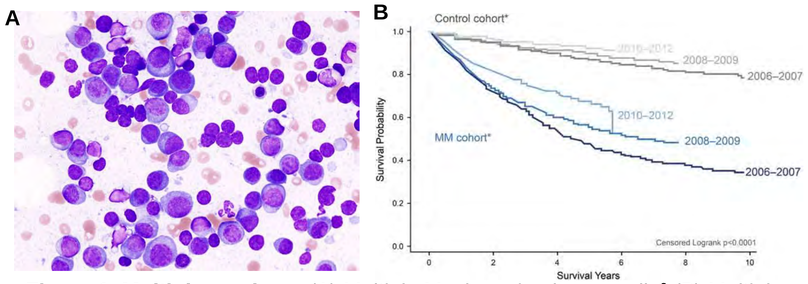


Figure 1. Multiple myeloma (A) Multiple Myeloma in plasma cells[6] (B) Multiple myeloma survival in different cohorts from 2006-2012[7]

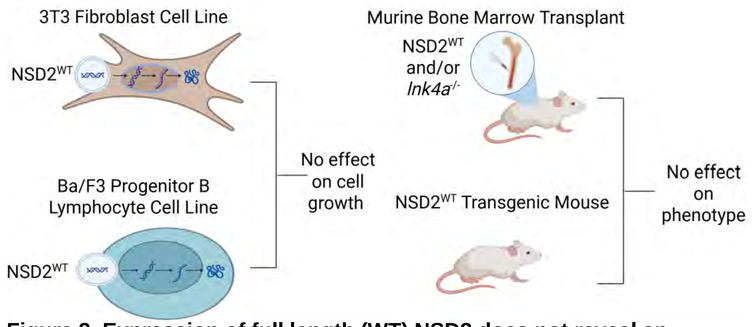


Figure 2. Expression of full length (WT) NSD2 does not reveal an oncogenic function. [8]

Central Question

What is the role of NSD2 in primary cells?

Methods

Step 1. Viral transduction of Mice with NSD2^{WT}, NSD2Δ3, and empty vector[4]

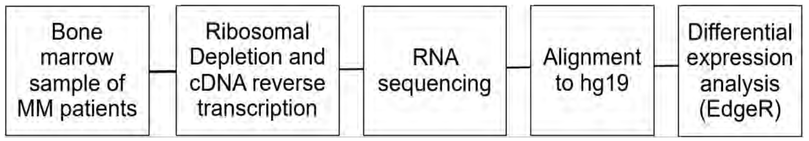
1. C57BL/6 mice
2. B cells isolation
3. Stimulate with LPS+IL-4
4. Virus transduction with empty vector, NSD2^{WT} and NSD2Δ3



Figure 3. Methods of viral transduction[4]

Methods

A Step 2. Sequencing and analysis of bone marrow RNA of MM patients[4]



B Step 3. Analysis of Human Bone Marrow Atlas v.2.0[9]

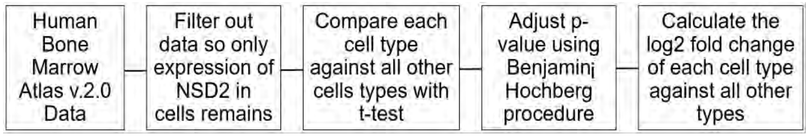


Figure 4. Methods of MM patient data and bone marrow atlas (A)MM patient bone marrow methods (B) Human bone marrow atlas analysis methods

Results

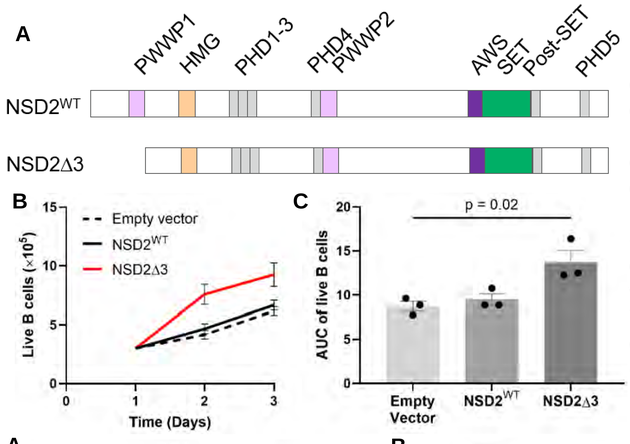


Figure 5. NSD2Δ3 increases oncogenic effects (A) Representative construct[4] (B) Cell growth[4] (C) Area under the curve (AUC) and compared by one-way ANOVA with Tukey post hoc comparisons (Empty vector vs NSD2Δ3, p=0.02).[4]

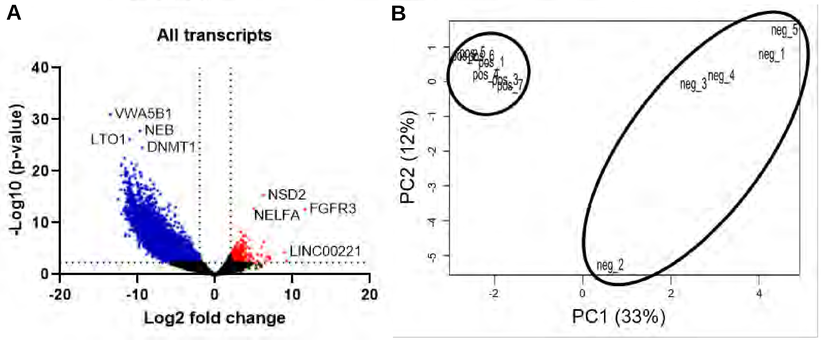


Figure 6. Analysis of t(4;14) MM patient data reveals NSD2 is highly expressed in t(4;14)+ MM patients and t(4;14)+ MM is associated with down regulation of transcripts (A) Volcano plot shows gene expression change in t(4;14)+ MM patients compared to t(4;14)- patients.[4] (B) Principal component analysis of MM patient data shows that t(4;14)+ MM patients have strong correlation with each other compared to t(4;14)- MM patients. [4]

Results

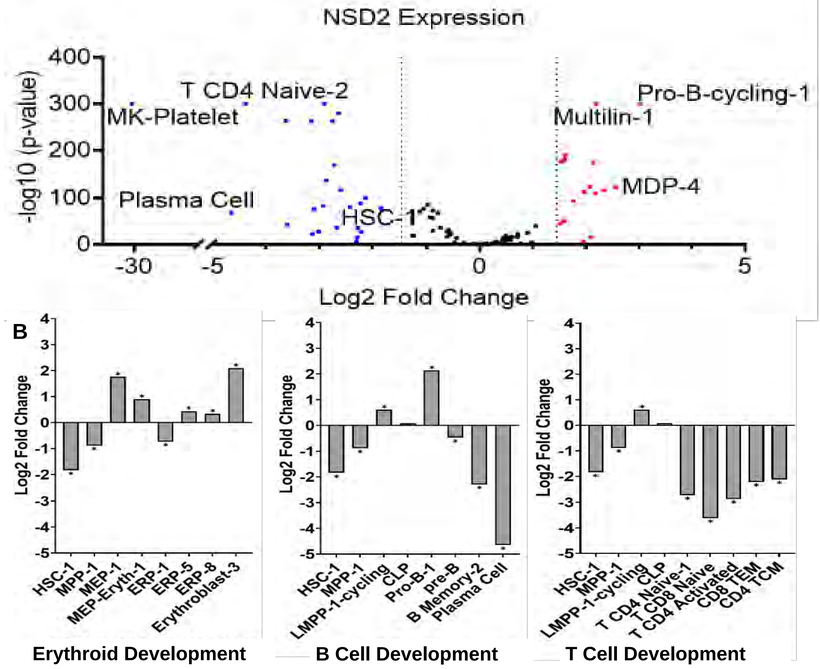


Figure 7. Expression of NSD2 within human bone marrow atlas (A) Volcano plot of bone marrow atlas cells shows NSD2 expression in human bone marrow atlas. Each point signifies a cell type, with p-value showing significance of T-test results. (B) Expression of NSD2 in B cell development (C) Expression of NSD2 in erythroid cell development (D) Expression of NSD2 in T cell development

Conclusions

- NSD2Δ3 expresses more oncogenic effects than NSD2^{WT}
- Multiple myeloma patients with t(4;14) show strong downregulation of transcripts, compared to upregulation.
- In human bone marrow cells, NSD2 shows low expression in HSC, high expression in progenitor cells, low expression within fully developed T and B cells, and high expression in erythroblast-3 cells.

Future Directions

- Further investigation is required regarding the t(4;14) ribosomal depletion data to see whether the reads are exonic, intronic, or intergenic. This will provide insight into what specifically is being upregulated
- Analysis of different library preparation methods and their impact on gene expression results

Acknowledgements

My thanks to Dr. Tomasson, Dr. Bates, Dr. Vasileva, Dr. Buckman and Dr. Ma for all the guidance, support, and mentorship. Thank you to SSTP for this amazing opportunity. Figures were made using BioRender and Graphpad Prism

References

Two-Stage Classifier of Non-Small-Cell Lung Cancer Subtypes Based on CT Radiomics Features

Shreya Polavarapu[1]; Fahim Zaman, PhD[2]; Xiaodong Wu, PhD[2,3]

[1]Northview High School, GA; [2]Department of Electrical & Computer Engineering, University of Iowa; [3]Department of Radiation Oncology, University of Iowa

Introduction

- Lung cancer is the leading cause of cancer death in the U.S., with over 600,000 people living with a diagnosis and around 229,410 new cases per year[1].
- Five-year survival has climbed to 29.5%, largely due to low-dose CT screening and targeted therapy[1].
- NSCLC subtype currently requires an invasive tissue biopsy and manual pathological, which leads to significant delays & missing reports[2,3].
- Such delays measurably affect treatment paths and outcomes, impacting quality of life[3].
- Deep learning models trained directly on CT images and machine learning models trained on extracted radiomics features have both been investigated as a non-invasive NSCLC subtype classification method[4,5].
- Radiomics-based models produce quantifiable image features, making them interpretable in medical settings[5].
- Khodabakhshi et al. showed CT radiomics features could predict NSCLC subtype from a single-cohort dataset, but adenocarcinoma was severely underrepresented and served as the reference category in their multinomial model[6,7].

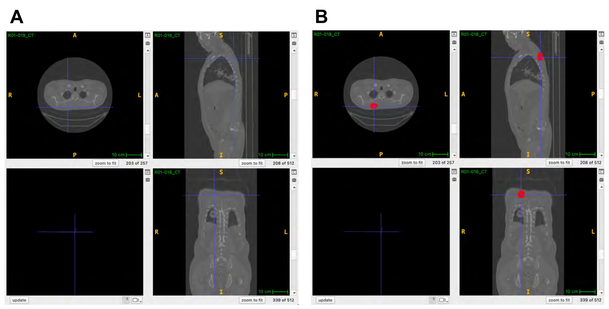


Figure 1. Representative CT Imaging and ROI Segmentation. (a) Axial, coronal, and sagittal views of an unannotated 3D CT volume for Case ID R01-018 (Squamous Cell Carcinoma). **(b)** Corresponding views with the lung region-of-interest (ROI) tumor segmentation overlaid in red.

Hypothesis

Combining multi-center CT radiomics cohorts with fold-safe, linear feature selection and a soft-blended two-stage hierarchical classifier will improve histopathological subtype classification in non-small-cell lung cancer.

Methodology

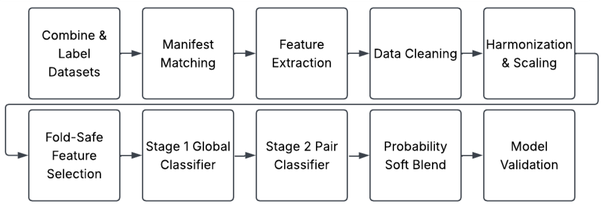


Figure 2. Two-Stage Radiomic Classification Pipeline. Overview of the two-stage machine learning framework for non-small-cell lung cancer histological subtyping, detailing data assembly, preprocessing, fold-safe feature selection, classification, and model validation.

1. **Combine & Label Datasets:** Combined NSCLC-Radiomics[7] and NSCLC-Radiogenomics[8] collections from TCIA and mapped free-text pathology notes into four standardized histopathological subtype classes.
2. **Manifest Matching:** Matched labeled patient records against disk inventory for available 3D CT volumes and lung ROI segmentation masks to retain 513 out of 591 patients.
3. **Feature Extraction:** Extracted 1,781 PyRadiomics features per patient across Original, Wavelet, and Laplacian of Gaussian filters at isotropic 1 x 1 x 1 mm resolution, retaining 455 patients after removing failed extractions.
4. **Data Cleaning:** Applied numeric type coercion, deleted all NaN or zero-variance columns, and performed median imputation on remaining missing values.
5. **Harmonization and Scaling:** Corrected inter-cohort scanner variations using ComBat harmonization with cohort source set as batch variable and histology set as protected covariate, followed by StandardScaler normalization.
6. **Fold-Safe Feature Selection:** Executed embedded L1-logistic regression and high-correlation pruning ($|r| > 0.85$) strictly inside cross-validation folds using training data only to prevent data leakage.
7. **Stage 1 Global Classifier:** Trained a class-weighted balanced multinomial logistic regression model on 15 globally-selected features to generate a baseline 4-class probability distribution.
8. **Stage 2 Pair Classifier:** Trained six dedicated RBF-SVM expert classifiers on pair-specific feature subsets ranked by ExtraTrees to resolve subtle distinctions between subtype pairs.
9. **Probability Soft Blend:** Blended probabilities between expert model output and Stage 1 model output at a fixed weight alpha = 0.50 when Stage 1 top two candidate classes matched an expert pair.
10. **Model Validation:** Evaluated performance using a 5-split x 10-repeat Stratified Cross-Validation scheme totaling 50 folds, calculating final metrics once over pooled out-of-fold predictions.

Results

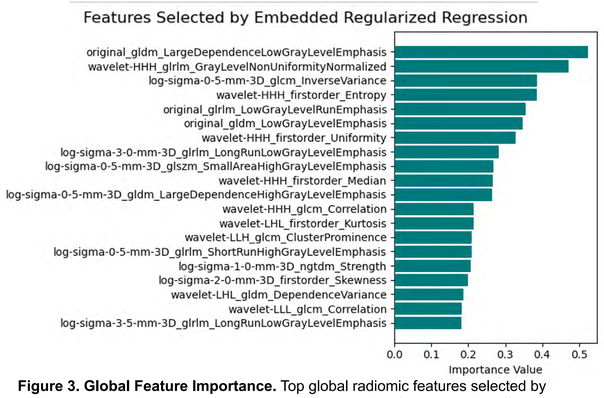


Figure 3. Global Feature Importance. Top global radiomic features selected by embedded L_1-regularized regression, ranked by absolute fitted model coefficient magnitude in the Stage 1 baseline classifier.

Subtype	Precision	Sensitivity	F1-Score	Specificity	Accuracy	AUC (One vs. Rest)
NOS	0.846	0.894	0.870	0.979	0.969	0.919
Adenocarcinoma	0.824	0.781	0.802	0.922	0.877	0.864
Squamous	0.805	0.825	0.815	0.891	0.867	0.884
Large-Cell	0.926	0.932	0.929	0.980	0.970	0.954
Average	0.850	0.858	0.854	0.943	0.921	0.905

Figure 5. Subtype Performance Metrics. Out-of-fold performance summary detailing precision, sensitivity, F_1-score, specificity, accuracy, and One vs. Rest AUC across individual subtypes alongside the overall average.

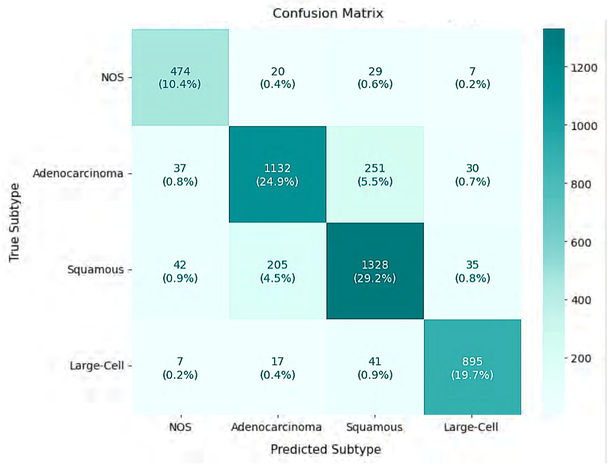


Figure 4. Multi-Class Confusion Matrix. Pooled out-of-fold confusion matrix across all 50 cross-validation folds ($N = 4{,}550$ total predictions across 455 patients and 10 repeats) demonstrating classification distribution across the four subtypes.

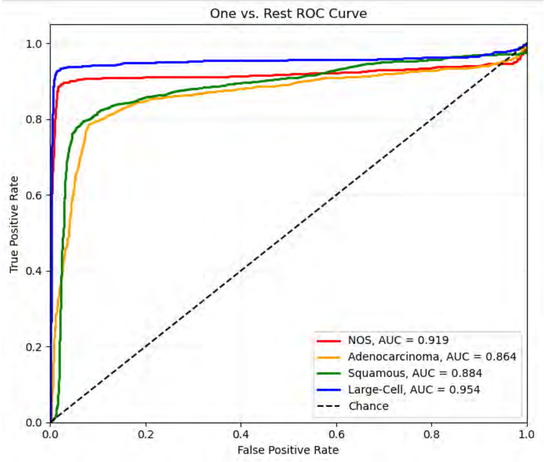


Figure 6. Receiver Operating Characteristic (ROC) Curves. Out-of-fold average and subtype-specific One-vs-Rest ROC curves, with class-specific AUC values detailed in the lower-right legend.

Discussion

- Surpassed baseline across all reported metric averages: precision (0.710 to 0.850), sensitivity (0.703 to 0.858), F1-score (0.706 to 0.854), and specificity (0.906 to 0.943), with an average ROC-AUC of 0.905 achieved.
- Evaluated accuracy using One vs. Rest, achieving an average binary accuracy of 0.921 across all four subtypes - outperforming the baseline's single-class reference approach by reflecting multi-class balance without majority-class bias.
- Confusion between adenocarcinoma and squamous cell carcinoma remained the primary source of error, with adenocarcinoma recording the lowest sensitivity (0.781) among the four subtypes.
- Findings aligned with prior literature confirming that gray-level texture heterogeneity features serve as the primary subtype indicators over shape or simple intensity statistics.
- Prevented optimistic performance estimates caused by feature-selection leakage in baseline procedures by refitting feature selection strictly on training partitions across 50 cross-validation folds.
- Applied ComBat location-scale corrections to eliminate linear inter-scanner batch effects prior to downstream linear classification, noting that non-linear scanner differences remain an area for future extension.

Conclusion

The results supported the hypothesis. Average precision, sensitivity, F1-score, and ROC-AUC all exceeded the corresponding baseline values. The adenocarcinoma class, previously underrepresented, achieved out-of-fold metrics comparable to the other three subtypes while preserving model interpretability and avoiding the feature-selection leakage pattern identified in the baseline study's methodology.

Future Directions

- Improve pair distinction between adenocarcinoma and squamous cell carcinoma.
- Increase dataset size to improve feature selection and subtype classification.
- Introduce clinical features such as sex, ethnicity, smoking history, and location of tumor, as they are highly correlated with certain subtypes[9,10].
- Expand the amount of imaging sources to improve generalizability.
- Find an alternative to ComBat harmonization that removes both linear and nonlinear scanner artifacts.
- Expand to low-dose CT scans while taking into consideration the impact of Gaussian and Poisson noise on extracted radiomics features, since patients at high risk for lung cancer are screened with low-dose CT[11].

Acknowledgements

I would like to thank Professor Xiaodong Wu, Dr. Fahim Zaman, and PhD student Tarun Roy for their incredible guidance throughout this project. I also extend my sincere gratitude to the Takotsubo research team for providing valuable medical and statistical insights and for offering a firsthand look into inter-lab collaboration. Finally, I would like to thank the Belin-Blank Center and the Iowa Secondary Student Training Program for making this wonderful opportunity possible.

References

Scan the QR Code to view the references:

Does Interpreter Use Affect Neuropsychological Assessment in Monolingual Asian Language Speakers?

Qiao, Sophie[1,3], Martin, Ashby, Ph.D[1]., Tranel, Daniel, Ph.D. [1,2]

[1]Department of Neurology, [2]Department of Psychological and Brain Sciences, University of Iowa, Iowa City, IA, [3] Concord Academy, Concord, MA

Discussion

Limited English Proficiency (LEP) population, **5.4 million** of whom are Asian, makes up 9% of the U.S. population.[4] In neuropsychological testing, LEP patients engage in a **three-way interaction** between them, clinician, and interpreter. [2] [3]

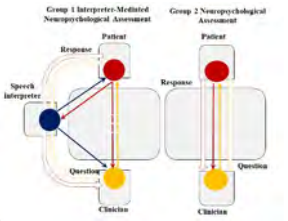


Figure 1 Dotted arrows represent vocalized speech communication, solid arrows represent nonvocal communications (gestures, etc) three dashes represents that nonvocal communications are not received at the same time as verbal communication[2]

Existing research on Spanish-speaking LEP patients associated interpreter-assisted testing with **lower performance, greater variability in, and less definitive interpretations of assessment results**. However, no studies have examined **effect of interpreter use in Asian LEP patients**.[2]

Hypothesis

- Asian-language-speaking LEP patients tested with a speech interpreter will demonstrate **lower test performance** and **higher score variability** on neuropsychological assessments,
- Results will be further impacted by **ad hoc interpretation**

Methods & Materials

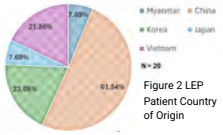


Figure 2 LEP Patient Country of Origin



Figure 3 Patient Matching Documentation

Asian Language-speaking LEP patients tested with the use of a speech interpreter (n=20)

Matched 1:2

Comparison Group of fluent English patients with similar demographics and diagnostics (n=40)

Analyze Clinical Impressions and Test Scores

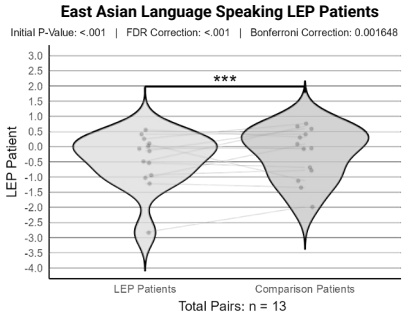
Results - East Asian Language Speaking LEP Patients

East Asian Language Speaking LEP Patients One Tailed t-test and F-test Results

Analysis Type	LEP Patient Mean (SD)	Comparison Group Mean (SD)	t-value	Initial p-value	FDR Correction	Bonferroni Correction	Cohen's d	F-test	p-value
Weighted (By Test Proportion)	-0.17973 (11.97)	-0.09279 (13.45)	-1.014	<.001	<.001	0.00165	-0.281	1.263	0.220
Unweighted (equal pair comparisons)	-0.45 (0.91)	-0.24 (0.86)	-1.734	<.001	<.001	0.00165	-0.481	1.102	0.208

East Asian Language & Vietnamese Speaking LEP Patients One Tailed t-test and F-test Results

Analysis Type	LEP Patient Mean (SD)	Comparison Group Mean (SD)	t-value	Initial p-value	FDR Correction	Bonferroni Correction	Cohen's d	F-test	p-value
Weighted (By Test Proportion)	-0.19796 (15.07)	-0.06985 (12.03)	-2.858	<.001	<.001	<.001	-0.656	1.754	0.115
Unweighted (equal pair comparisons)	-0.85(0.98)	-0.33 (0.78)	-2.971	<.001	<.001	<.001	-0.682	1.547	0.147



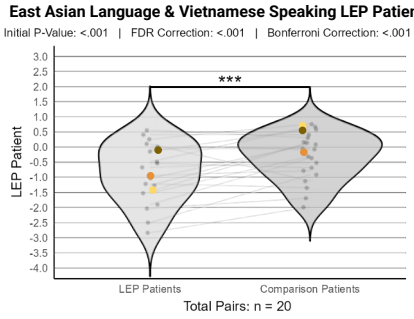


Figure 4 & 5 Violin Plot of LEP Patient Test Performance Compared to Comparison Group. Ad hoc cases marked in color

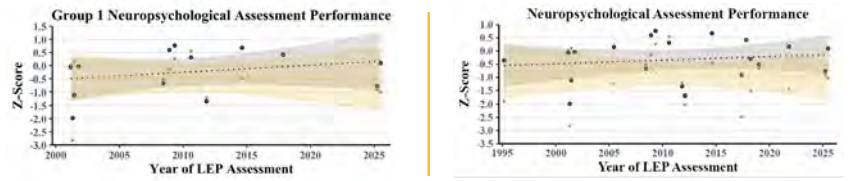


Figure 6 & 7 Scatter Plot of LEP Patient Test Performance Compared to Comparison Group (LEP: Yellow, Comparison Group: Gray)

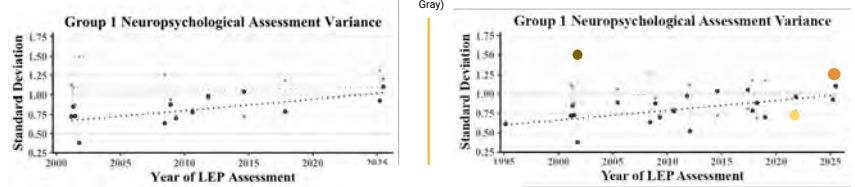


Figure 8 & 9 Scatter Plot of LEP Patient Assessment Score Variance Compared to Comparison Group (LEP: Yellow, Comparison Group: Gray) Ad hoc cases marked in color.

Patient Demographics

Patient Eduction	$\bar{x} \pm \sigma$	Range
Asian LEP Patients	13.500 ± 3.762698	[2.000000 : 20.000000]
Comparisons	13.475 ± 3.601905	[1.000000 : 20.000000]
Education Matching Quailty	0.005535896	

Patient Age	$\bar{x} \pm \sigma$	Range
Asian LEP Patients	61.405701 ± 15.449662	[27.874429 : 79.024658]
Comparisons	60.650253 ± 15.193038	[29.955023 : 87.160046]
Age Matching Quailty	0.040024602	

	Males	Females	Total
Asian LEP Patients	8	12	20
Comparisons	18	22	40
Total Cases	26	34	60

Patient's Primary Neurological Condition Asian LEP Patients	
Progressive Dementia (AD, FTD, LBD)	1
Vascular Dementia	1
Mixed Dementia	2
Mild Cognitive Impairment (MCI)	2
Cerebrovascular Accident	2
Movement Disorder (PD, MS, HD, other)	1
Traumatic Injury (PTHI, LOC, PTSD)	4
Psychiatric or Mood Disturbance(s)	5
Renal Dysfunction	1
Cerebrovascular Disease	1
Totals	20

Discussion & Conclusions

Findings are **consistent with prior research** demonstrating adverse effects of interpreter use in Spanish-speaking LEP patients and suggest that similar effects are present in Asian language-speaking LEP patients, although to varying extents[2]. **Interpreter use was associated with:**

- **significantly lower test performance** (p<.001)
- **nonsignificant trend toward greater test score variability** (p>.05)
  - small sample size (n = 20) may have limited statistical power to detect a small-to-moderate effect

Findings highlights the need for:

- **Standardized guidelines for interpreter-assisted neuropsychological assessment.**
- **Developing normative data for LEP patients.**

Acknowledgements

I would like to express gratitude to Dr. Ashby Martin and Dr. Dan Tranel for your amazing mentorship and support. I am also thankful towards everyone in the Tranel Lab and Benton Neuropsychology Clinic for providing me with wonderful opportunities to shadow and listen to valuable insights in morning meeting. I have learned so much from you all. Thank you to all the friends that supported me. Special thanks to Luke Bruderer and Emma Yang for all the conversations and great times at the lab.

References

Lab Website

Salt-Dependent Rheology of Silk Fibroin: Experimental Analysis and AI Prediction

Sunney Que[1], Alvis Yu-Wei Chen[2], Reza Amouzandeh[2], Xuan Mu[2]*

[1] Ames High School, IA; [2] Roy J. Carver Department of Biomedical Engineering, University of Iowa; Email: xuan-mu@uiowa.edu

Introduction

- Silk fibroin is a biocompatible structural protein with tunable mechanical properties, making it promising for biomedical materials[3,5]
- Conventional silk gelation methods often use chemical, thermal, or pH-based triggers that can alter protein conformation[4,5].
- Salt ions may provide a milder method for controlling silk fibroin assembly and gelation[2,4].
- **Aim: Determine how salt identity and concentration influence silk fibroin viscoelasticity and evaluate Gaussian Process Regression for trend modeling and prediction.**

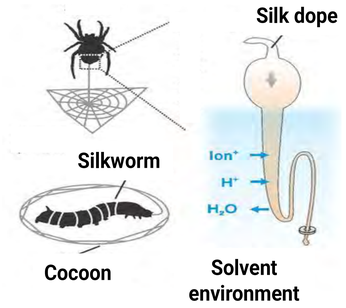
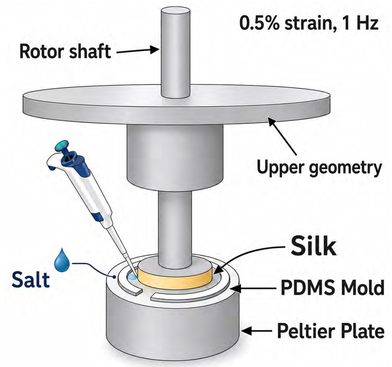


Figure 1. Ionic composition regulates protein assembly during natural silk spinning[2,4].

Methods

- Regenerated silk fibroin solution was prepared using a previously established protocol.
- Amplitude sweeps identified the linear viscoelastic region, while flow sweeps characterized the viscosity profile of each sample. Oscillatory time sweeps were then conducted under the selected conditions.
- Rheological measurements (Storage & loss modulus) with salt addition on SF were performed using a rotational rheometer and a plasma-treated PDMS mold to monitor viscoelastic behavior over time (500 sec).
- Gaussian Process Regression Model used for data analysis and curve fitting.



The original schematic was created with BioRender.com and subsequently refined using ChatGPT.

Figure 2. Schematic of the in situ rheological measurement setup.

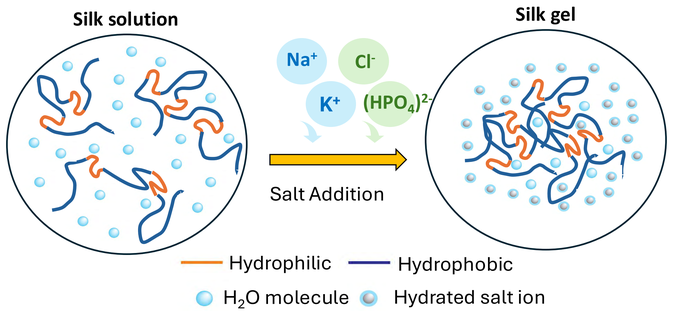


Figure 3. Schematic of macromolecular crowding in silk fibroin induced by salt ions.

Results

Salt Ion Effect

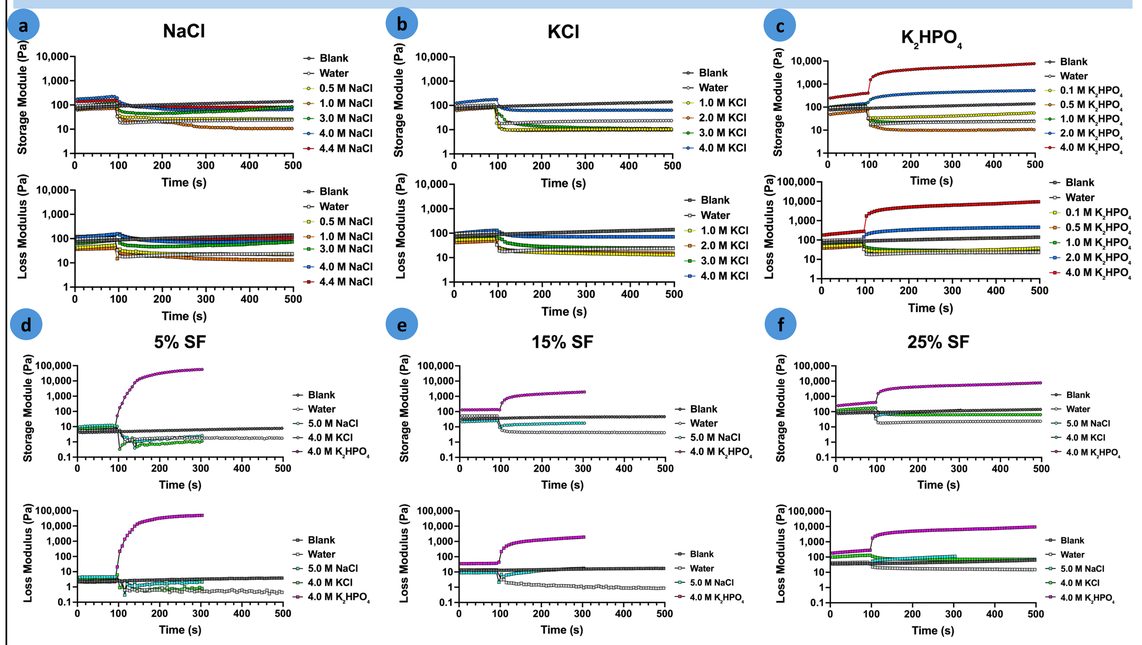


Figure 4. Effects of salt identity & concentration (a-c) and SF concentration (d-f) on the storage modulus(G') and loss modulus (G'') of silk fibroin. G' measures solid-like stiffness; G'' measures liquid-like behavior.

Gaussian Process Regression

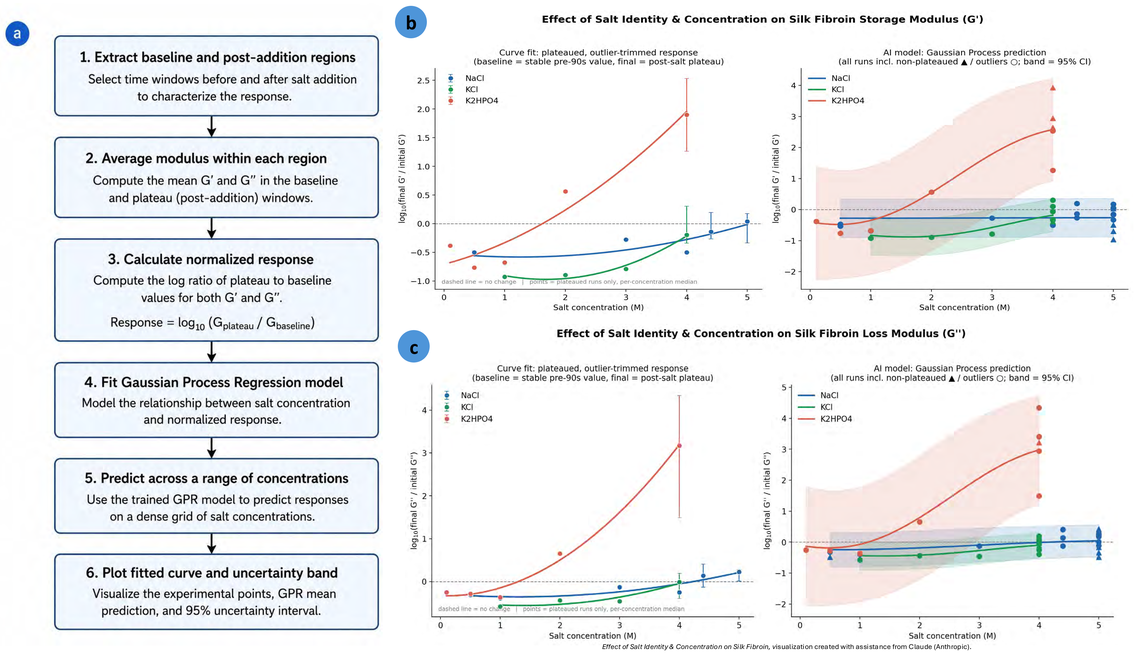


Figure 5(a-c). Gaussian Process Regression (GPR) modeled the nonlinear relationship between salt concentration and modulus[6]. Figure 5(b-c) GPR fit to plateaued, outlier-trimmed data (left) vs. full-dataset GPR with uncertainty quantification (right).

Gaussian Process Model Validation

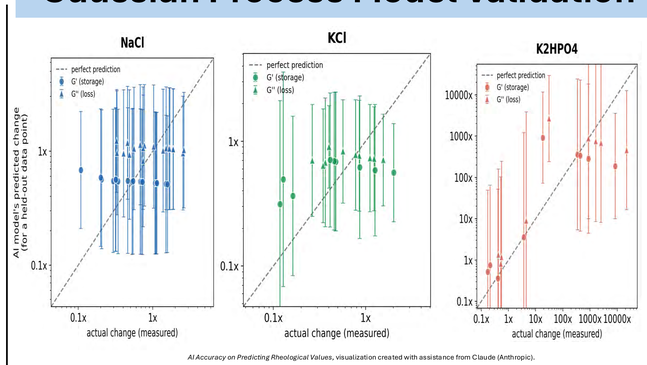


Figure 6. Model accuracy assessed via leave-one-out cross-validation.
NaCl (n=19): R^2 = −0.16, median error ×1.9.
KCl (n=10): R^2 = 0.20, median error ×1.9.
K_2HPO_4 (n=9): R^2 = 0.74, median error ×3.0.

Conclusions and Implications

- Silk fibroin rheology depends strongly on anion identity and salt concentration.
- Chloride salts had a milder effect on viscoelastic network formation, with limited differences between Na^+ and K^+.
- HPO_4^{2-} showed a clear concentration-dependent effect: low concentrations had limited effects, whereas high concentrations increased stiffness and promoted network formation.
- Gaussian Process Regression captured these ion-dependent trends and quantified prediction uncertainty.
- Ultimately, combining rheology with machine learning could support the more efficient design of silk fibroin hydrogels with tunable mechanical properties.

Acknowledgements

I want to thank Alvis Yu-Wei Chen, Reza Amouzandeh, and Dr. Xuan Mu for mentoring me during this project and giving me the opportunity to work in this lab. Also, thank you to Belin-Blank and especially Ashlee Donithan for creating this program.

References

[1] Chen, H., Liu, Y., Balabani, S., Hirayama, R., & Huang, J. (2023). Machine learning in predicting printable biomaterial formulations for direct ink writing. *Research*, *6*, Article 0197. https://doi.org/10.34133/research.0197
[2] Koeppel, A., Laity, P. R., & Holland, C. (2020). The influence of metal ions on native silk rheology. *Acta Biomaterialia*, *117*, 204–212. https://doi.org/10.1016/j.actbio.2020.09.045
[3] Laity, P. R., Gilks, S. E., & Holland, C. (2015). Rheological behaviour of native silk feedstocks. *Polymer*, *67*, 28–39. https://doi.org/10.1016/j.polymer.2015.04.049
[4] Mu, X., Amouzandeh, R., Vogts, H., Luallen, E., & Arzani, M. (2023). A brief review on the mechanisms and approaches of silk spinning-inspired biofabrication. *Frontiers in Bioengineering and Biotechnology*, *11*, Article 1252499. https://doi.org/10.3389/fbioe.2023.1252499
[5] Mu, X., Yuen, J. S. K., Choi, J., Zhang, Y., Cebe, P., Jiang, X., Zhang, Y. S., & Kaplan, D. L. (2022). Conformation-driven strategy for resilient and functional protein materials. *Proceedings of the National Academy of Sciences of the United States of America*, *119*(4), Article e2115523119. https://doi.org/10.1073/pnas.2115523119
[6] Sourroubille, M., Miranda-Valdez, I. Y., Mäkinen, T., Koivisto, J., & Alava, M. J. (2025). Thermogelation of methylcellulose: A rheological approach with Gaussian Process Regression. *Colloids and Surfaces A: Physicochemical and Engineering Aspects*, *709*,

Using Sunlight to Produce Sustainable Hydrogen: Optimizing Titanium Substrates for PEC Water Splitting

Sean Anirudh Sathish[1], Samuel Adesanoye Ph.D[2,3], Syed Mubeen Ph.D[2,3]

[1]Fort Zumwalt West High School, MO; [2]SunHydrogen, Inc.; [3]Department of Chemical and Biochemical Engineering, University of Iowa

Introduction

Why is Hydrogen Production Important?

- Hydrogen is a fuel of the future, but over 95% of today's hydrogen is produced from fossil fuels, generating significant CO_2 emissions.[1, 5]
- Green hydrogen, produced using renewable energy, offers a sustainable, zero-carbon alternative for industry, transportation, and energy storage.[5]
- Goldman Sachs projects the hydrogen market could exceed $1 trillion annually by 2050, with global demand expected to increase up to sevenfold.[1]

Why Use PEC Water Splitting?

- Photoelectrochemical (PEC) water splitting uses energy directly from sunlight to convert water into hydrogen, eliminating the need for external electricity.[5]
- Produces hydrogen with zero operational carbon emissions, making it a sustainable fuel pathway.[5]

$$2H^+ + 2e^- \rightarrow H_2(g)$$

What Improvements Can be Made?

- Hydrogen Evolution Reaction (HER) efficiency remains limited by energy losses caused by overpotential.[2, 4]
- Electrode materials and catalyst deposition methods are not yet fully optimized.[2, 4]

Purpose

Research Question

How do electrodeposition parameters and titanium substrate properties affect catalytic activity, stability, and overall HER performance?

Objectives

- Achieve high HER activity with an initial overpotential < 75 mV
- Achieve long-term stability over 20 hours with a degradation rate < 3 mV/hr

Methodology

Experimental Setup

Preparing the Titanium Substrates

- Cut samples into a uniform size and clean to remove surface impurities
- Titanium selected for its corrosion resistance, electrical conductivity, and compatibility with acidic PEM conditions

Electrodeposition

- Two-electrode system used: Ti substrate (cathode), Pt mesh (anode)
- Platinum selected for its excellent HER catalytic activity

Testing

- Three-electrode system used; reference electrode ensures standardized potential measurements
- Sulfuric acid used as the electrolyte to provide abundant H^+ ions for HER

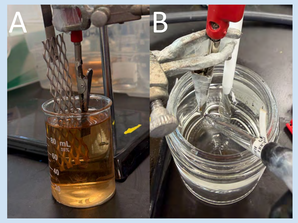
Optimization Workflow

Guidelines

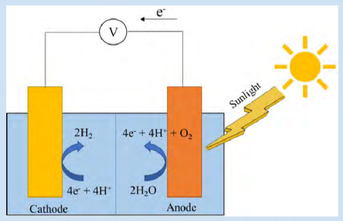
- Vary one parameter at a time while keeping all others constant
- Carry the best-performing condition forward based on HER activity

Parameters Tested (in order)

1. Substrate Material: Ti foil vs. Ti felt
2. Charge Density: 0.4 vs. 0.6 C cm^{-2}
3. Deposition Voltage: 1.3, 1.5, and 1.7 Volts
4. Annealing: Non-annealed vs. 2hr annealing at 200 °C
5. Substrate Porosity: Standard vs. High-porosity

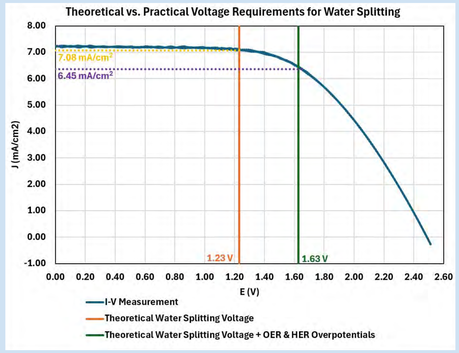


(A) Electrodeposition **(B)** HER Testing

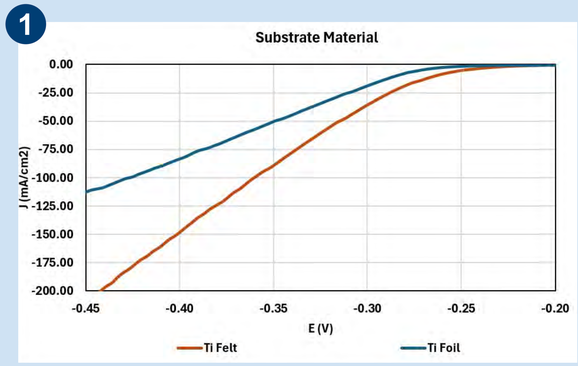


Schematic diagram of photoelectrochemical water splitting. Reproduced from Shahazi et al. (2024).

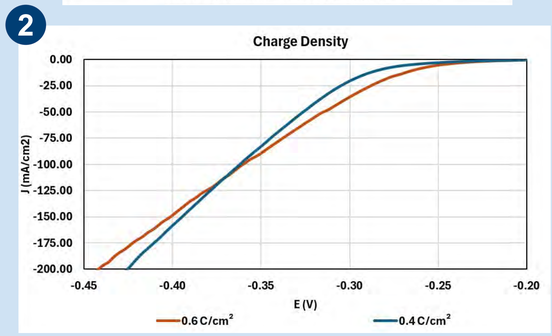
Results



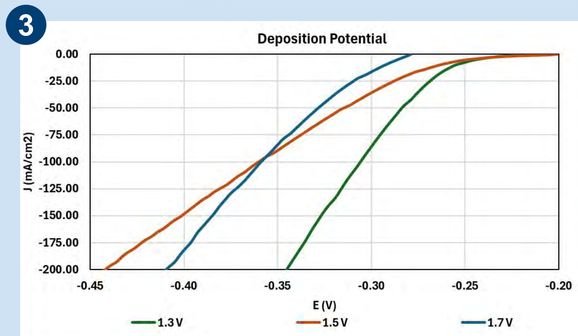
1



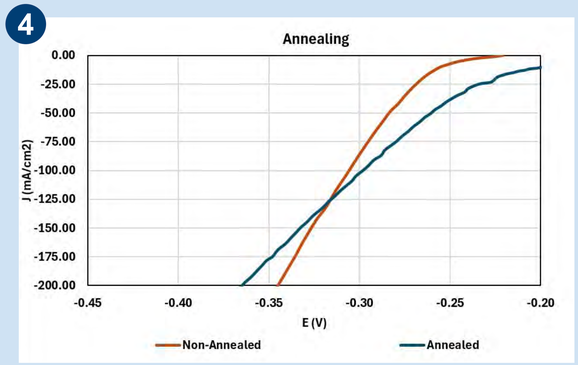
2



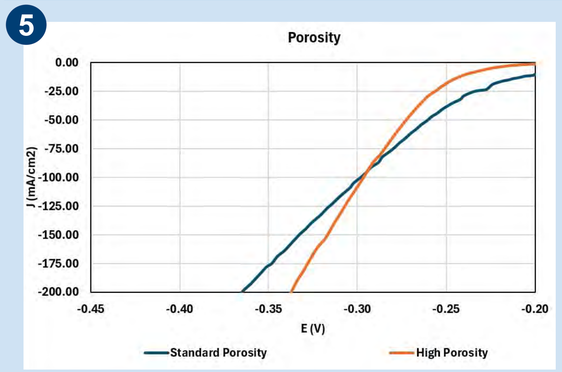
3

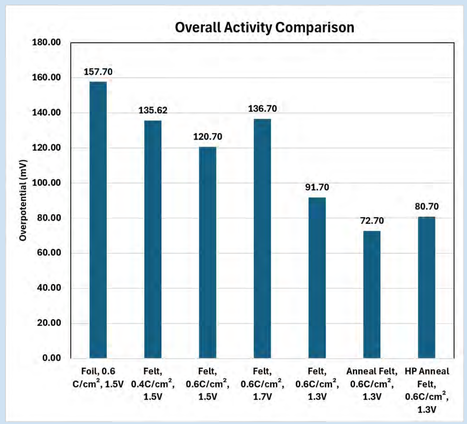


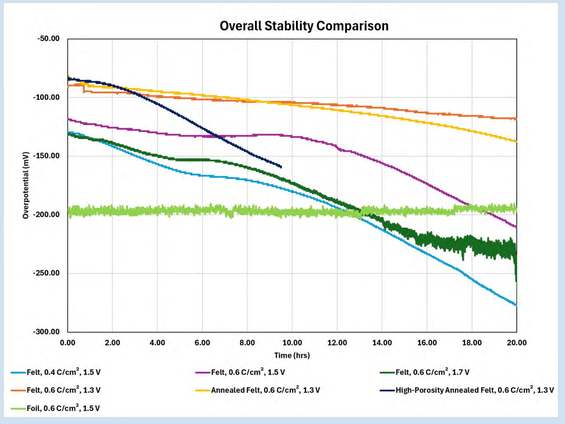
4



5







Conclusions

Sample	Overpotential(mV)	Degradation Rate (mV/hr)
Ti Foil, 0.6 C/cm², 1.5 V	157.70	~0
Ti Felt, 0.6 C/cm², 1.5 V	120.70	−4.65
Ti Felt, 0.4 C/cm², 1.5 V	135.62	−7.41
Ti Felt, 0.6 C/cm², 1.3 V	91.70	−1.35
Ti Felt, 0.6 C/cm², 1.7 V	136.70	−5.70
Annealed Ti Felt, 0.6 C/cm², 1.3 V	**72.70**	**−2.71**
High-Porosity Annealed Ti Felt, 0.6 C/cm², 1.3 V	80.70	−8.12*

*Measured over 9.5 hours instead of 20 due to time constraints during experimentation.

Key Takeaways

- Ti felt significantly outperformed Ti foil in catalytic activity, while titanium foil exhibited superior stability
- Electrodeposition parameters (charge density and deposition potential) had a substantial impact on both HER activity and long-term stability
- Annealing improved catalytic activity but also reduced long-term stability
- High-porosity felt had poorer activity and stability compared to standard porosity felt
- The optimal electrode configuration was annealed Ti felt deposited at 1.3 V and 0.6 C/cm², meeting both the activity and stability benchmarks
- Optimization reduced HER overpotential by approximately 85 mV
- Ultimately, catalytic activity and stability must be optimized together to develop commercially viable PEC hydrogen devices

Applications/Future Directions

Applications

- Lower-Cost Green Hydrogen: Improving the Solar-to-Hydrogen (STH) efficiency of PEC cells can enable greater hydrogen production at lower cost
- Scalable Hydrogen Production: More efficient and durable electrodes support the development of larger, commercially viable PEC hydrogen systems

Future Directions

- Test more deposition parameters (e.g. more annealing temperatures, deposition voltages, and charge densities) to further optimize performance
- Etch titanium felt to create a rougher surface, potentially allowing for more catalyst binding sites and improving activity
- Test stability of samples for an even longer time (>100 hours) to evaluate electrode durability and performance on industry standards

Acknowledgements

I would like to thank Dr. Mubeen for the incredible opportunity to work on this project and Samuel Adesanoye along with the entire SunHydrogen team for their guidance and support. Thank you also to all affiliated with the SSTP program.

References

1. Goldman Sachs Global Investment Research. (2022). *Carbonomics: The clean hydrogen revolution.* https://www.goldmansachs.com/insights/pages/carbonomics-the-clean-hydrogen-revolution.html
2. Liu, L., Nam, K. H., Yuan, Y., Yan, Y., Chiu, Y.-L., & Du, S. (2026). Chloride-induced morphology control of Pt coatings on titanium porous transport layers for proton exchange membrane water electrolyzers. *Advanced Energy and Sustainability Research, 7*(1), e202500399. https://doi.org/10.1002/aesr.202500399
3. Shahazi, R., Saddam, A. I., Majumdar, S., Islam, M. R., Rahman, M. M., Alam, M. M., Kumer, A., & Paimard, G. (2024). *Advancements in water splitting for sustainable energy generation: A review. Characterization and Application of Nanomaterials, 7*(1), 5834. https://doi.org/10.24294/can.v7i1.5834
4. Tao, Y., Wu, M., Hu, M., Xu, X., Abdullah, M. I., Shao, J., & Wang, H. (2024). High-performance porous transport layers for proton exchange membrane water electrolyzers. *SusMat, 4*, e230. https://doi.org/10.1002/sus2.230
5. Vilanova, A., Dias, P., Lopes, T., & Mendes, A. (2024). The route for commercial photoelectrochemical water splitting: A review of large-area devices and key upscaling challenges. *Chemical Society Reviews, 53*(5), 2388–2434. https://doi.org/10.1039/D1CS01069G

From Detection to Attitude and the Space Between: A Two-Stage Machine Learning Analysis of AI Companion and Mental Health Discourse

Kai Seifan[1], Haixia He[2], Weiguo Fan[2]

[1]Horace Mann School, New York City, NY; [2]Department of Business Analytics, University of Iowa, Iowa City, IA

Introduction

AI Companionship Background

- In recent years, the field of AI Companionship has only **grown** (Nakagomi et al., 2026).



- Companions provide **support**, allowing users to escape from reality (Nakagomi et al., 2026).
- Need for **research** to find out more about AI Companionship's growing role and **effects**.

Reddit Context

- Reddit **succeeds** where surveys do not: submissions are genuine as people are anonymous and speak their minds.

Sentiment Analysis Gaps

- Field dominated by **binary** classifications such as positive vs negative (Wang et al., 2020).
- **Debate** on best way to classify mixed (positive and negative) sentiment (Tak, 2022).
- We not only classify **ambivalence**, but do so under a **specific** mental health context, which is largely unexplored.

Objectives

Purpose: Develop + **mathematically** analyze ML pipeline, test if the **difficulty** of classifying is a limitation of models or inherent ambiguity, **shape** how methods should be improved and used.

RQ1: How can machine learning models be used to detect **mental health-related** content in AI companion posts and **classify** users' **sentiment** toward AI companions?

RQ2: What **factors** influence the **performance** of these machine learning models?

RQ3: How can these models **support future research** on AI Companions and mental health?

Methodology

Data Preparation

- Collected Reddit posts from
  - **38 mental** health communities
  - **30 AI** Companion communities
- **Ranked** posts using
  - TF-IDF (keyword similarity)
  - SBERT (semantic similarity)
- Selected the top **25%** for manual review
- Two **annotators labeled**
  - 2000 posts
  - 2000 comments

	AIC+MH	AIC	Excluded	MH
AIC+MH	633	260	1	1
AIC	84	2955	4	0
Excluded	0	0	13	0
MH	0	0	0	2

	Positive	Negative	Mixed	NA
Positive	212	1	9	8
Negative	5	273	33	18
Mixed	51	47	129	28
NA	4	5	3	3109

Methodology

Metrics

$$\kappa = \frac{p_0 - p_e}{1 - p_e}$$

- Labeling agreement: **κ = 0.73, AC1 ($\hat{\gamma}_1$) = 0.91**

$$\hat{\gamma}_1 = \frac{p_0 - p_e^{(\gamma)}}{1 - p_e^{(\gamma)}}$$

- Attitude agreement: **κ = 0.71**, **AC1 = 0.90**.

$$\text{Macro-}F1 = \frac{1}{K}\sum_{k=1}^{K} F1_k$$

- Unweighted **average** of all F1-scores.

$$\text{Accuracy} = \frac{TP+TN}{TP+TN+FP+FN} \qquad \text{Precision} = \frac{TP}{TP+FP} \qquad \text{Recall} = \frac{TP}{TP+FN}$$

$$F1 = 2 \cdot \frac{\text{Precision} \cdot \text{Recall}}{\text{Precision} + \text{Recall}}$$

- **Main** metrics for performance.

$$BC(h_n, g_n) = \frac{1}{N}\sum_{n=1}^{N}\sqrt{h_n g_n}$$

- Higher BC = more **overlap** between two classes.

$$\text{Sim}(A,B) = \cos(\theta) = \frac{A \cdot B}{\|A\|\,\|B\|}$$

Cosine Similarity:

Two posts embed as **vectors** u, v ∈ $\mathbb{R}^{768}$. Sim calculates angle between them → the posts' **semantic** similarity.

Training the Models

Stage 1: Mental Health Classification

1.1 Trained a **DistilBERT** baseline model on **4000** posts and comments.

1.2 **MentalBERT** model pretrained on Reddit mental health data (Ji et al., 2021).

Stage 2: Sentiment Classification

2.1 **Cardiff** model pretrained on **124 million** tweets for sentiment (Cardiffnlp, 2024).

2.2 **NLI** model given 3 **hypotheses** and **inferenced** sentiment in posts.

2.3 Converted submissions into vectors + used **UMAP** to identify **structure.** Trained an **MLP** and **Log Reg** model.

2.4 **Combined**: Cardiff scored every **sentence**, yielding probabilities inputted into the **conflict** feature. Joint with **embeddings** and ran through **Log Reg**.

$$\textbf{conflict} = \min(\max_i \mathbf{s}_i^{+}, \max_i \mathbf{s}_i^{-})$$

2.5 Prompted the LLM Qwen2.5-7B to classify sentiment in a **similar** way humans would.

Results

Stage 1

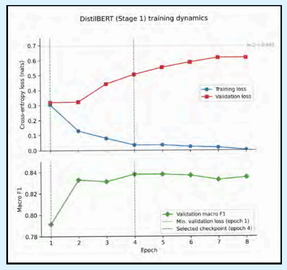


Figure 1. DistilBERT. Top: Validation increases while training decreases. Bottom: **Validation** macro F1 peaks at epoch 4 **(0.838).**

Model	Class	Prec.	Rec.	F1	Supp.
DistilBERT	AIC	0.94	0.92	0.93	624
	AIC+MH	0.72	0.77	0.75	163
MentalBERT	AIC	0.94	0.95	0.94	624
	AIC+MH	0.80	0.75	0.78	163
DistilBERT macro F1 / accuracy			0.838 / 0.89		
MentalBERT macro F1 / accuracy			0.861 / 0.91		

Table 1. Test performance for both models at selected **checkpoints.**

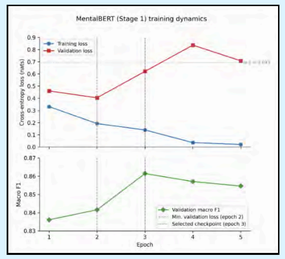


Figure 2. MentalBERT. Pattern of Figure 1 **amplified.** form. Macro F1 peaks at epoch 3 **(0.861).**

Stage 2

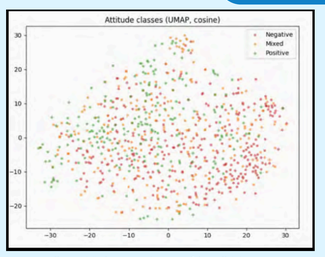


Figure 3. UMAP projections of the 814 embedded posts. All three attitude classes, **no structure**.

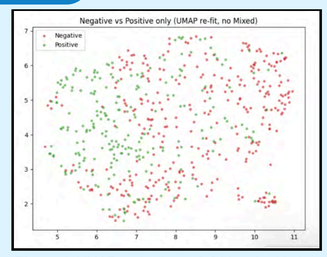


Figure 4. UMAP projections of 814 embedded posts. Negative and Positive only, **distinct** regions.

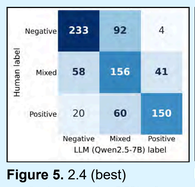


Figure 5. 2.4 (best) confusion matrix; **85%** of **errors** involve mixed.

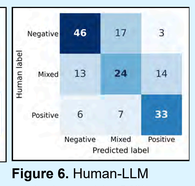


Figure 6. Human-LLM confusion matrix: **91%** disagreement involves **mixed**.

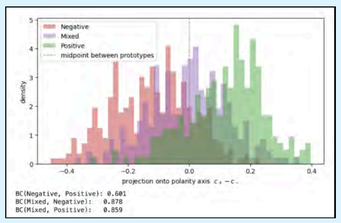


Figure 7. 814 posts projected onto **polarity** axis. Mixed peaks at midpoint but **overlaps** both poles heavily.

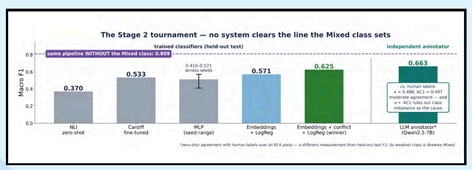


Figure 8. Macro F1 for **ALL** Stage 2 approaches. Dashed line: the same pipeline without the Mixed class **(0.809).**

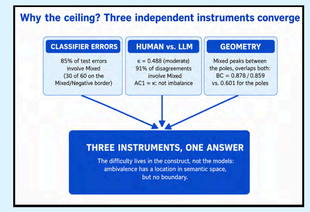
Discussion

RQ1:

- MentalBERT **ourperformed** DistilBERT (Macro-F1 0.861).
- Cardiff + conflict feature + embeddings + Log Reg (2.4) **best** approach with Macro-F1 of **0.625.**

RQ2:

- Attitude **specificity** affects model.
- **Joint** human-LLM annotation.
- Small **parameter** models better: Log Reg outperforms → does not memorize **noise.**



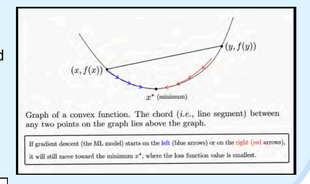
RQ3:

- Model 2.4 shows **promise** for multi-class sentiment classification.
- Mixed predictions not failure but **flags** for posts with **entanglement** that **humans** can fail to classify.
- **Future** research into practical applications of models to **help** people.
- Can any **representational** space give Mixed a **boundary**?

Extra Findings

- Log Reg with **same** scores every time
- Loss **function** convex in weights: second **derivative** along any direction ≥ 0.
- Came from analyzing these three model functions **together**:

$$p_k = \frac{e^{z_k}}{\sum_j e^{z_j}} \qquad -log(p_y) \qquad z_k = w_k x + b_k$$



Mathematical analysis → **insight**

Acknowledgements

- Secondary Student Training Program (SSTP)
- Tippie College of Business
- Professor Weigou Fan and Dr. Haixia He
- James Cao, Sarah Li, and Elizabeth Wang

Contact info: kseifan237@gmail.com

Full paper:

References

1. AI Companion Market Size to Hit USD 552.49 Billion by 2035. (n.d.). Retrieved July 15, 2026, from https://www.precedenceresearch.com/ai-companion-market
Aghakhani, E., & Rezapour, R. (2026). Like a therapist, but not: Reddit narratives of AI in mental health contexts (arXiv:2601.20747). arXiv. https://doi.org/10.48550/arXiv.2601.20747
2. Cardiffnlp/twitter-roberta-base-sentiment-latest · Hugging Face. (2024, January 4). https://huggingface.co/cardiffnlp/twitter-roberta-base-sentiment-latest
3. Ji, S., Zhang, T., Ansari, L., Fu, J., Tiwari, P., & Cambria, E. (2021). MentalBERT: Publicly available pretrained language models for mental healthcare (arXiv:2110.15621). arXiv. https://doi.org/10.48550/arXiv.2110.15621
4. Nakagomi, A., Akutsu, Y., Yasuoka, M., Abe, N., Ihara, S., Teroh, T., & Tabuchi, T. (2026). AI companions and subjective well-being: Moderation by social connectedness and loneliness. Technology in Society, 85, 103229. https://doi.org/10.1016/j.techsoc.2026.103229
5. Tak, R. (2022). A quantifiable analysis of ambivalence in tweets. International Journal for Research in Applied Science and Engineering Technology, 10(4), 691–699. https://doi.org/10.22214/ijraset.2022.41340
6. Wang, Z., Ho, S.-B., & Cambria, E. (2020). Multi-level fine-scaled sentiment sensing with ambivalence handling. International Journal of Uncertainty, Fuzziness and Knowledge-Based Systems, 28(04), 683–697. https://doi.org/10.1142/S0218488520500294

Do Disasters Drive Emigration? A Global Granger-Causality Analysis Across Country Income Levels

Rushil Sengupta[1], Caglar Koylu[2]

[1]Monta Vista High School, Cupertino, CA; [2]School of Earth, Environment, and Sustainability, University of Iowa, Iowa City, IA

Introduction

Background

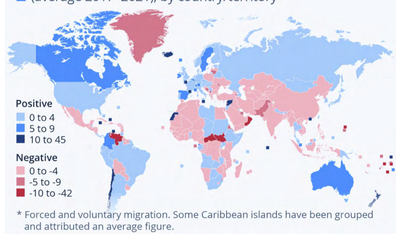
- Natural disasters displace millions of people each year, and climate change continues to elevate global hazards
- Migration is quite expensive, and extreme events like disasters destroy people's assets including housing and valuables, immobilizing the most vulnerable

Past Research

- A U.S. study demonstrating flood damages sorted outbound migration by income, showing trends of higher income levels migrating, while lower income levels were trapped
- Previous Geo-Social lab work used Granger-Causality models for data recorded over time, which works on using migration mechanics to assess predictive patterns

Problems to Solve

- Existing research on displacement caused by natural disasters, especially on the difference in effects across income levels, remains limited in global reach and general impact
- Past research has been limited by bad data, caused by factors such as forced conflict escapes and seasonal baselines causing migration data to be hard to interpret



Research Objectives

Research Question: How are changes in countries' migration trends associated with disaster frequency, and how does income of those countries affect those changes during high disaster periods?

Hypotheses:

- Lower income populations face mobility constraints, so disasters may cause higher increases in emigration rates in high income countries whose residents can afford to move compared to lower income countries
- As the frequency of disasters per month increases, the outward migration will increase, though it may have a cap on this increasing outward migration as the number of disasters per month increases

Objectives: Build monthly migration metrics for 180 countries (2019–2022) while removing forced migration and seasonality from the data. Then, test in what ways disasters influence migration, and compare disaster month vs normal month migration across different income levels.

Methodology

1. Data Collection and Transformation

Two original datasets:

- EMDAT natural disaster
- Global migration flows dataset from Meta x Humdat

Transformed migration data into new dataset with:

- The country's name and month of data collection
- Number of outward and inward migrants
- Population
- Emigration rate (out migration rate)

$$\text{Out-Migration Rate} = \frac{\text{Number of Out-Migrants}}{\text{Total Population}} \times 1{,}000$$

- Migration efficiency rate

$$\text{Migration Efficiency Ratio} = \frac{\text{In-migrants} - \text{Out-migrants}}{\text{In-migrants} + \text{Out-migrants}} \times 100$$

Migration Flows Data

country_from	country_to	migration_month	num_migrants
AD	AE	2019-01	12
AD	AE	2019-02	2
AD	AE	2019-03	1
…	…	…	…
BO	UY	2022-11	13
BO	UY	2022-12	18

Disasters Data

country	start_date	end_date	people_affected
Ecuador	2022-04-25	2022-04-25	85121
Kenya	2021-03-06	2021-03-31	270143
Afghanistan	2022-08-31	2022-08-31	1304600
…	…	…	…
Uruguay	2020-06-22	2020-06-23	15097
Bosnia and Herzogovina	2020-06-22	2020-06-24	36024

2. Cleaning & Controls

- Remove data influenced by factors other than disasters (i.e. wars)
- Deseasonalize the migration data

3. Income and Distance

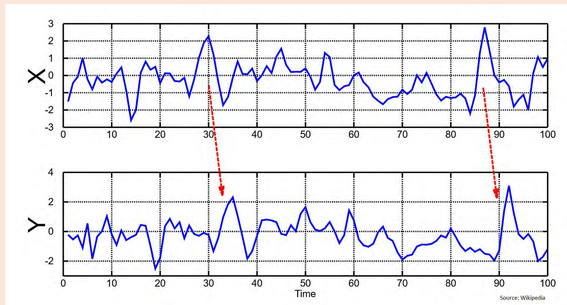
- Split countries into GDP-per-capita quartiles
- Compare disaster- vs normal-month migration
- Test the across-income trend
- Measure migration distances

4. Granger-Causality

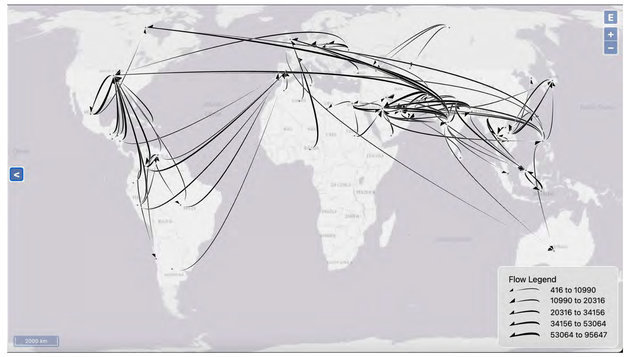
- R^2-score and AIC based model comparison for selecting best lag

$$R^2 = 1 - \frac{\Sigma_i^N (y_i - \hat{y}_i)^2}{\Sigma_i^N (y_i - \bar{y})^2} \qquad AIC = -2\ln(L) + 2k$$

- Granger-Causality Test & Lag Selection (time series relationships)



Top 100 Largest Migration Flows



Results

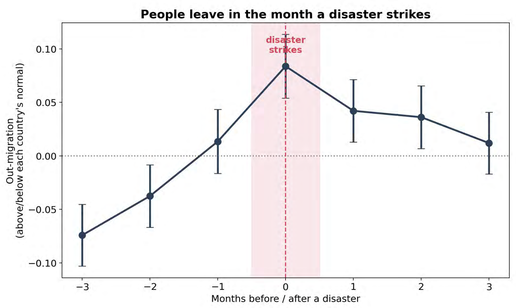


Figure 1: In terms of relationship to disaster timing, the emigration rate sits below each country's normal before a disaster, peaks in the exact month it strikes, then decays over the next ~3 months.Granger F-tests (restricted vs. unrestricted models, ADF-stationary series, AIC-selected 1–3 month lags) confirm disasters add predictive power beyond migration's own history.

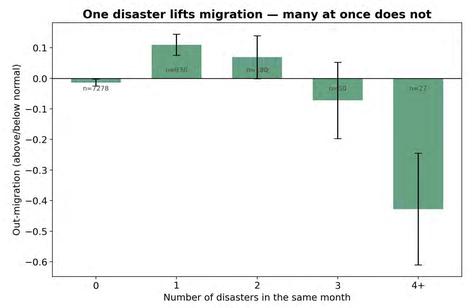


Figure 2: The out-migration rate increases with 1–2 disasters, but decreases when disaster frequency reaches high counts, showing high disaster frequency traps people while general disasters provoke migration out of a country. A single disaster lifts standardized out-migration to +0.11, but the effect turns negative at 3 and 4+, a signature of trapped populations.

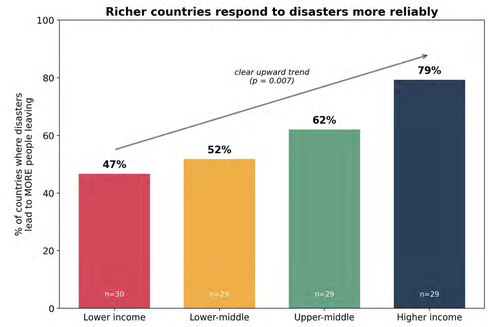


Figure 3: A clear relationship can be seen where higher income levels mean higher migration rates when a disaster occurs. The share of countries where disasters raise out-migration climbs across income quartiles, and the median country's response rises the same way. Based on this, oth the probability and magnitude of leaving scale with income.

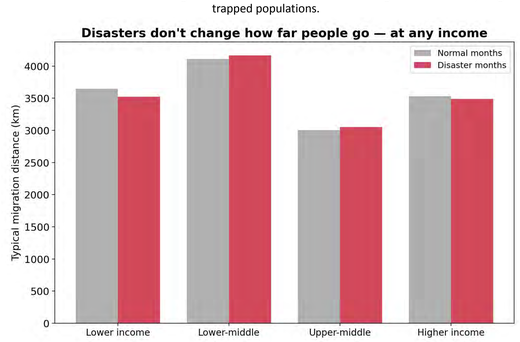


Figure 4: For each income level, the typical migration distance doesn't change between normal months and disaster months, with income also not showing any trend with how far people migrate, so how many people migrate. Distance shows no income relationship ($\rho \approx 0.04$) and shifts only ~1% in disaster months — it likely depends on geography, not income or disasters.

Conclusion and Discussion

Conclusions

- Disasters have a heavy influence on increasing international migration month-to-month, an influence also following disaster timing rather than only coinciding with it
- Income determines disaster response, as richer countries are more likely to migrate and in greater numbers, while only around half of the poorer countries respond, also showing a suppression in their ability to migrate
- The relationship between disaster frequency and migration is non-linear, as although the migration rate goes up during months with 1-2 disasters, it goes back down, even further below normal, at higher disaster frequencies

Impact

This is the first global, monthly test of how disaster frequency relates to international migration, including income as a moderator, on fully open data. This research brings awareness to the necessity of aid towards countries with people who are trapped by natural disasters, and can act as a first step towards even stronger research to identify more migration patterns relating to the environment.

Future Work

The most important is to analyze data over longer stretches of time (past 48 months), allowing for extended Granger-Causality tests. Subnation migration data can provide further insight on countries with a lack of disaster-provoked migration and help us understand what might trap them aside from income.

Acknowledgements

Thank you to my Geo-Social Lab mentor, Dr. Koylu, who went far beyond simply teaching me the necessary concepts, and made sure I understood the entire research process. His constant support and advice have positively shaped how I will approach learning and research in the future. I would also like to thank my lab mates Jay, Josh, and Aditya, who made the research process even more fun.

Key References

Clark, Mallory B., et al. "Exodus of the Affluent? Examining Climate Hazards, Migration, and Household Income in the U.S." Population and Environment, vol. 47, no. 3, 2025, article 28. Springer, https://doi.org/10.1007/s11111-025-00496-5.

Gallaway, Lowell, and Richard Vedder. "Migration Efficiency Ratios and the Optimum Distribution of Population." Growth and Change, vol. 16, no. 1, 1985, pp. 3–7. Wiley Online Library, https://doi.org/10.1111/j.1468-2257.1985.tb01033.x.

Kwon, Hyesop, and Caglar Koylu. "Revealing Associations between Spatial Time Series Trends of COVID-19 Incidence and Human Mobility: An Analysis of Bidirectionality and Spatiotemporal Heterogeneity." International Journal of Health Geographics, vol. 22, no. 1, 2023, article 33. BioMed Central, https://doi.org/10.1186/s12942-023-00357-0.

Tenerelli, Patrizia, et al. "Population Density Modelling in Support of Disaster Risk Assessment." International Journal of Disaster Risk Reduction, vol. 13, 2015, pp. 334–341. ScienceDirect, https://doi.org/10.1016/j.ijdrr.2015.07.015.

Zhao, Pengjun, et al. "The Effective Intervening Opportunity Model for Seasonal Human Mobility." The Innovation, vol. 6, no. 6, 2025, article 100992. ScienceDirect, https://doi.org/10.1016/j.xinn.2025.100992.

The Effect of Free Surface on Vortex Shedding Behind Wedges

Arjun Shankar[1], Skinder A. Dar[2], Cong Wang[2]

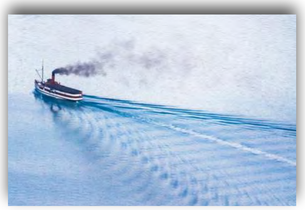
[1]Mountain View High School, Mountain View, CA
[2]IIHR - Hydroscience and Engineering, Department of Mechanical Engineering, University of Iowa, Iowa City, IA

Introduction

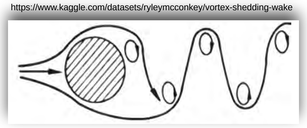
Vortex shedding is the alternating, periodic formation and release of swirling vortices from sides of a bluff (non-streamlined) object.

Vortex shedding occurs behind **boats**, impacting their energy efficiency, stability and stealth. It is extremely difficult to model because of complexities of the **surface** of the water [1].

Previous studies have focused on **cylindrical** bodies [2,3] that do not represent the sharp geometry and shape of real ship hulls.



https://www.kaggle.com/datasets/ryleymcconkey/vortex-shedding-wake

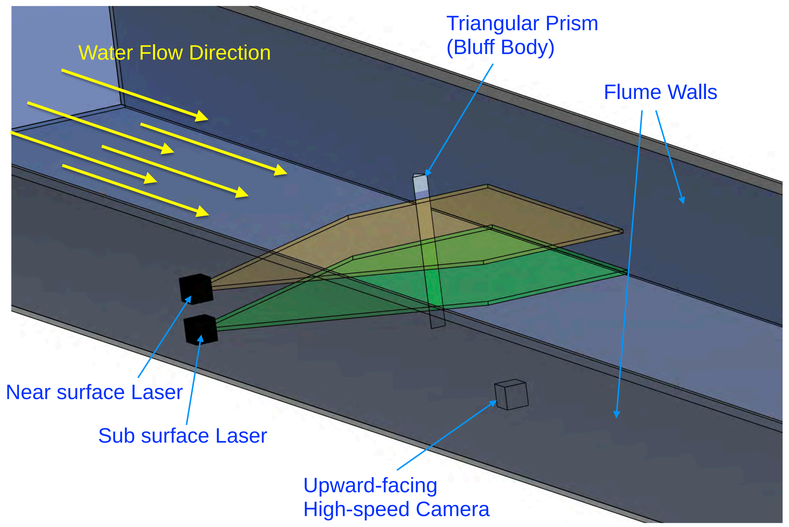


https://en.wikipedia.org/wiki/Vortex_shedding

Objective: To study the **effect of free surface** on **vortex shedding behind triangular prisms.**

Experimental Setup

Experiments were conducted in a clear flume, seeded with 13 μm reflecting Silver-coated beads. We performed **Particle Image Velocimetry (PIV) analysis** on two horizontal cross-sections: **Near-Surface**, 2mm below the surface and **Sub-Surface**, well below (180mm) the surface. The unique experimental facilities of IIHR were integral to collecting meaningful data.

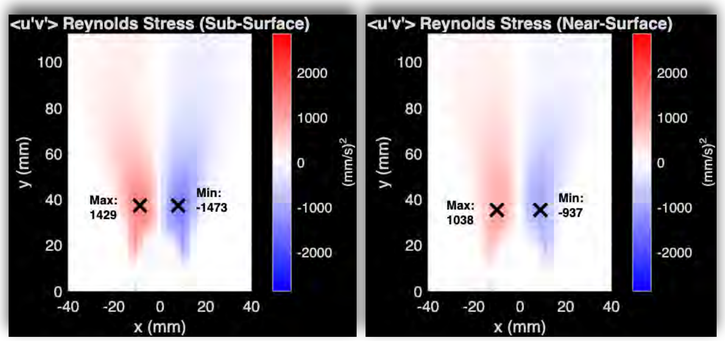


Model of the experimental setup, using the flume developed by Butler et al. [1].

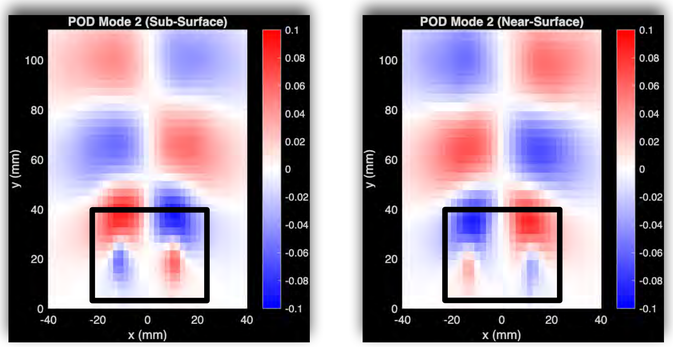
Key Parameters

- Flow medium: **Water**
- Flow speed: **140 mm/s**
- Reynolds number: **2800**
- Froude number: **0.316**
- Strouhal number: **0.21**
- Bluff geometry: **Equilateral triangular wedge with 20 mm side length**
- Blockage Ratio: **3.3%**
- Imaging Frame rate: **450 Hz**
- PIV Resolution: **2.1-3.5mm/pix**

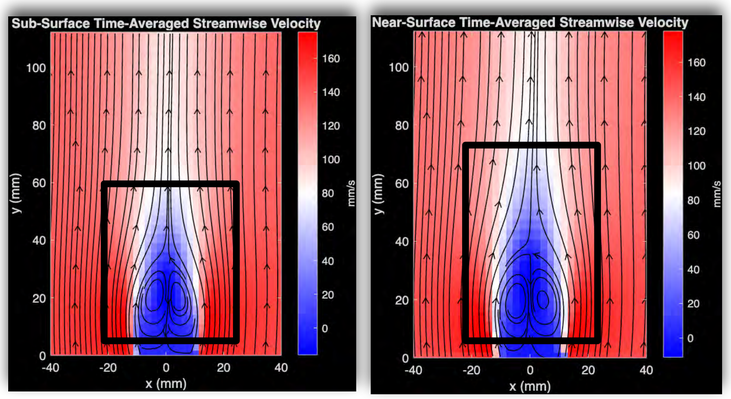
Results



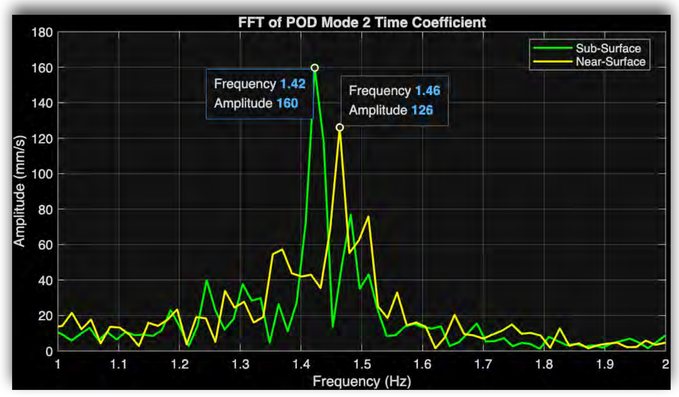
Shear Reynolds Stress *for Sub-Surface and Near-Surface vortex shedding. This represents momentum transfer from turbulent mixing. Peak shear Reynolds Stress for the* ***Sub-Surface is 1.42x stronger*** *than Near-Surface.*



The second dominant mode of the fluctuating streamwise velocity field for Sub-Surface and Near-Surface vortex shedding, by applying Proper Orthogonal Decomposition (POD) techniques. ***Near-Surface velocity fluctuations are gentler than the Sub-Surface.***



Average streamwise velocities for Sub-Surface and Near-Surface vortex shedding. The ***Near-Surface has a lengthened recirculation region*** *(approximately 40% longer, as shown in blue), which* ***delays vortex formation and reduces strength*** *of resulting vortex shedding structures [4].*



Fourier Transform of temporal coefficients of the second POD mode, showing nearly ***identical shedding frequencies*** *for Sub- and Near-Surface (1.42Hz vs 1.46Hz).* ***However,*** *Sub-Surface fluctuations have 1.27x higher spectral amplitude, suggesting* ***Near-Surface wake exhibits weaker and less coherent vortex shedding structures.***

Conclusions

Key Findings:

- Free surface **suppresses turbulent mixing**, but **doesn't affect the shedding frequency.**
- The lengthened recirculation region close to the surface **stabilizes the wake** behind the wedge, causing **weaker, less-coherent vortex shedding**.

New insights into influence of free-surface on bluff-body wake dynamics have been developed.

Future studies can utilize this work to design ships that account for this difference in wake near and far from the surface of the water.

Acknowledgements

I would like to thank my mentors **Prof. Cong Wang** and **Skinder Dar** (PhD candidate) for their amazing guidance, and to the **Secondary Student Training Program** at **Belin-Blank Center** for making this research possible.

References

[1] Butler, D., Dar, S., Nguyen, M., and Wang, C., 2026, "Design of a High-Speed, Low-Turbulence Water Flume With Initial Application to Free Surface Turbulent Wake Flow," Theoretical and Applied Mechanics Letters, 16(1), Art. No. 100621. https://doi.org/10.1016/j.taml.2025.100621
[2] Gaster, M., 1971, "Vortex Shedding From Circular Cylinders at Low Reynolds Numbers," Journal of Fluid Mechanics, 46(4), pp. 749–756. https://doi.org/10.1017/S002211207100082X.
[3] Perry, A. E., Chong, M. S., and Lim, T. T., 1982, "The Vortex-Shedding Process Behind Two-Dimensional Bluff Bodies," Journal of Fluid Mechanics, 116, pp. 77–90. https://doi.org/10.1017/S0022112082000378
[4] Tong, X., Jiang, H., Cao, S., Kang, L., and Fan, D., 2026, "Recirculation-Mediated Wake Control of a Near-Wall Cylinder Under Downstream Plate Oscillation," Journal of Ocean Engineering and Science, https://doi.org/10.1016/j.joes.2026.06.014

Assessing the Relationship Between Climate and Wetlands Across Iowa Watersheds, 2004–2024

Joshua Shi[1]; Caglar Koylu PhD[2]

Charter School of Wilmington, Wilmington, DE[1]; School of Earth, Environment, and Sustainability, University of Iowa, Iowa City, IA[2]

INTRODUCTION

Background Information

- Approximately 90–95% of Iowa's wetlands that existed prior to European settlement have been drained, primarily for agricultural development. (Iowa DNR, n.d.; USDA NRCS, 2025)
- Many wetland restoration efforts have taken place in Iowa since the 1980s. Today, Iowa's landscape comprises of natural, restored, and constructed wetlands (Iowa Geological Survey, 2005).
- Palmer Drought Severity Index (PDSI) estimates relative wetness or dryness based on historical precipitation, temperature, and soil conditions. Positive values indicate wetter-than-normal conditions, while negative values indicate drier than normal (Palmer, 1965)



Extent of Wetlands overlaid on Iowa HUC 10 Watersheds, 2024

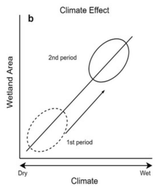
U.S. Fish and Wildlife Service National Wetlands Inventory; U.S. Geological Survey Watershed Boundary Dataset (HUC10)

Introducing the Problem

- Restored or constructed wetlands may differ from undisturbed natural wetlands in their hydrology, vegetation, and ecological function.
- The relationship between climate conditions, such as PDSI, and mapped wetland area may be weakened or obscured across Iowa's modern day wetlands.

Previous Research

- Research on wetlands in Prairie Pothole Region has shown that for each individual wetland, climate and wetland area will form a natural linear relationship. A land-use effect will show up as a change in the slope or intercept of that relationship. (McKenna et al., 2019). McKenna et al. applied a framework originally created by Gupta et al. (2015).
- However, previous research has mostly been limited to individual wetlands or study areas where there have been minimal land-use, so it is unclear if this relationship exists throughout Iowa's modern day watersheds (McKenna et al., 2019).



Adapted from McKenna et al. (2019), Figure 3b, based on Gupta et al. (2015).

Objectives

- Determine the relationship between climate, measured by PDSI and mapped wetland fraction across Iowa HUC10 watersheds over the last 20 years
- Evaluate spatial models that account for geographic patterns among watersheds across the study years

References

DATA AND METHODOLOGY

Data Collection

Wetland Data:

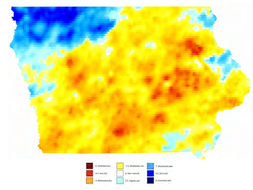
- USGS Annual NLCD land-cover data
- 30 meter resolution
- Classes 90 and 95 are wetlands
- Wetland fraction: Wetland pixels ÷ total valid pixels within each HUC10 watershed



July 2024 Iowa land-cover raster. Source: USGS Annual NLCD land-cover data

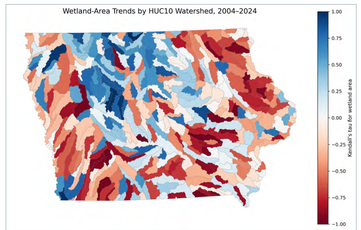
PDSI Data:

- PDSI Data was obtained from GRIDMET/DROUGHT via Google Earth Engine
- 4.6 km resolution
- Watershed value: Mean PDSI across pixels within each HUC10 watershed

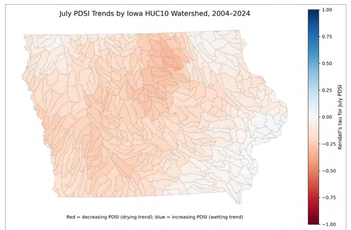


July 2024 Iowa PDSI raster. Source: GRIDMET/DROUGHT via Google Earth Engine.

Data Preparation



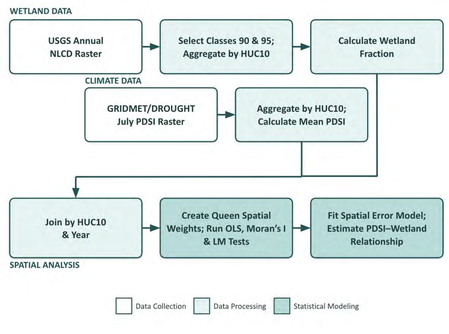
Kendall's tau for Wetland Fraction, 2004–2024



Kendall's tau for July PDSI, 2004–2024

How to Interpret Kendall's τ

- It measures the direction and consistency of change over time
- Positive τ: mostly increasing trend
- Negative τ: mostly decreasing trend
- τ near 0: little consistent trend
- |τ| near 1: strong, consistent trend



Modeling

	Accounts for spatial dependence	Selection evidence	Model Decision
OLS	No	Does not account for spatial dependence	Rejected - Significant Moran's I value
Spatial Lag (ML_Lag)	Yes	Similar to but less significant than error model	Considered, but less favorable
Spatial Error (ML_Error)	Yes	Best Fit (LM-error test had lower p-value than LM-lag)	Selected - LM Error test was more favorable than the LM Lag test

- Since data points are repeated over time and spatially correlated with their neighbors, the data is represented using one cross-sectional spatial regression per year (2004–2024) rather than a standard OLS model.
- Spatial analysis was conducted in Python using packages provided on PySAL
- Spatial weights: Queen contiguity (watersheds sharing an edge or corner are considered neighbors)

General Spatial Error Model:

$$y_i = \alpha + \sum_{j=1}^{m} \beta_j X_{ij} + u_i$$

$$u_i = \lambda u_{lag-i} + \epsilon_i$$

$$u_{lag-i} = \sum_k W_{ik} u_k$$

y_i: wetland fraction in watershed i

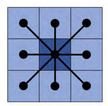
X_j: July PDSI

β_j: PDSI coefficient

W_{ik}: neighboring-watershed weights

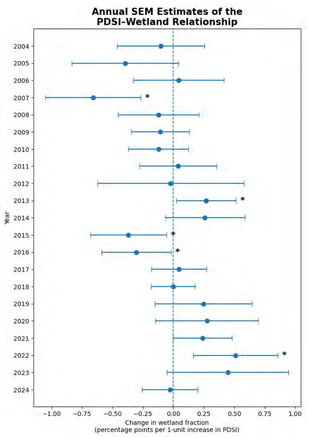
λ *(lambda)*: spatial dependence among unexplained influences

Queen Contiguity:



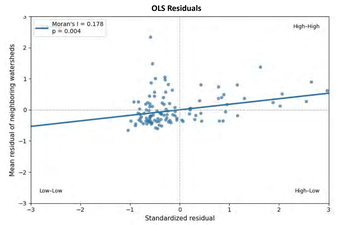
RESULTS

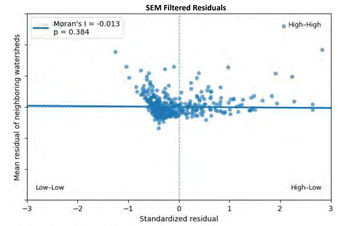
Each point represents a watershed, N=383 HUC10 watersheds



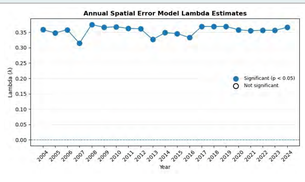
- **Dot:** annual PDSI effect
- **Bar:** 95% confidence interval
- **Asterisk:** p<0.05
- **Crossing zero =** not significant

Example: 2024 Spatial Autocorrelation Analysis

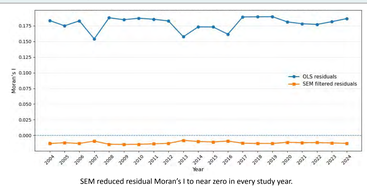




Annual Spatial Error Model Lambda Estimates



Residual Spatial Autocorrelation Before and After SEM



SEM reduced residual Moran's I to near zero in every study year.

DISCUSSION

Model Evaluation:

- The Spatial Error Model accounted for geographic clustering among neighboring watersheds.
- The spatial regression model found little evidence of a consistent relationship between July PDSI and wetland fraction from 2004–2024.
- A positive Moran's I means unexplained values cluster geographically.
- SEM residual Moran's I was near zero and nonsignificant in every study year, indicating there was little remaining spatial correlation.

Spatial Effects

- Positive and significant lambda values in every study year suggest that unexplained factors are spatially correlated among neighboring watersheds
- It implies that wetland patterns may be influenced more strongly by other spatial factors, such as agricultural land modification, than by July PDSI alone.

Limitations:

- NLCD data measured mapped annual land cover rather than short-term water-level changes
- July PDSI may not capture seasonal or delayed wetland responses.
- I used separate spatial regressions for each year, a simpler version of a standard spatial-temporal regression
  - Annual models treated each year separately and did not model temporal dependence within watersheds
  - A full spatial-temporal regression model would account for both similarity among neighboring watersheds and repeated measurements of the same watershed over time

CONCLUSION

Findings:

- Wetlands across Iowa did not show a consistent relationship between climate conditions and wetland area from 2004-2024
- Land modification, agricultural drainage, and other spatial factors may explain the weak climate-wetland fraction relationship. However, the specific factor was not tested.
- However, neighboring watersheds appeared to share similar unmeasured spatial influences

FUTURE WORK

Building off the Unmeasured Spatial Features:

- Determine whether human intervention has weakened the relationship between PDSI and wetland area across Iowa watersheds
- Analyze different influences such as cropland expansion, agricultural drainage, and use machine learning tools such as XGBoost to determine predictive factors.

Improved Data:

- Separate natural, restored, and constructed wetlands and see if results differ for each type
- Use soil, topography, and hydrology data to better determine wetland area coverage

Improved Analysis:

- Test the relationship using a spatial-temporal regression

ACKNOWLEDGEMENTS

I want to thank Professor Koylu, my lab mates Jay, Rushil, and Aditya, the SSTP program, as well as my parents for giving me this incredible opportunity to work in a professional lab environment. Their support and encouragement helped make my experience at SSTP both enjoyable and memorable.

Investigating the Role of Sleep in Menopause Related White Matter Damage

William Shin[1,2], Giovanna Novi[3,4], Liam Campbell[3,4], Michelle Voss[3,4]

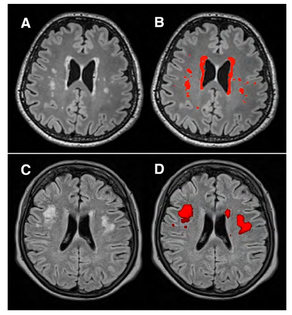
Harvard Westlake High School[1], Secondary Student Training Program[2], Department of Psychological and Brain Sciences[3], Health, Brain, and Cognition (HBC) Lab[4]

Introduction

White matter hyperintensities (WMH) represent white matter damage on MRI. They are associated with neurological disease, cognitive decline, and depression.[1]

After **menopause**, females have a faster rate of WMH progression[2]

- Higher estrogen levels are linked to lower WMH volume (WMHV)[3]
- **Hormone Replacement Therapies (HRTs)** have a negative effect on WML progression.[4]



FLAIR MRI with WMH in red[7]

The exact mechanism behind accelerated WMH progression after menopause as well as why reintroducing estrogen does not counteract this mechanism is not known.

Studies have mainly focused on cardiovascular risks, not considering sleep alterations in menopause as a possible mechanism.

- Healthy amounts of sleep are independently associated with lower WMHV[5]
- Menopause related sleep disturbances are independently associated with WMHV[6]

Aim: Determine whether whether menopause or HRT affect the relationship between sleep and WML volume.

Methods

Initial Screening

- Applicants were initially screened based on cardiovascular risk, neurological disorders, psychiatric conditions, menopausal status, and medical history/medications
- There were initially 54 non HRT females, 19 HRT females, and 41 males

Sleep Measurements

- Sleep duration was measured by actigraph watches

WMH Data

- A Lesion Prediction Algorithm (LPA) pipeline was used to identify WMH on FLAIR scans and calculate WMHV
- WMHV was adjusted for intracranial volume (ICV) and log-adjusted

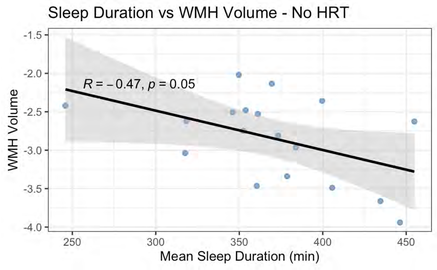
MatchIt: Adjusting for Confounders

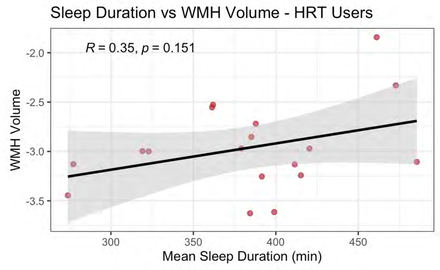
Confounds	No HRT	Male	Std. mean diff.
Age	62.38	62.69	-0.063
Education	16.31	16.54	-0.102
BMI	29.87	30.00	-0.021
Non-smoker	0.69	0.69	0.000
Smoker	0.31	0.31	0.000

Confounds	HRT	No HRT	Std. mean diff.
Age	64.44	64.50	-0.009
Education	17.00	16.61	0.170
BMI	27.81	27.31	0.100
Non-smoker	0.72	0.72	0.000
Smoker	0.28	0.28	0.000

Results

How does HRT affect the relationship between sleep and WMHV?

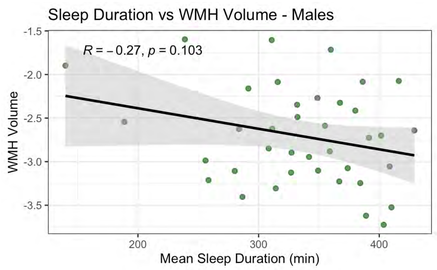


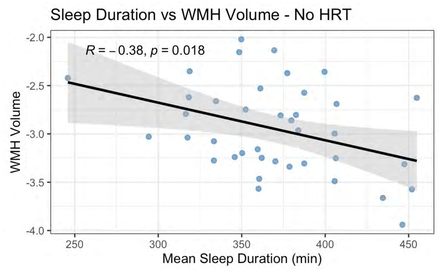


	SEX.HRT	Sleep Duration (min)	WMHV
N	FNo	18	18
	FYes	18	18
Mean	FNo	370	-2.84
	FYes	384	-2.96
Median	FNo	365	-2.69
	FYes	387	-3.00

- **HRT Group:** positive but not statistically significant correlation (r=0.35, p>0.05)
  - Note: when H_a was positive correlation p=0.076
- **Control Group (no-HRT):** statistically significant negative correlation (r=-0.27, p ≤ 0.05)

How does the relationship between sleep and WMH differ between males and females?





	SEX-HRT	Sleep Duration (min)	WMHV
N	FNo	39	39
	M	38	39
Mean	FNo	370	-2.95
	M	335	-2.70
Median	FNo	369	-3.00
	M	345	-2.70

- **Post-Menopausal Group (No-HRT):** positive but not statistically significant correlation (r=-0.38, p>0.05)
- **Control Group (Males):** statistically significant negative correlation (r=-0.27, p ≤ 0.05)

Discussion

Females w/ HRT vs Females w/o HRT

While the results from the HRT group were not statistically significant, the results are still worth discussing considering the small sample size and small p-value (0.076)

As of yet, no studies have found a positive correlation between sleep and WMHV

Possible implications if sleep duration and WMHV are positively correlated in a later study with a larger sample size:

- Discovery of a new risk factor for WMH related to HRT
- New understanding of HRT effects
- Greater importance of sleep in future studies researching HRT and WMHV

Females w/o HRT vs Males

Post-menopausal females have a stronger association between sleep duration and WMHV than men.

- Sleep is likely not one of the main mechanisms behind accelerated WMH progression after menopause

Oddities in the data set:

- Males had more WMHV than females, which goes against prior literature[8]
  - Could be because of unmeasured confounders
- There was not a significant correlation in males (p>0.05)
  - Could be because of the small sample size

Limitations

1. Lack of premenopausal females included in the analysis allowed for sex-specific confounders, and menopause was not isolated.
2. Cross-sectional design limits ability to determine causality and account for confounders.
3. Small sample size limited statistical power.

Acknowledgments

A special thanks to Dr. Michelle Voss, Giovanna Novi, and Liam Campbell for their guidance and support. We thank the support from the National Institute on Aging (NIA) (R01 AG055500) that funded the BrainEXTEND trial, and the MR imaging equipment supported by a high-end instrumentation grant (S10OD025025).

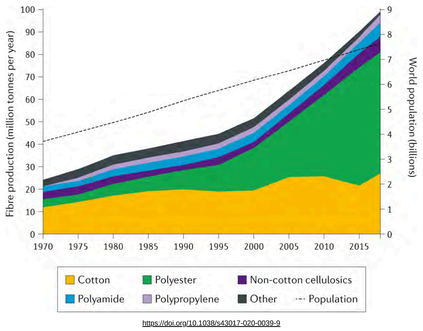
References and Citations

Optimizing RNA-FISH to Analyze Bacterial Cellulose Production in *Escherichia coli*–*Komagataeibacter xylinus* Co-Culture

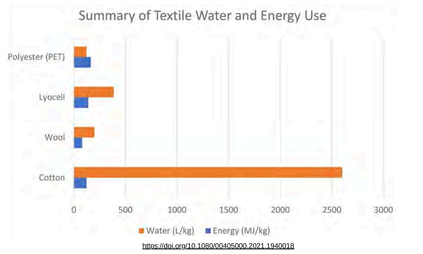
Trisha Shivakumar[1], Ji Woo Han[2], Cole Southard[2], Hyeongmin Seo, PhD[2]

[1]The Harker School, San Jose, CA; [2]Department of Chemical and Biochemical Engineering, University of Iowa

Introduction

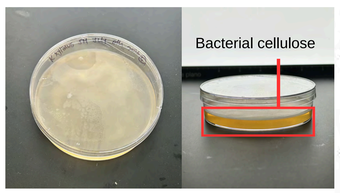


https://doi.org/10.1038/s43017-020-0039-9



https://doi.org/10.1080/00405000.2021.1940018

- The world generates over **92 million tons** of textile waste per year
- We now operate in a linear economy, so this waste is burned or landfilled
  - Emits **1.2 billion tons** of greenhouse gas (Chen et al., 2021)
- Growing cotton costs **2,230 L of water** per shirt (Kranthi et al., 2025)
  - **2 years of drinking water** for one person
- Causing **drought, deforestation, and disease** in regions like Brazil, India, Burkina Faso
- **Bacterial cellulose (BC)**, a cotton alternative grown by bacteria, is a promising alternative that **lowers water usage** and can be grown sustainably using waste products



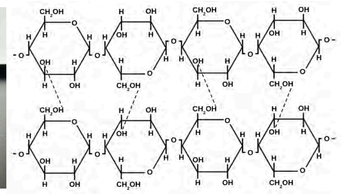


Figure 1. Bacterial cellulose structure consists of hydrogen bonds on the atomic scale and a dense fibrous network on the nanoscale, giving a "pure cellulose" cotton replacement.

- Through co-culture, *B. cereus* increased BC ~3x, better for widespread adoption (Li et al., 2023)

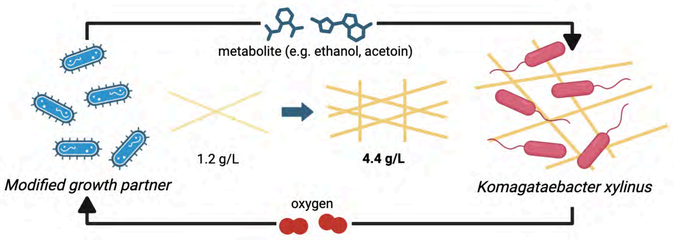


Figure 2. Positive feedback growth loop with co-culture partner providing metabolites for *K. xylinus* to grow cellulose and *K. xylinus* providing oxygen for partner to grow.

Research Goals

1 Optimize RNA-FISH hybridization time, optical density, and dehydration to increase efficiency of co-culture analysis

2 Analyze bacterial cellulose production and properties in *K. xylinus* monoculture versus modified co-culture.

Methods

Preparation/ Setup | Reaction | Separation/ Purification | Optimization | Imaging/ Analysis

Cloning Partner Enzyme

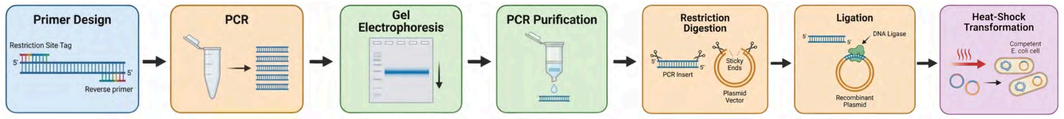


Figure 3. Cloning procedure used to express nitroreductase in *E. coli* for textile dye degradation. This procedure is also used to engineer *E. coli* to produce the ethanol metabolite.

RNA-FISH Optimization

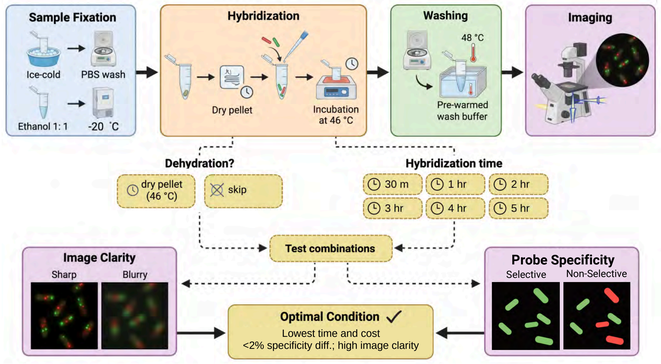


Figure 4. RNA-FISH protocol; optimizing dehydration, hybridization time, and optical density in order to increase cell viability and image clarity for co-culture analysis.

Bacterial Cellulose Production

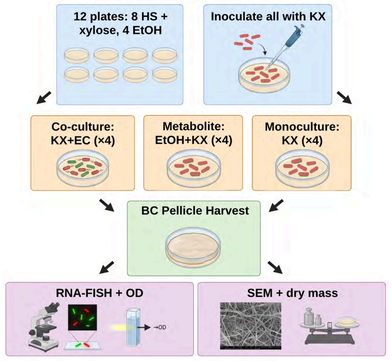


Figure 5. Preparation and analysis of bacterial cellulose in co-culture versus monoculture.

Results and Discussion

Experiment #1: RNA-FISH

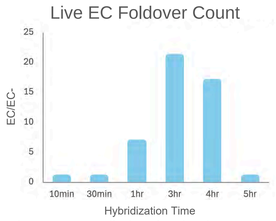


Figure 6. *E. coli* Signal-to-background peaked most at 3 hours.

Probe Specificity Differences

Modification	% Difference
No dehydration	−0.24
No wash incubation	+1.30
3 h hybridization	+0.02

Table 1. All 3 optimization approaches show specificity within 2% of standard.

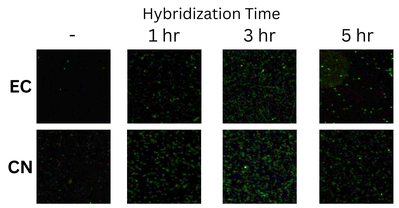


Figure 7. Image clarity increases until 3 hours then makes insignificant difference, justifying 3 hour hybridization time.

Experiment #2: Bacterial Cellulose Co-Culture

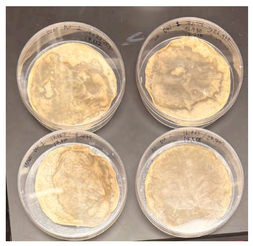


Figure 8. BC grown with mono-culture (left) versus co-culture (right), showing similar properties.

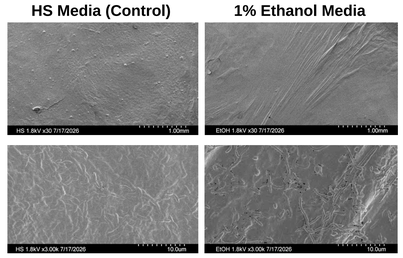


Figure 9. SEM imaging showing that the addition of EtOH (right) does not damage BC's surface structure; it increases production while retaining strength.

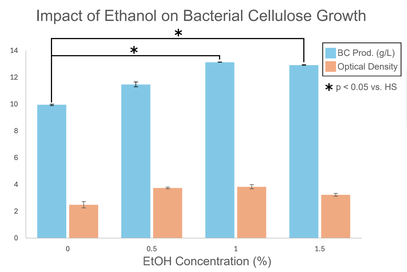


Figure 10. At 1% Ethanol concentration, BC shows optical density of +54% and dry mass of +32%, indicating higher *K. xylinus* productivity and growth.

Reducing hybridization to 3 hours and eliminating dehydration and wash incubation preserved specificity and image clarity while **halving protocol time**. Adding 1% ethanol produced **13.14 g/L** of bacterial cellulose, with **32% greater dry mass** and **54% higher optical density** than the control.

Conclusions

2x faster FISH | **>10x** cheaper FISH | **+32%** BC growth | **117x** less water

- Optimized RNA-FISH showed **98%+ specificity** at 3-hour hybridization; cell counter reduced cost ~10x over flow cytometer
- Identified 1% EtOH as optimal; effect diminished above 1%
- At 1% EtOH, one "BC T-shirt" uses only **19.03 L** of water

Engineered *E. coli* could form a positive feedback loop with *K. xylinus* to produce ethanol gradually within the culture, helping *K. xylinus* generate more sustainable cellulose in the optimal range.

Future Work and Applications

- Genetically modify *E. coli* to produce ethanol and monitor growth to validate feedback loop
- Inoculate BC with different co-culture ratios to analyze population dynamics over time
- Our optimized RNA-FISH procedure can be used as a cheaper bacterial sensor due to our use of a cell counter
  - Isolate species in water sample or wound site to identify toxicity and optimal treatment method
- Co-cultured BC with an ethanol metabolite could offer a sustainable, infection-resistant alternative to state-of-the-art wound dressings
  - When coupled with an Ag/GM-CSF layered, works as antimicrobial agent



https://doi.org/10.1007/978-3-319-76573-0_30-1

Acknowledgements

I would like to thank Dr. Seo, Ji Woo Han, Cole Southard, and the rest of the Engineered BioSynthesis Lab for their mentorship and guidance throughout this project. I also thank SSTP and the Belin-Blank Center for this opportunity.

References

Chapagain, A. K., Hoekstra, A. Y., Savenije, H. H., & Gautam, R. (2006). The water footprint of cotton consumption: An assessment of the impact of worldwide consumption of cotton products on the water resources in the cotton producing countries. *Ecological Economics, 60*(1), 186-203.

Chen, X., Memon, H. A., Wang, Y., Marriam, I., & Tebyetekerwa, M. (2021). Circular economy and sustainability of the clothing and textile industry. *Materials Circular Economy, 3*(1), 12.

Fahma, F., Firmanda, A., Cabral, J., Pletzer, D., Fisher, J., Mahadik, B., ... & Wulandari, A. (2023). Three-dimensional printed cellulose for wound dressing applications. *3D Printing and Additive Manufacturing, 10*(5), 1015-1035.

Hill, J. D., & Papoutsakis, E. T. (2024). Species-specific ribosomal RNA-FISH identifies interspecies cellular-material exchange, active-cell population dynamics and cellular localization of translation machinery in clostridial cultures and co-cultures. *Msystems, 9*(10), e00572-24.

Kranthi, K. R. (2025). Water Footprint in Cotton 2020–2024: A Global Analysis. *International Cotton Advisory Committee.* Washington DC-20006–1635-USA. https://www.icac.org.

Li, W., Huang, X., Liu, H., Lian, H., Xu, B., Zhang, W., ... & Zhong, C. (2023). Improvement in bacterial cellulose production by co-culturing Bacillus cereus and Komagataeibacter xylinus. *Carbohydrate Polymers*, 313, 120892.

Zhang, B., Huang, Z., Guo, T., Jing, J., & Dang, Y. (2025). Accelerating infectious wound healing through bacterial cellulose/ag composite film enriched with GM-CSF. *Scientific Reports, 15*(1), 22142.

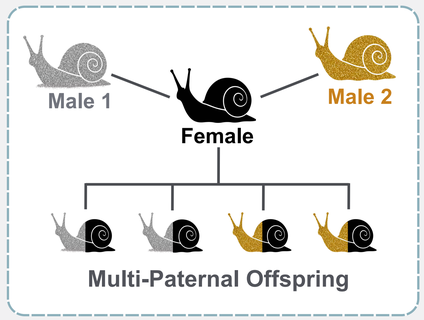
Do Male New Zealand Mud Snails Prefer Virgin Females?

Daniel Sun[1], Clare Mulcahy B.S.[2], Winnie Gavin B.A.[2], Maurine Neiman, Ph.D.[2]

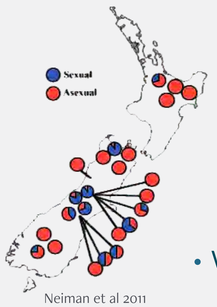
IOWA College of Education Belin-Blank Center
NEIMAN LAB
THE SCIENCE OF SEX @ UNIVERSITY OF IOWA

Sperm Competition in Animals

- **Sperm competition** shapes reproductive success
- **Male mate choice** may reduce sperm competition[1]
- Many species exhibit **virgin female preference**[1]
- **Asexual females** increase the stakes of **male sperm investment**



Why *Potamopyrgus antipodarum*?



Neiman et al 2011

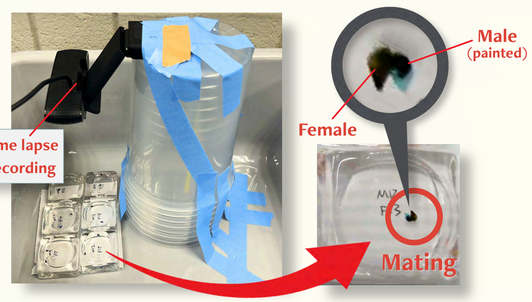
- **Sexual and asexual lineages**
- **Multiple paternity** documented[2]
- Ideal for **mate choice studies**
- Widely used **evolutionary model**

Photo by Christian Böck

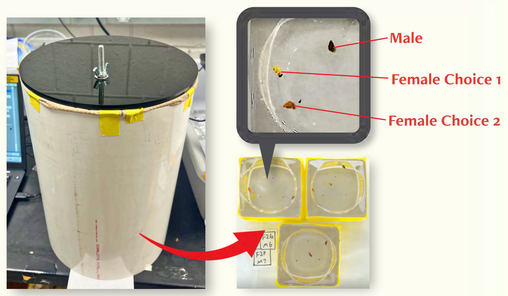
Testing Mate Choice

1. Collect **virgin and recently inseminated females** → Controlled mating to generate inseminated females
2. **Male is given a choice** between female types
3. Analyze **mating preference** through **recording & behavioral scoring**[3, 4]

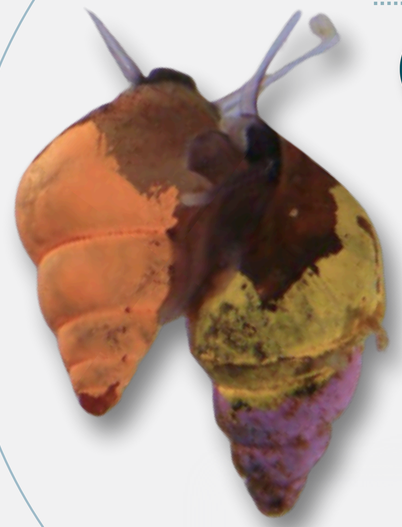
The Setup



1. Controlled Mating



2. Mate Choice Trials

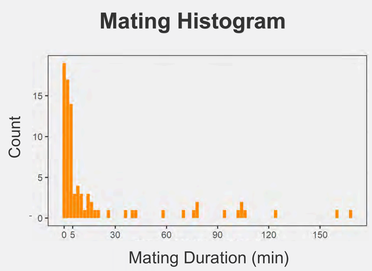


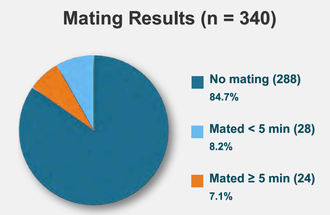
"they just don't wanna mate 😭😭"

Controlled Mating

Virgin females were paired with males to create recently inseminated females.

1. Scored **340 video recordings**
2. Classified matings as **none, <5 min, or ≥5 min**
3. Females with **≥5 min matings** were used in mate choice trials

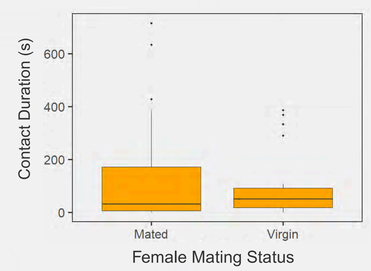




Mate Choice Trials

Males were given a choice between a virgin and a recently inseminated female.

1. Recorded **all interactions**
2. Measured **# of contacts, duration, and matings**
3. Compared **behavioral responses** toward each female



What we determined

- Contact frequency
- Contact duration
- Female Choice

Results & Discussion

- **No clear evidence** of virgin female preference
- On average, males showed **more and longer contact behavior** toward **recently inseminated females**
- **Limited sample size** reduces reliability

Potential Outcomes

- **More matings with virgins** — Male choice reduces sperm competition
- **No preference** — Unable to distinguish / not under strong selection
- **More matings with mated females** — Mated status may imply increased fecundity

Future Directions & Implications

- Increase the number of mate choice trials to **improve statistical power**
- **Potential future experiment:** Test male mate choice under **different conditions** (e.g., increased environmental stress, increased male-male competition)

References & Acknowledgements

[1]The Hill School, Pottstown, PA | [2]Department of Biology, University of Iowa, IA

Hill IOWA Department of Biology

Sex- and Region-Biases in the Effect of Tamoxifen on the Dopamine Transporter

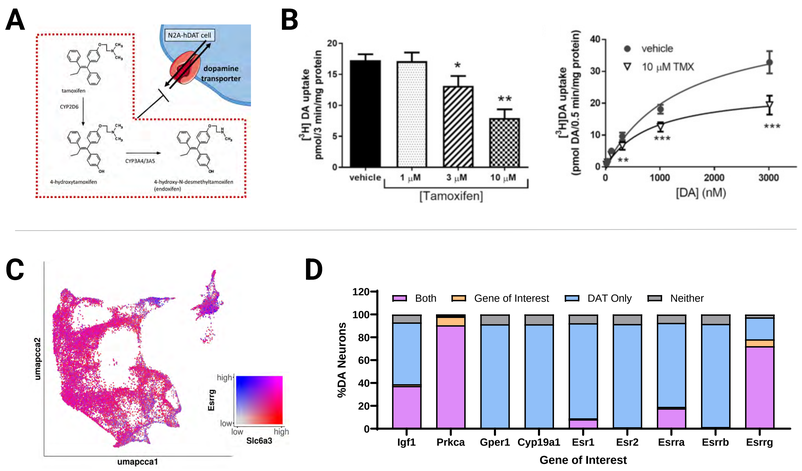
Yihan (Eason) Tang[1], Brenna A. Powers[2], Julia I. Neuharth[2,3], Nathan Fassett[2], and Adele Stewart[2-4]

[1]Liberty High School, Frisco, TX, [2]Department of Neuroscience & Pharmacology, [3]Interdisciplinary Graduate Program in Neuroscience, [4]Iowa Neuroscience Institute, University of Iowa, IA

Abstract

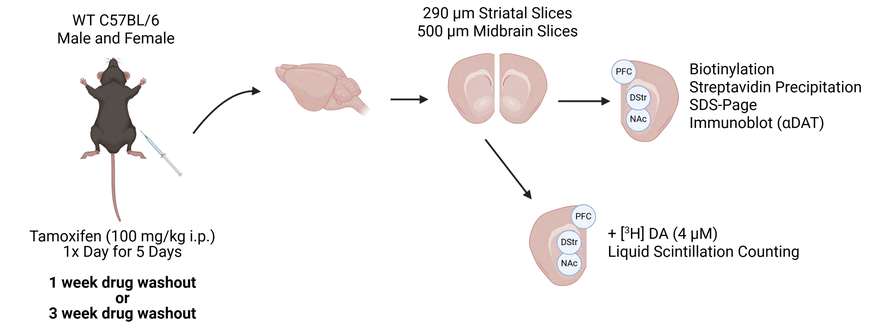
Dopamine (DA) is a catecholamine neurotransmitter involved in motor control, reward processing, and other brain functions. The presynaptic dopamine transporter (DAT) is a membrane protein that clears DA from the synaptic cleft through reuptake into presynaptic neurons. Several aspects of dopaminergic neurotransmission exhibit sex-dependent differences. Tamoxifen (TAM) is a selective estrogen receptor modulator commonly used to treat breast cancer. In preclinical research, TAM is also used to initiate Cre-dependent recombination in inducible rodent models. Previous studies using cultured cells and *ex vivo* synaptosomes from male mice suggest that TAM and its active metabolites can reduce DAT-mediated DA uptake. However, the underlying mechanism, duration, and potential sex dependence of this effect remain unclear. To assess the effects of TAM on dopaminergic neurotransmission in both sexes, male and female C57BL/6 mice received TAM (100 mg/kg, i.p.) or corn oil vehicle for 5 consecutive days followed by a drug washout period. We collected brain slices containing dorsal striatum (DStr), nucleus accumbens (NAc), and prefrontal cortex (PFC), which represent projection regions of the three major dopaminergic pathways. We also collected slices containing dopaminergic cell bodies in the substantia nigra pars compacta (SNc) and ventral tegmental area (VTA). *Ex vivo* [^{3}H] DA uptake and biotinylation assays were performed after 1 and 3 weeks of drug washout. An additional cohort of mice underwent open-field locomotor testing 1 week after treatment. TAM treatment produced a female- and DStr-specific decrease in DA uptake. No significant changes were detected in males or in the other female projection regions examined. TAM also had no significant effect on amphetamine-induced locomotor activity in either sex. These findings suggest that TAM modulates DAT through an alternative, sex-dependent mechanism that may not be fully explained by its conventional actions at estrogen receptors. One possibility is that TAM acts through an alternative receptor or signaling pathway, potentially involving estrogen-related receptor gamma. Alternatively, active TAM metabolites, including 4-hydroxytamoxifen and endoxifen, may engage distinct signaling pathways in females. These mechanisms may produce sex- and time-dependent effects on DAT function.

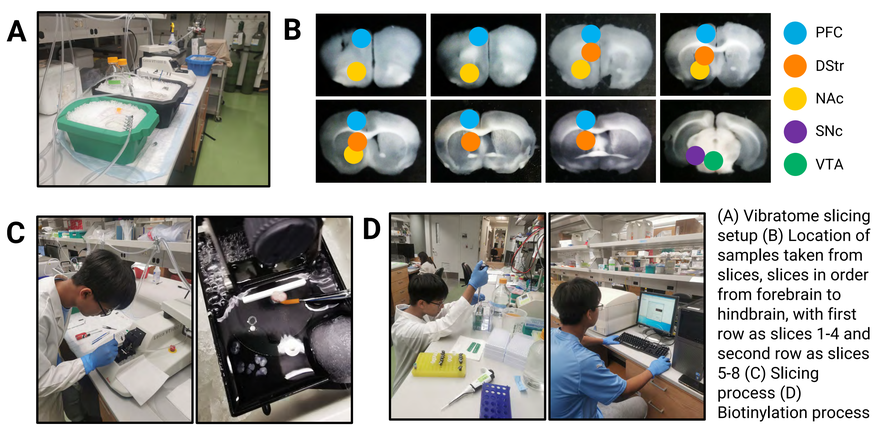
Background



Tamoxifen (TAM) and its active metabolites modulate dopamine transporter (DAT) function, resulting in reduced [^{3}H]DA uptake. Estrogen-related receptor gamma (ERRγ) is a potential molecular target. (A) Previous studies suggest that TAM and its active metabolites 4-hydroxytamoxifen and endoxifen inhibit DAT function in transfected cells (Mikelman et al., 2017). (B) Acute TAM treatment reduces [^{3}H]DA uptake in male striatal synaptosomes. Synaptosomes treated with 3 or 10 μM TAM exhibited significantly lower [^{3}H]DA uptake than vehicle treated controls (Mikelman et al., 2018). (C) ERRγ, encoded by *Esrrg*, is co-expressed with DAT, encoded by *Slc6a3*, in approximately 72% of dopaminergic neurons (Dopabase.org). (D) Among potential targets of TAM and its metabolites, ERRγ exhibits relatively high co-expression with DAT in dopaminergic neurons (Dopabase.org).

Methods and Results





(A) Vibratome slicing setup (B) Location of samples taken from slices, slices in order from forebrain to hindbrain, with first row as slices 1-4 and second row as slices 5-8 (C) Slicing process (D) Biotinylation process

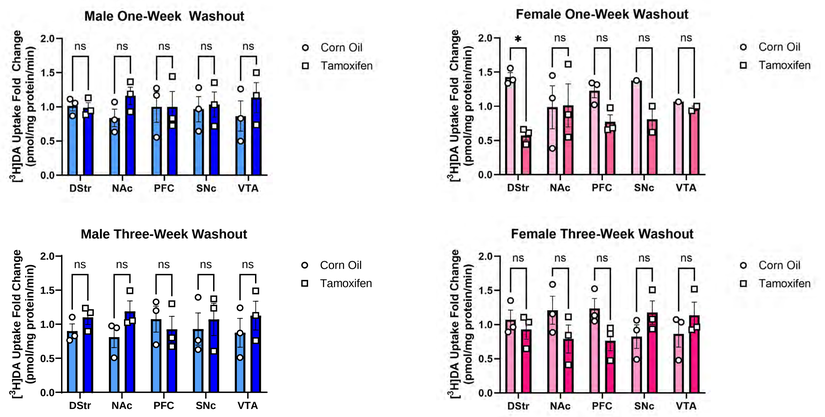


Figure 1: Tamoxifen treatment results in a decrease in [^{3}H]DA uptake in the female, but not male, DStr after a 1-week washout period. DAT-mediated [^{3}H]DA uptake was assessed in slices containing DStr, NAc, PFC, SNc, and VTA of male and female C57BL/6 mice following completion of either a one-week or three-week drug washout period. TAM significantly decreased uptake in the DStr of female mice compared to vehicle treated controls at the one-week time point. This decrease was not present following three weeks of drug washout. No significant treatment-dependent differences in DAT-mediated uptake were observed in males or in the other brain regions examined in females at either timepoint. Data were analyzed by two-way ANOVA and are presented as mean ± SEM. *P < 0.05.

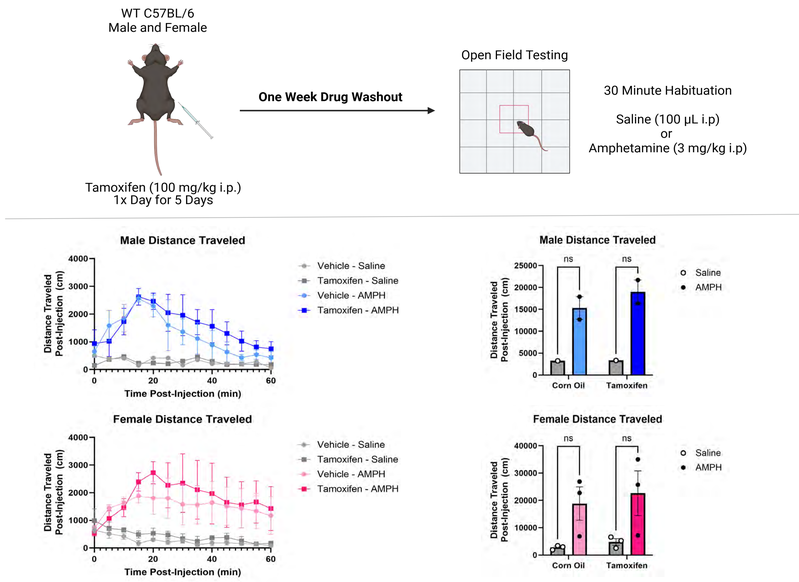
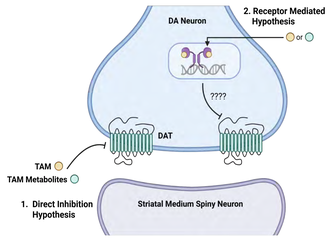


Figure 2. Tamoxifen treatment does not alter amphetamine-induced locomotor activity after a 1-week washout period. Male and female mice treated with tamoxifen or vehicle received a single injection of amphetamine (AMPH, 3mg/kg i.p.) or saline (100 μL i.p.) following habituation in the open-field chamber. Locomotor activity was recorded for 60 minutes after injection. No significant effects of tamoxifen treatment on AMPH-dependent locomotion were observed in either sex. Data were analyzed by two-way ANOVA and are presented as mean ± SEM. ns = not significant.

Conclusions



- Significant decrease in DA uptake in the DStr of females indicates differing mechanisms of DAT regulation by tamoxifen in males and females.
- Variability across timepoints suggest tamoxifen's active metabolites may regulate DAT.
- These findings suggest two potential mechanisms of DAT regulation by TAM:
  - Direct interaction and inhibition of DAT
  - Action at a receptor upstream of DAT to influence DAT Function

Future Directions

- Replicate experiment at 48-hour washout timepoint to match the timepoints run in the literature
- Run same uptake, biotinylation, and behavior procedures with larger sample sizes
- Further investigate intermediate steps in TAM regulation based on proposed mechanisms

Acknowledgments

This work was supported by NIH Grants 1R21DA060410 (A.S.) and T32GM144636 (B.A.P.). I would like to express my sincere gratitude to Dr. Adele Stewart for her mentorship and for the opportunity to contribute to this project, and Brenna Powers, Julia Neuharth, and Nathan Fassett for their guidance throughout the research process. I am also grateful to the entire Stewart Lab for fostering a welcoming and supportive environment. Additionally, I would like to thank Ashlee Donithan and the SSTP staff for making this invaluable experience possible.

References

1. Mikelman SR, Guptaroy B, Gnegy ME. Tamoxifen and its active metabolites inhibit dopamine transporter function independently of the estrogen receptors. J Neurochem. 2017;141(1):31-6. Epub 20170214. doi: 10.1111/jnc.13955. PubMed PMID: 28075498.
2. Mikelman SR, Guptaroy B, Schmitt KC, Jones KT, Zhen J, Reith MEA, Gnegy ME. Tamoxifen Directly Interacts with the Dopamine Transporter. J Pharmacol Exp Ther. 2018;367(1):119-28. Epub 20180814. doi: 10.1124/jpet.118.248179. PubMed PMID: 30108161; PMCID: PMC7250473.
3. Dopabase.org

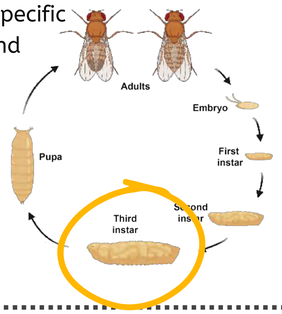
Assessing Larval Associative Learning in Fly *prickle* Mutants

Sophia Tian[1], Letong Chen[2], Brady Williquett[3], J. Robert Manak, PhD[3]

[1]Cinco Ranch High School, [2]Westtown School, [3]University of Iowa

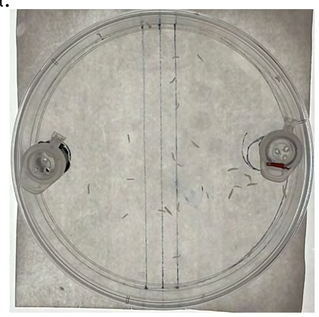
Introduction

- *prickle* is involved in nervous system development and function in *Drosophila melanogaster*.
- *prickle* mutations increase seizure susceptibility through oxidative stress and glial immune activation, making *Drosophila* a model for studying epilepsy-related disorders.[1,2]
- Understanding how individual *prickle* mutations affect behavior may reveal isoform-specific roles in neural development and neurological disease.
- This study investigates whether *prickle* mutations affect associative learning in third-instar *Drosophila* larvae.



Methodology[3]

1. Thirty feeding third-instar *Drosophila melanogaster* larvae of each genotype were collected, rinsed with water, and transferred to experimental plates.
2. Larvae completed three 5-minute training cycles pairing one odor (1-octanol or amyl acetate) with a 2 M fructose reward and the alternate odor with agarose.
3. A reciprocal training group was tested by reversing the odor–reward pairing to minimize bias.
4. Larvae were placed on an agarose-only test plate containing both odor sources. After 5 minutes, the number of larvae on each side of the plate and in the center was recorded.
5. The Performance Index (P.I.) was determined. Three biological replicates were completed for each genotype.



Materials

All relevant mutations were outcrossed into a Canton-S genetic background.

prickle gene variants			
+/+	All isoforms of *prickle* functional	No seizures, low neuronal cell death, robust learning in adults	learning at larval Stage?
pk^{pk}	Loss-of-function mutation in the *prickle-prickle* isoform	No seizures, very high neuronal cell death, normal learning in adults	
pk^{sple}	Loss-of-function mutation in the *prickle-spiny-legs* isoform	Seizures, high neuronal cell death, poor learning in adults	
pk^{M}	Loss-of-function mutation in the *pkM* isoform	Unknown effects	
$pk^{pk-sple13}$	Loss-of-function mutation of the entire *prickle gene*		

Results

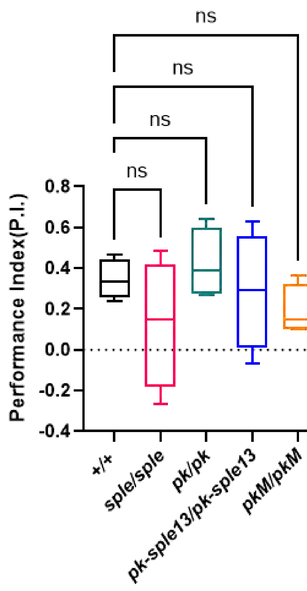


Figure 1. Naïve Sugar Preference Is Similar Across Genotypes. Data shown are mean ± SD. Brown-Forsythe and Welch ANOVA test with Dunnett's T3 multiple comparisons test, *n* ≥ 3 assays per condition, 30 larvae per assay. ns = not significant, * = $p < 0.05$.

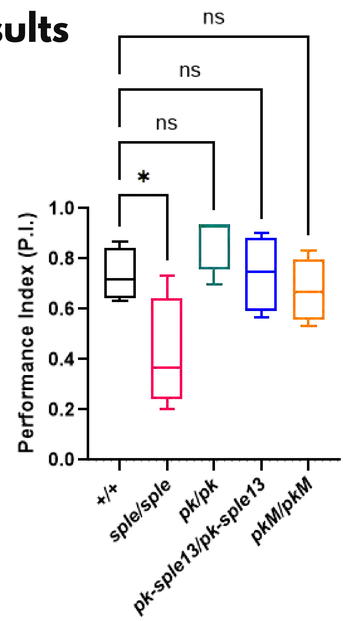


Figure 2. Naïve AM Preference Is Reduced for *sple* mutants. Data shown are mean ± SD. Brown-Forsythe and Welch ANOVA test with Dunnett's T3 multiple comparisons test, *n* ≥ 3 assays per condition, 30 larvae per assay. ns = not significant, * = $p < 0.05$.

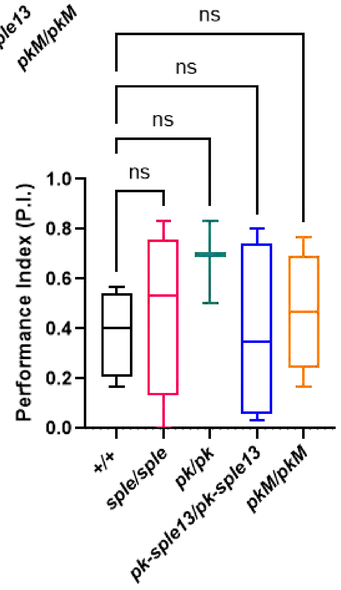


Figure 3. Naïve OCT Preference Is Similar Across Genotypes. Data shown are mean ± SD. Brown-Forsythe and Welch ANOVA test with Dunnett's T3 multiple comparisons test, *n* ≥ 3 assays per condition, 30 larvae per assay. ns = not significant, * = $p < 0.05$.

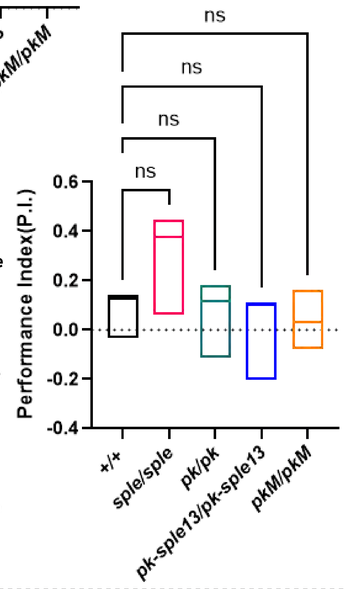


Figure 4. Associative Learning Is Similar Across *prickle* Mutants. Data shown are mean ± SD. Brown-Forsythe and Welch ANOVA test with Dunnett's T3 multiple comparisons test, *n* ≥ 3 assays per condition, 30 larvae per assay. ns = not significant, * = $p < 0.05$.

Conclusions

- Associative learning performance was not significantly different across prickle mutant genotypes compared to wild type, suggesting that loss of specific *prickle* isoforms may not substantially impair larval olfactory learning.
- Despite genetic disruption of *prickle*, larvae maintain the ability to perform some degree of associative learning (PI > 0), thus indicating that early neural circuits required for learning may remain functional.
- The absence of larval learning deficits in pk^{sple} mutants suggests that seizure susceptibility and learning impairment may arise at different developmental stages.
- Early larval neural circuits may be resilient to *prickle* disruption, allowing normal associative learning despite the mutations affecting later neuronal function.
- Differences in quantifications of adult neuronal cell death across different *prickle* mutants do not directly correspond with differences in larval associative learning performance.

Future Direction

Wild-type larvae showed a lower performance index than the generally expected range for this assay (~0.3-0.5).[3]

Further optimization is needed by:

- Increasing biological replicates
- Standardizing larval age and hydration
- Improving odor container consistency
- Minimizing handling stress during transfers.

Future studies should examine additional behavioral phenotypes, including coordination of locomotion, to determine whether *prickle* mutations impact broader nervous system function.

1. Lilienthal, A. J., Parida, M., & Manak, J. R. (2022). Characterization of *prickle* isoform-specific *pk pk1* and *pk sple1* mutations in *Drosophila melanogaster*. *microPublication biology*, *2022*, 10.17912/micropub.biology.000656.
2. Nukala, K. M., Lilienthal, A. J., Lye, S. H., Bassuk, A. G., Chtarbanova, S., & Manak, J. R. (2023). Downregulation of oxidative stress-mediated glial innate immune response suppresses seizures in a fly epilepsy model. Cell Reports, 42(1), 112004. https://doi.org/10.1016/j.celrep.2023.112004
3. Apostolopoulou, A. A., Widmann, A., Rahwedder, A., Pfitzenmaier, J. E., & Thum, A. S. (2013). Appetitive associative olfactory learning in Drosophila larvae. Journal of Visualized Experiments, 72, e4334. https://doi.org/10.3791/4334

References & Acknowledgements

We are grateful to Dr. Manak, Brady Williquett, and the Manak Lab for their mentorship throughout this project. We also thank the University of Iowa and the Belin-Blank Center for making this experience possible.

Who Fears AI? Understanding AI-Related Job Concerns Across Employment Groups on Reddit

Elizabeth Wang[1], Haixia He[2], Weiguo Fan[2]

[1]Middleton High School; [2]Department of Business Analytics, University of Iowa;

Background

- AI is rapidly transforming the workplace (Voigt, 2025), raising concerns about job security and unemployment (Baholli et al., 2026).
- These concerns may differ across employment groups
- Reddit provides large scale anonymous discussions. about AI, work, and mental health, offering honest opinions regarding jobs and employment (Iordache & Iancu, 2026).
- Machine learning enables analysis of user sentiment and employment related concerns.

Objectives

Purpose: Identify how different groups of people are affected by AI in the workplace.
RQ1: How do Reddit users perceive the impact of artificial intelligence on work?
RQ2: How do perceptions of AI-related job concerns differ across users with different employment statuses?
RQ3: How can machine learning models detect users' employment statuses and identify AI-related job concerns from Reddit posts?

Methods

Reddit posts and comments from job/work and mental health communities

Manual annotation
- AI related job concern
- Sentiment
- Employment status

1576 posts and comments containing AI job/work related sentiments labeled "Negative", "Mixed", or "Positive"

1143 posts labeled "True" or "False" in employment status: Student, Seeking Work/Unemployed, Employed

Analyze and compare sentiment across employment status groups

Apply embeddings and train models
- RoBERTa
- Logistic Regression
- LinearSVC
- Zero-shot classification
- Cosine Similarity

Results

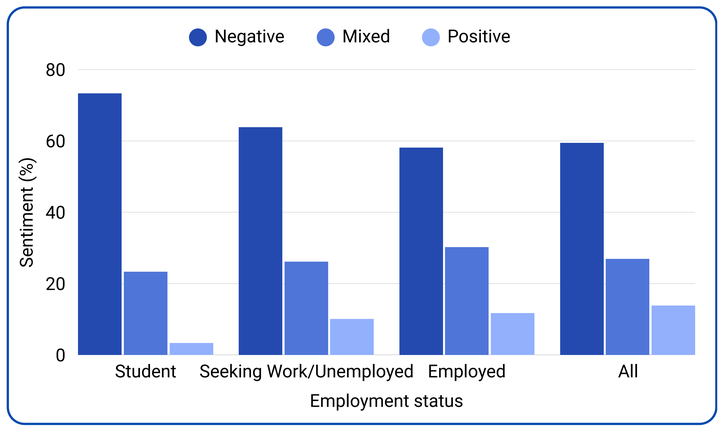


Figure 1. Sentiment distribution across employment statuses

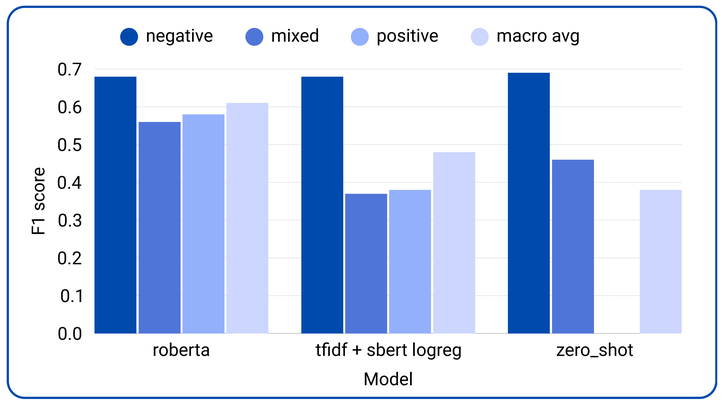


Figure 3. Comparison of F1 scores for sentiment type prediction

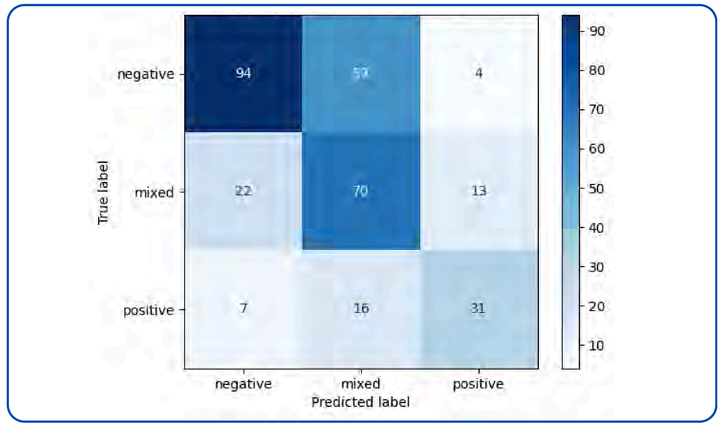


Figure 4. RoBERTA Confusion Matrix for sentiment type evaluation



Figure 2. Frequently seen words in posts with the corresponding employment status label

Step	Model	Accuracy	Precision	Recall	F1
student	**tf-idf + cosine**	0.896	0.725	0.771	0.747
seeking work/unemployed	**tf-idf + sbert + linear_svc**	0.826	0.736	0.831	0.750
employed	**tf-idf + linear_svc**	0.801	0.845	0.822	0.833
sentiment presence	**sbert + linear_svc**	0.845	0.711	0.857	0.777
sentiment type	**RoBERTa**	0.62	0.63	0.61	0.61

Figure 5. Models with highest F1 score for each step of the process

Discussion

Findings:
- The overall sentiment regarding AI-related job loss is negative, with 59.4% of users having negative sentiment compared to 13.8% of users having positive sentiment.
- Students had more negative opinions on AI-related job loss, largely because of either concern for the future or because they returned to school to acquire more skills in face of AI.
- People who were seeking work or unemployed also had more negative sentiments, but not as much as students.
- Models tended to perform well, with exception of sentiment type detection.
- For sentiment type detection, only RoBERTa achieved an F1 score of 0.6 or higher.

Future Directions:
- Increase the amount of data collected to strengthen model performance.
- Investigate how factors such as age, gender, occupation, etc., affect AI-related job concerns.
- Test more models for predicting sentiment type.

Acknowledgements

- Haixia He and Professor Fan for their mentorship and support
- James Cao, Kai Seifan, and Sarah Li for their assistance in data collecting
- The SSTP program for this opportunity and their support while I was hospitalized :(

References

- Baholli, I., Tigno, G., Hidri, F., Sholla, A., Meka, E., & Kruja, S. (2026). Tracking Topic Drift in AI and Workforce Narratives on Reddit: A Longitudinal Visualization from 2010–2024. International Journal of Innovative Technology and Interdisciplinary Sciences, 9(1), 1–24. https://doi.org/10.15157/ijitis.2026.9.1.1-24
- Iordache, D.-M., & Iancu, C. (2026). Unveiling IT job market sentiment and trends: A Reddit-based study using sentiment analysis and named entity recognition. In C. Ciurea, P. Pocatilu, & F. G. Filip (Eds.), *Proceedings of the 24th International Conference on Informatics in Economy (IE 2025): Recent results in education, research, and applications in the AI era* (pp. 423–434). Springer Nature Singapore. https://doi.org/10.1007/978-981-95-6136-0_33
- Voigt, J. (2025). Exploring public sentiment on the impact of AI on work. SSRN. https://doi.org/10.2139/ssrn.5229091

For questions, please email: flyingfalcon25@gmail.com

Glial immune molecules influence synapse levels in young *Drosophila melanogaster*

Laura Wang[1,2], Sierra Feeney[3], Taylor Jay[3]

[1]Ames High School, Ames, Iowa, [2]Secondary Student Training Program, Belin-Blank Center, University of Iowa College of Education, Iowa City, Iowa,
[3]Department of Neuroscience and Pharmacology, Carver College of Medicine, University of Iowa, Iowa City, Iowa

Belin-Blank Center
College of Education
The University of Iowa

IOWA
Carver College of Medicine

Background:

- Inflammation is broadly linked with aging, suggesting exaggerated immune responses may contribute to physiological decay[1]
- Previously, the Jay lab has identified several transcripts upregulated in *Drosophila* **astrocytes**, a primary class of glial cells, with age, which encode immune molecules, many of which are **anti-microbial peptides (AMPs)**
  - AMPs have also been linked to long-term memory in *Drosophila*[2]
- The Jay lab has conducted previous **Brp-GFP ELISA** testing to quantify synapse levels in flies with knockdowns (KD) of these transcripts at 10-12 and 30-35 days post-eclosion (dpe)
  - Brp, or Bruchpilot, is a molecule present in presynaptic zones and serves as a canonical synapse marker[3]

Research Question:

To what degree do glial immune molecules, such as antimicrobial peptides, play a role in synaptic development and elimination, and how do these roles differ with age?

Methods:

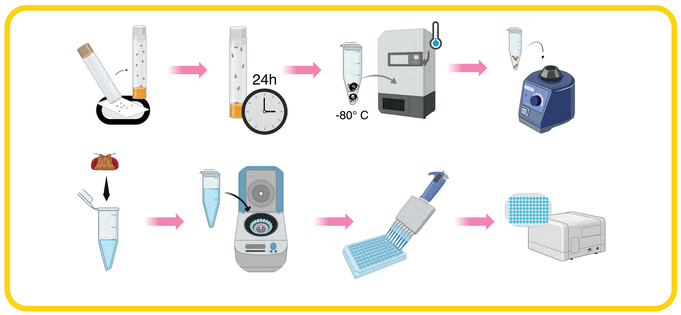


Figure 1. Fly preparation and Brp-GFP ELISA protocol.

Fly preparation:

- All knockdowns were generated using the UAS-Gal4 system with a glial-specific Gal-4 line and transcript-specific RNAi lines
  - Additionally, crosses were created to tag Brp with green fluorescent protein
- Flies were collected and separated by sex at 0-2 dpe, then aged for 24 hours to obtain 1-3 dpe flies
  - Flies were then immediately transferred to -80° C freezer
- Flies were vortexed in eppendorf tubes to remove heads prior to usage in ELISA

Methods:

ELISA (96-well plate):

Day 1: Coat plate in 100 µl of 1:5000 GFP antibody in coating buffer overnight (4 C°)
Day 2: Wash 4x with 0.1% PBST, coat with 300 µl 2% milk in 0.1% PBST overnight (4 C°)
Day 3:

- Homogenize heads with 120 µl PBST, centrifuge at 13,000 rpm for 2 minutes
- Wash wells 4x with PBST, load 100 µl of homogenates, incubate for 90 minutes at 37°
- Wash 4x in PBST, add 100 µl 1:2500 detection Ab in 2% milk PBST overnight (4 C°)

Day 4: Wash 4x with PBST, add 100 µl HRP Ab at 1:2000 Ab overnight (4 C°)
Day 5: Wash 4x with PBST, add 100 µl TMB substrate, then 100 ul 1N HCl to stop reaction; read plate at wavelengths 450 and 630

Data analysis:

- Raw 630 nm values and blank cell averages were subtracted from 450 nm values; these values were then normalized against 10-12 dpe AttP2 controls to be used in an Analysis of Variance

Results:

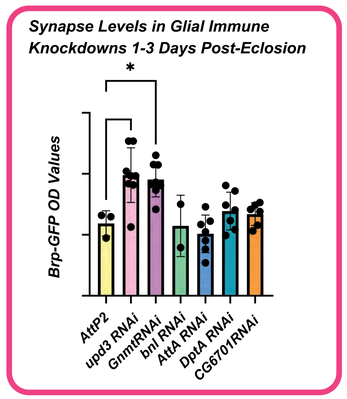


Figure 2. 1-way ANOVA with multiple comparisons test in 1-3 dpe flies. Only significant results between control and experimental flies shown

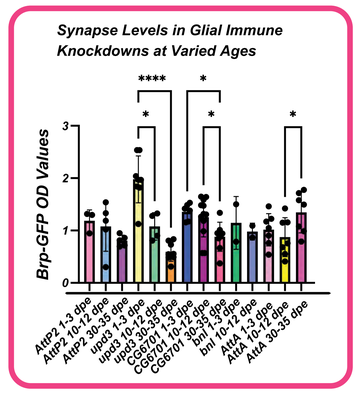


Figure 3. 1-way ANOVA with multiple comparisons test in 1-3, 10-12, and 30-35 dpe flies. Only significant results between same genotypes shown

Discussion:

- Gnmt and upd3 KD flies exhibited higher Brp-GFP levels than age-matched controls, indicating crucial roles in synapse regulation or elimination during the young adult period
- **Upd3** encodes a **cytokine** produced in the fat body, the primary immune organ in the fly, which regulates the immune response[4]; its regulatory role may increase AMP activity, which often target bacteria[5]
  - Because mitochondria evolutionarily originate from bacteria, the **AMPs may nonspecifically target mitochondria and trigger apoptosis[6] in neural cells as a result of cytokine activity, contributing to fewer synapses** in the 1-3 dpe control as compared to the 1-3 dpe upd3 flies
- **Gnmt** encodes **glycine N-methyltransferase** and is expressed in the fat body, the main immune fly organ[7]
  - Knockdown of this gene affecting synapse levels further links increased immune activity to neurodegeneration, implying that production of glycine N-methyltransferase in the glia may play a role in young adult synapse regulation

Conclusions:

The cytokine encoded by upd3 and glycine N-methytransferase in glia play crucial roles in synapse level regulation post-pupal development and in early adulthood, as demonstrated in varied age comparisons and with age-matched controls.

Future Directions:

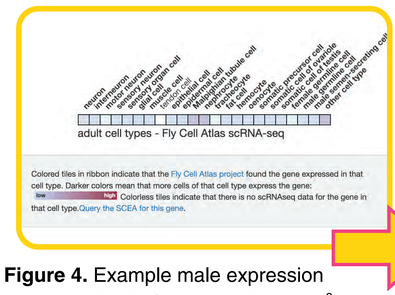


Figure 4. Example male expression ribbon for DptB. Souce: FlyBase.org[9].

- Potentially, conduct a survivorship study to determine the effects of synapse differences between genotypes and ages on **longevity and overall physiological health**
- Complete similar 1-3 dpe Brp-GFP ELISA with knockdowns of transcripts in the fat body, the primary immune organ and primary producer of AMPs[8]
- Complete synapse quantification experiment with knockdowns in the Malpighian tubules to see whether immune molecules produced there affect synapse levels
- Relevant expression data for these transcripts and other immune transcripts upregulated in astrocytes with age demonstrated many were highly expressed in renal cells (nephrocytes) and the Malpighian tubules
  - Malpighian tubules are homologous to human kidneys
  - These included **DptB** (Malpighian tubules and nephrocytes), **bnl** (Malpighian tubules), **AttB** (nephrocytes), and **SPH93** (Malpighian tubules and nephrocytes), all of which encode immune molecules

Acknowledgements:

I'd like to extend my gratitude to Sierra Feeney for her guidance, advice, and knowledge in each step of my work this summer. I'd like to thank Dr. Taylor Jay and each of the members of the Jay lab for welcoming me into their space and allowing me to share in their resources this summer, as well as providing expert guidance and feedback for my work. I'd also like to thank the Secondary Student Training Program for providing me with the opportunity to complete this work. BioRender and GraphPad Prism were used in this poster.

References: https://tinyurl.com/36ejywwh

ARABIC SPEECH INTERPRETER USE IMPAIRS NEUROPSYCHOLOGICAL ASSESSMENT PERFORMANCE

College of Education
Belin-Blank Center

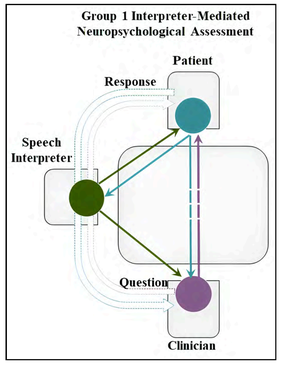
Emma, Yang[1,3]; Ashby, Martin, Ph.D.[1]; Daniel, Tranel, Ph.D.[1,2]

[1]Department of Neurology, [2]Department of Psychological and Brian Sciences, University of Iowa, Iowa City, IA

The University of Iowa

Introduction

- **Neuropsychological assessments** are a collection of cognitive/behavioral tests that aid in diagnosing conditions.
- Arabic-speaking **Limited English Proficiency (LEP)** individuals report speaking, reading, or writing English "less than well" or "not at all" (Martin, 2026). Thus, must rely on a **speech interpreter** for health services.



Research Aim

Research Question: *Does reliance on an Arabic speech interpreter during neuropsychological assessments lead to false judgment of cognitive performance for LEP patients?*

Aims:

- Analyze differences in the testing results of Arabic patients who used a speech interpreter, versus English-speaking patients who did not.
- Examine whether reliance on a speech interpreter during testing can lead to superficial cognitive impairment or misleading diagnostics.

Methodology

- Patient neuropsychological **reports** from Benton Neuropsychology Clinic were compiled.
- Test scores were **converted** to Z-scores for statiscal analysis.

Patient's Primary Neurological Condition	LEP
Progressive Dementia (AD, FTD, LBD)	3
Vascular Dementia	0
Mixed Dementia	3
Encephalitis	1
Tumor(s)	1
Psychiatric or Mood Disturbance(s)	6
Seizure Disorder	3
Neurotoxin Exposure (CO, Hypoxia)	1
Multifactorial Brain Dysfunction	1
Totals	19

Gender	Males	Females	Total
LEP (n=19)	4	15	19
Non-LEP (n=38)	9	29	38
Total	13	44	57

Patient Age	Avg. (±SD)	Range
LEP	53.94737 ± 19.67729	[22-90]
Non-LEP	51.44737 ± 36.27559	[17-89]
Age Matching Quality (SMD)	0.085670847	

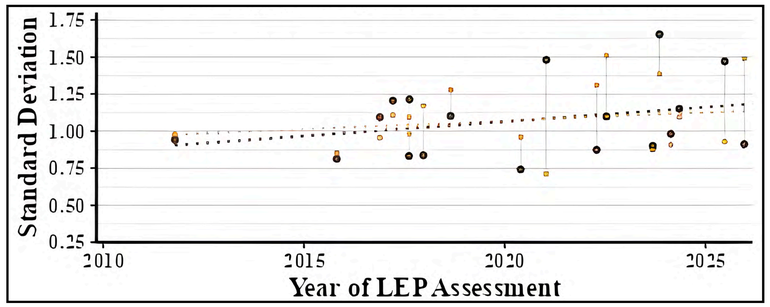
Patient Education	Avg. (±SD)	Range
LEP	10.52632 ± 10.2639	[2-16]
Non-LEP	10.76316 ± 10.3619	[1-16]
Education Matching Quality (SMD)	-0.0229653	

NOTE: A SMD value <0.1 suggests difference is negligible and indicates good balance.

Results

Finding 1: Overlap indicates that the difference in variance between the LEP group and the non-LEP group is not significant.

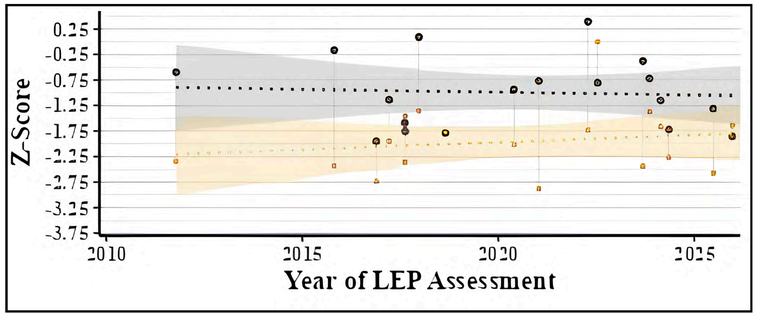
Figure 1: *Neuropsychological Assessment Variance*



Note. This figure shows the assessment variance for each LEP patient (gold) and their respective comparison patients (black).

Finding 2: Reliance on a speech interpreter significantly impairs performance of LEP patients (p < 0.001) on assessments.

Figure 2: *Neuropsychological Assessment Performance*



Note. This figure shows the average performance of LEP patients (gold) and non-LEP patients (black). Negative Z-score values indicate a performance lower than the norm while positive values represent average or above average performance.

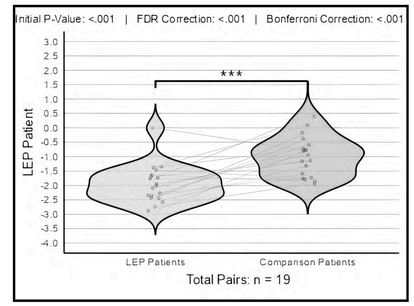
Table 1. *Two-tailed t-test and F-test Results*

Analysis Type	LEP Patient Mean (SD)	Comparison Group Mean (SD)	Degrees of Freedom	t-value	p-value	Cohen's d	F-test	p-value
Weighted (by test proportion)	-0.394(8.4919)	-0.1852(11.73)	18	-4.2715	< 0.001	-0.97996	1.2927	< 0.001
Unweighted (equal pair comparisons)	-1.95(0.6571)	-1.000(0.686)	37	-4.6675	< 0.001	-1.0708	1.2399	< 0.001

Finding 3: There is a significant difference between average z-scores for LEP patients compared to non-LEP patients (p < 0.001).

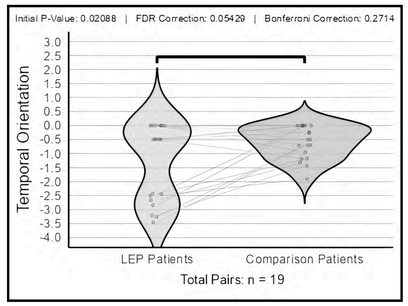
Finding 4: Z-score differences between the two groups specific to the temporal oreintation test was not significant (due to a limited sample size). However, data is trending towards signficance.

Figure 3: *Violin Plot of Data Values (with FDR correction)*



Note. This plot shows the distribution of z-scores, with a wider width indicating more concentrated data points.

Figure 4: *Violin Plot of Data Values for Temporal Orientation Test*



Note. This plot shows the distribution of z-scores specific to the temporal orientation test (a test administered to all patients).

Discussion

- Individuals who do not have a profiency in the English language can come across **barriers** with healthcare services.
- The lack of direct/dyadic interactions can disrupt the **accuracy** of medical interactions.

Study Limitations:

- A small sample size was used (n=19 compared to a expected minimum of n=35).
- Time constraint (5 weeks was utilized).

Future Aims

- Obtain a **larger** data set to effectively prove assessment impairment.
- Develop an all inclusive **protocol** for speech interpreted neuropsychological assessments that has little to no effect on cognitive performance.
- Expand the research to include **bilingual** individuals to study whether bilingualism can produce language specific assessment results.

[1] Brantuo, M. A., An, K., Biss, R. K., Ali, S., & Erdodi, L. A. (2022). Neurocognitive profiles associated with limited English proficiency in cognitively intact adults. Archives of Clinical Neuropsychology, 37(7), 1579–1600. https://doi.org/10.1093/arclin/acac019
[2] Casas, R., Treble, A., Yim, E., Obler, L. K., & Greenwald, B. S. (2012). Interpreter-mediated neuropsychological testing of monolingual Spanish speakers. The Clinical Neuropsychologist, 26(1), 88–101. https://doi.org/10.1080/13854046.2011.640641
[3] Malik, A., El-Haj, M., & Paasche-Orlow, M. K. (n.d.). Readability of Arabic vs. English patient educational materials [Conference poster]. https://elhaj.uk/docs/medicalRead.pdf
[4] Martin, A. (2026). Linguistic barriers in U.S. neuropsychological assessment: A state-of-the-art review. Archives of Clinical Neuropsychology, 41(3), Article acaf091. https://doi.org/10.1093/arclin/acaf091
[5] Nielsen, T. R., Segers, K., Vanderaspoilden, V., Beinhoff, U., Minthon, L., Pissiota, A., Stiglich, S., Tsolaki, M., Goudsmit, M., Palomo, A. F., & European Consortium on Cross-Cultural Neuropsychology (ECCroN). (2024). Interpreter-mediated neuropsychological assessment: Clinical considerations and recommendations from the European Consortium on Cross-Cultural Neuropsychology (ECCroN). The Clinical Neuropsychologist, 38(8), 1775–1805. https://doi.org/10.1080/13854046.2024.2335113

Key Sources & Acknowledgements

First and foremost, I would like to express my graditude to my mentors Dr. Ashby Martin, Dr. Daniel Tranel, and Luke Bruderer. Thank you all for your incredible insights and help! Secondly, I would like to thank everybody in the Tranel Lab and the Benton Neuropsychology Clinic for the amazing opportunities I was given. Furthermore, I am grateful to the Belin-Bank Center for making this research experience feasible. Finally, thank you to my friends and family who pushed me to where I am today.

STPV system with 0.0157% efficiency

Matteo Yu[1], Mihika Kamat[2], Jayden Leung[3], Fatima Toor[4]

[1]Georgetown Preparatory School [2]Los Altos High School [3]Noble and Greenough School [4]Electrical and Computer Engineering, University of Iowa

Intro

- Sub-bandgap and thermalization losses limit the maximum efficiency of a single-junction solar cell to 33%
- Pairing an absorber with a selective emitter can match the bandgap of photons to its PV cell

Methods

1. Designed two-stage concentrator with Fresnel lens and compound parabolic concentrator (CPC)
2. Measured indoor and outdoor I-V curves of absorber-emitter pairs

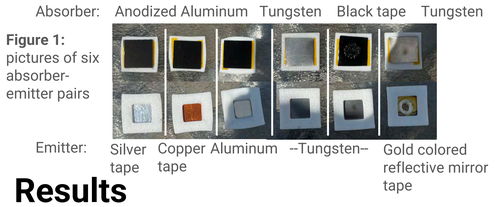


Figure 1: pictures of six absorber-emitter pairs

Results

Figure 2: Current-voltage curve of indoor-tested STPV

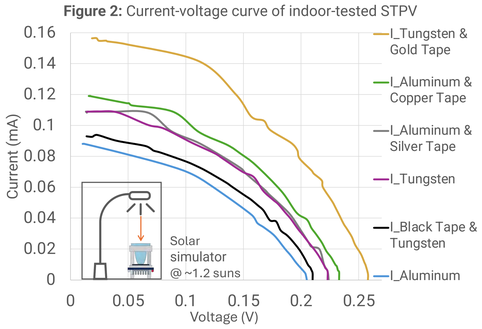
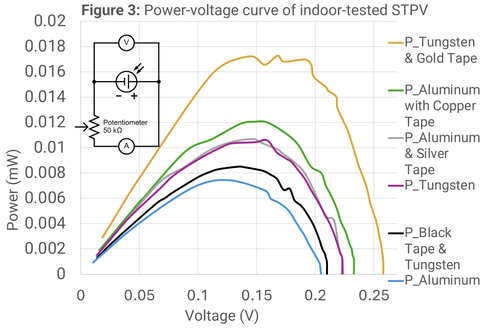


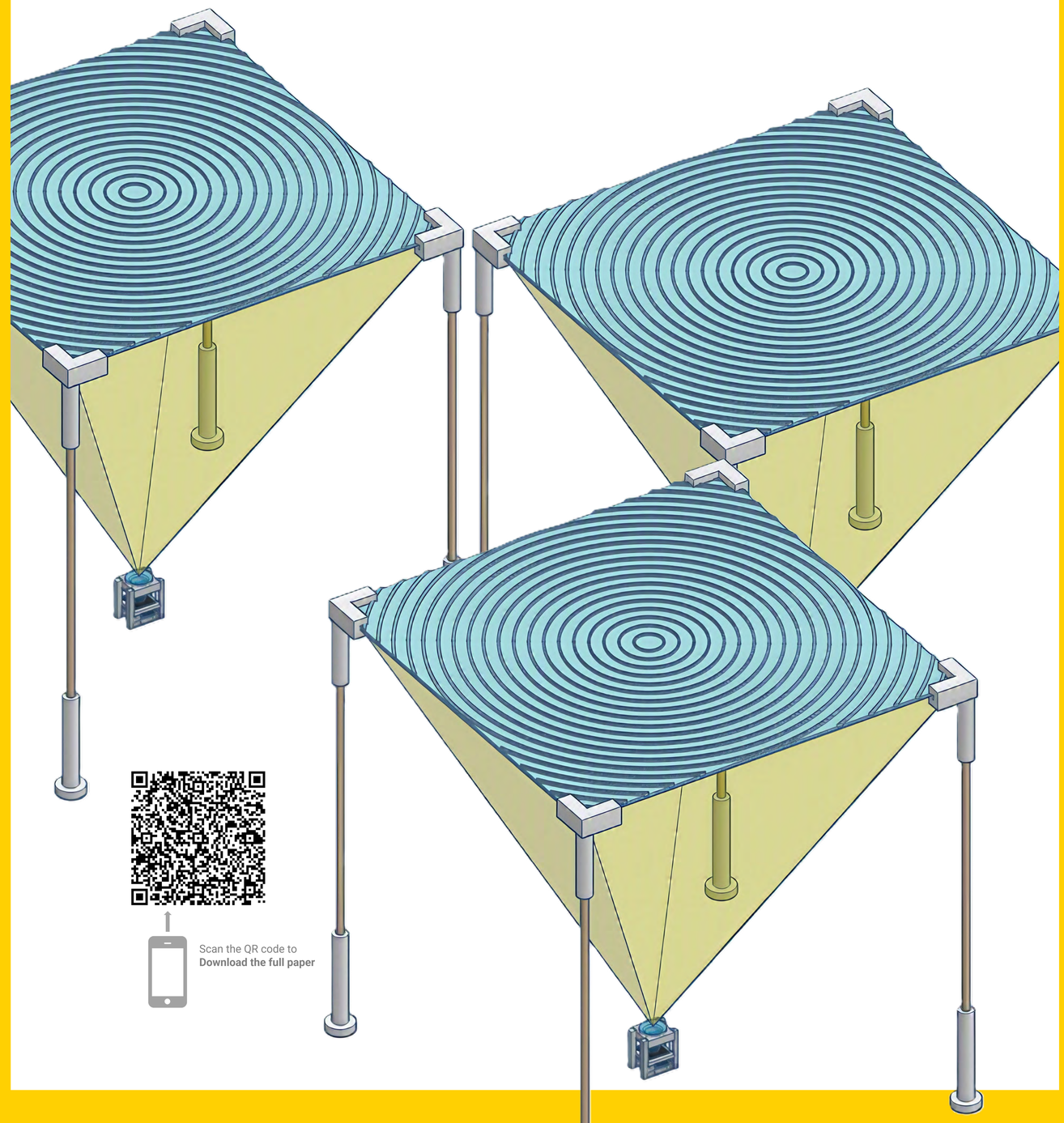
Figure 3: Power-voltage curve of indoor-tested STPV



- Tungsten absorber and gold colored reflective mirror tape achieved the highest power output both indoors and outdoors

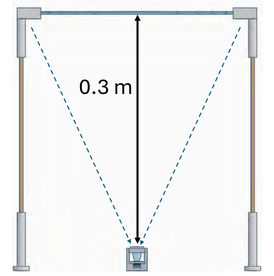
IOWA

Pairing a **tungsten absorber** with a **gold-colored reflective mirror tape emitter** maximizes the efficiency of **solar thermophotovoltaic systems.**



Scan the QR code to **Download the full paper**

Extra Tables & Figures



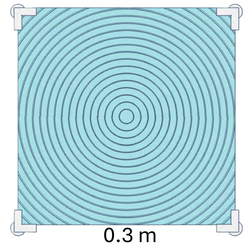
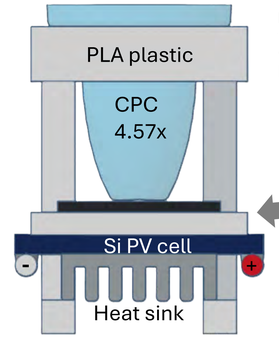


Figure 4: Side and top view of the STPV system with the Fresnel lens



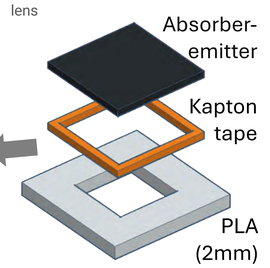


Figure 5: Diagram of the STPV system without the Fresnel lens

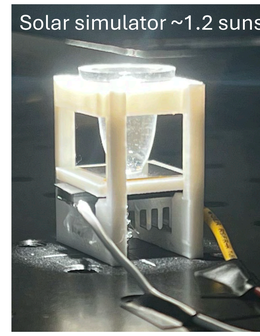


Figure 6: Picture of the indoor test setup using a solar simulator

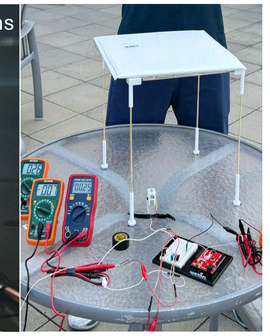


Figure 7: Picture of the outdoor (33℃) test setup with the Fresnel lens.

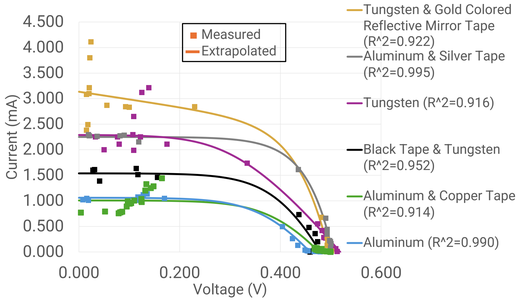


Figure 8: Current-voltage curve of outdoor-tested STPV system.

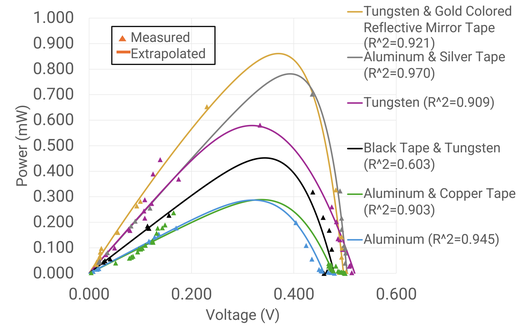


Figure 8: Power-voltage curve of outdoor-tested STPV system.

Caught in a Protein Craze: Influence of Diet on Tentacle Regeneration

Sophia Zeng[1]
Winnie Gavin, B.A.[2]
Peter Nitsche[2]
Maurine Neiman, Ph.D.[2]

[1]Tsinghua International School, Beijing, China
[2]University of Iowa, Department of Biology



Photo taken by Sophia Zeng

Potamopyrgus antipodarum

Does diet influence healing processes?

- Regeneration of tissue is energetically costly
- Resource allocation may depend on nutrient availability [4]

Why *Potamopyrgus antipodarum*?

- An established model for studying tentacle regeneration [1,5]
- Diverse array of asexual lineages allows for powerful controlled experiments holding genetic variation constant [3]
- Can readily manipulate diet [2,6]

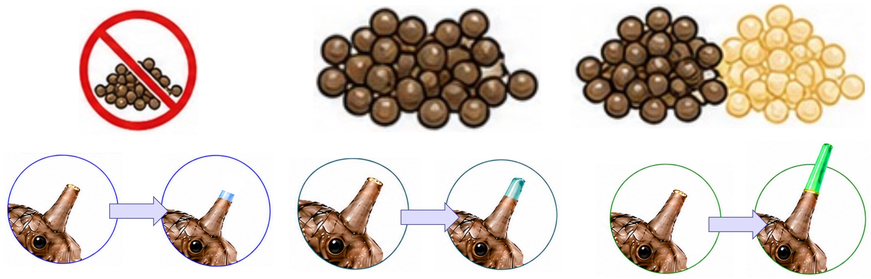


Photo taken by Dorota Paczesniak, CC BY 4.0

Does food and environmental nutrients matter?

How does food and protein availability affect the rate of tentacle regeneration?

Hypothesis: Tentacle regeneration will proceed the most rapidly with food and protein supplementation, while food-deprived snails will experience the slowest regeneration.



Diagrams rendered on BioRender and Canva

Experimental Design

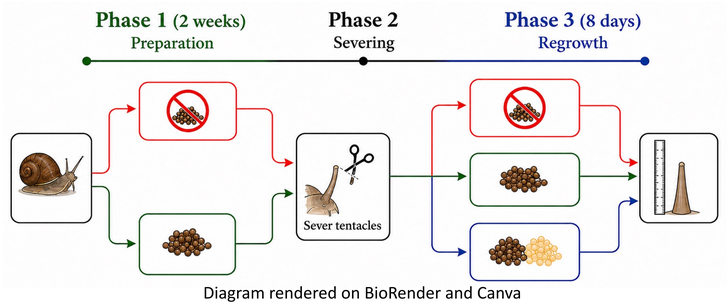
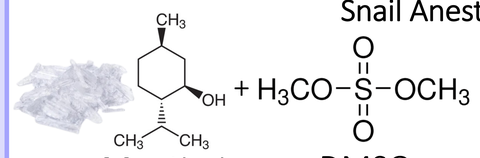


Diagram rendered on BioRender and Canva

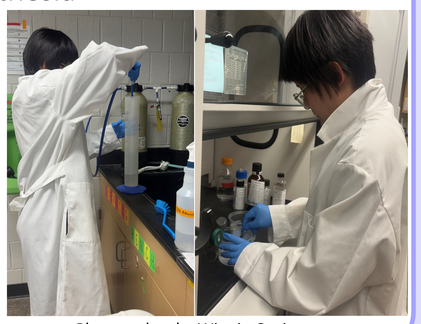
Snail Anesthesia



Menthol DMSO



Photo taken by Christian Böck, University of Innsbruck, Austria



Photos taken by Winnie Gavin

Analysis Reveals An Unexpected Correlation

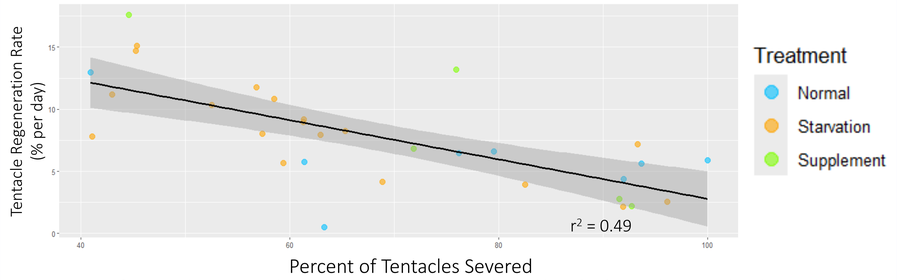


Figure 1. Significant and negative relationship between percent of initial length of tentacle severed and tentacle regeneration rate (β = -0.700, $p < 0.011$; $r^2 = 0.49$).

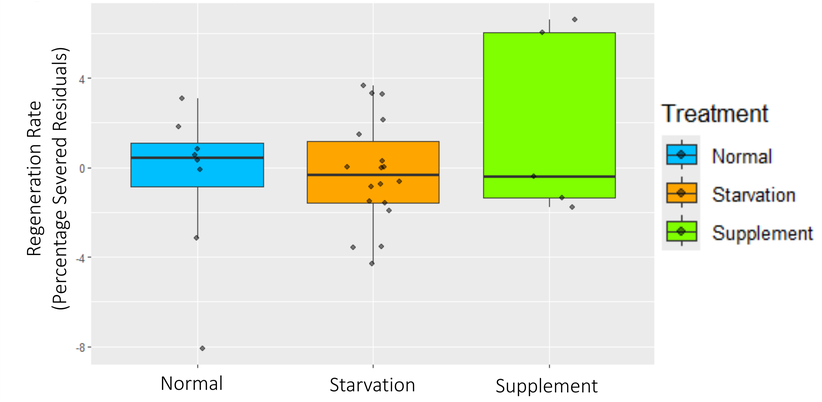


Figure 2. Regeneration rate by food treatment. There was no evidence for an effect of food treatment (ANOVA: $F_{(2,28)} = 1.142$, $p = 0.334$). We used residuals from the linear regression between the percent of each tentacle severed and regeneration rate for the ANOVA to correct for the negative effect of increased fraction of tentacle removal on the rate of tissue regeneration.

Charts rendered on R Studio

Conclusions & Next Steps

Results

- No evidence for a relationship between regeneration rate and diet treatment
- Confounding negative correlation between percent of tentacle severed and regeneration rate

Limitations

- Variation in fraction of tentacle removed across snails
- Challenges in standardizing measurement photos
- Small sample size (~ 30 snails)

Future Directions

- Increase the number of snails severed
- Standardize percent of tentacle severed
- Explore mechanism underlying relationship between severed tentacle percentage and regeneration rate

References & Acknowledgements

[1]Krois, N., Cherukuri, A., Puttagunta, N., & Neiman, M. (2013). Higher rate of tissue regeneration in polyploid asexual versus diploid sexual freshwater snails. *Biology Letters*, *9*(4), 20130422. https://doi.org/10.1098/rsbl.2013.0422

[2]Kröncke, N., & Benning, R. (2023). Influence of dietary protein content on the nutritional composition of mealworm larvae (*Tenebrio molitor* L.). *Insects*, *14*(3), 261. https://doi.org/10.3390/insects14030261

[3]Lively, C. M. (2024). *Through the looking glass: I. Why cross-fertilize?* Indiana University Bloomington Libraries Publishing. https://doi.org/10.5967/gbd3-ka07

[4]Rädecker, N., Chen, J. E., Pogoreutz, C., Herrera, M., Aranda, M., & Voolstra, C. R. (2019). Nutrient stress arrests tentacle growth in the coral model *Aiptasia*. *Symbiosis*, *78*(1), 61–64. https://doi.org/10.1007/s13199-019-00603-9

[5]Song, Q., Magnuson, R., Jalinsky, J., Roseman, M., & Neiman, M. (2021). Intraspecific genetic variation for anesthesia success in a New Zealand freshwater snail. *Genetica*, *149*(1), 47–54. https://doi.org/10.1007/s10709-020-00110-6

[6]Tuncha, N. P., Niba, A. T., & Banla, N. R. (2021). Effect of feeding different levels of protein supplementation on the growth performance of young snails (*Archachatina marginata*) in the western highlands of Cameroon. *Animal Husbandry, Dairy and Veterinary Science*, *5*, 1-6. https://doi.org/10.15761/ahdvs.1000186

I would like to acknowledge members of the Neiman Lab for helping me and to Belin-Blank Center and SSTP for providing me this research opportunity.

Effects of S_2Cl_2 as a Secondary Crosslinking Agent on Polydicyclopentadiene (pDCPD) Membranes

Patrick Zhang[1], Allen Ma[2], Saurav Katuwal[3], MS, Jett Tjaden[3], MS, Ned B. Bowden[3], PhD

[1]Head-Royce School, CA, [2]Princeton International School of Mathematics and Science, NJ, [3]Department of Chemistry, University of Iowa, IA

Introduction

Fatty acids are valued for their biodegradability, safety, and diversity, such as in biofuel and vegetable oil production. Traditional methods used to separate fatty acids, such as distillation and recrystallization, are energy-intensive or are restricted to specific molecules.[2] OSN (Organic Solvent Nanofiltration) membranes, however, can separate molecules at room temperature and can be engineered to separate specific mixtures.[5]
Various studies have aimed to separate fatty acids and fatty acid methyl esters with different membranes.[2, 3]

Dicyclopentadiene (DCPD, Figure 1) is an organic molecule that undergoes ring opening metathesis polymerization (ROMP) to produce the polymer, polydicyclopentadiene (pDCPD). pDCPD is a highly chemical-resistant polymer that swells in various organic solvents, opening its polymer chains and allowing for diffusion of molecules.[4] The C=C bonds allow for further customization of crosslinking density, establishing it as a great starting material to insert cross-linking agents such as S_2Cl_2, a strong electrophile able to bind to such sites.[1]

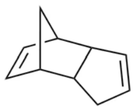


Figure 1. DCPD
Source: Wikipedia

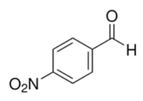


Figure 2. PNB
Source: Sigma-Aldrich

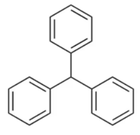


Figure 3. TPM
Source: Sigma-Aldrich

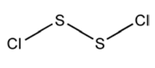


Figure 4. S_2Cl_2
Source: Wikipedia

Research Question:

How does the degree of secondary crosslinking using S2Cl2 affect the permeability of pDCPD membranes, and what fabrication conditions are required to make results replicable and applicable?

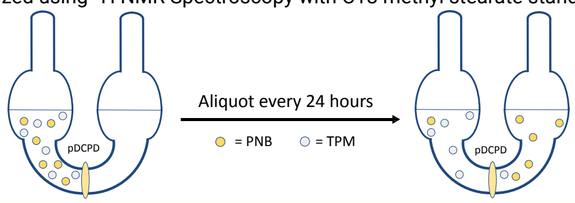
Methodology

pDCPD membranes were synthesized by combining DCPD and Grubbs catalyst (1st generation) in a 5000:1 ratio and pressed between two silanized glass plates on a 45°C hot plate. Selected membranes were measured to be approximately 60-100 μm thick and cut into circular discs of radius approximately 2 cm.

pDCPD membranes were swelled in DCM for 30 minutes before S_2Cl_2 (0.5, 0.8, 1.0, 1.2, 2.0 eq) was added with 20 mL DCM and stirred on an orbital shaker for 30 minutes.

Two bulbs were affixed together by two O-rings and a clamp, separated by the membrane. 1:1 of the components were prepared as the retentate. The retentate (1:1 ratio of PNB:TPM) was dissolved in 30 mL Dichloromethane (DCM) and placed in one bulb, while the permeate side contained only 30 mL DCM.

1 mL aliquots were extracted from each side every 24 hours and were analyzed using ^{1}H NMR Spectroscopy with C18 methyl stearate standard.



Results & Discussion

Raw pDCPD Membrane: PNB vs. TPM Separation

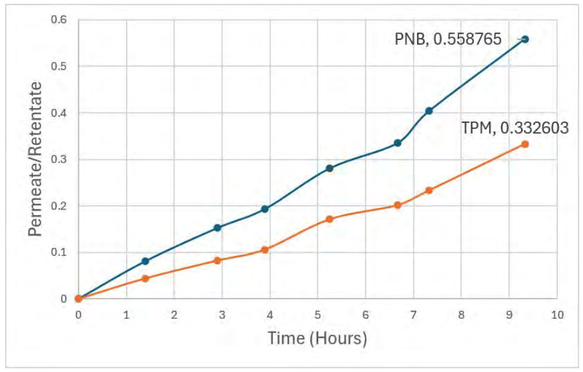


Figure 1. Baseline selectivity of PNB and TPM of uncrosslinked pDCPD membrane (0.0 eq S_2Cl_2).

30 min. Swelling: PNB vs. TPM Separations

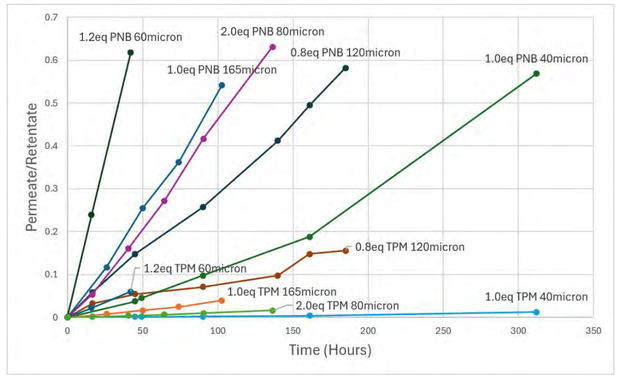


Figure 2. Effect of S_2Cl_2 equivalence on PNB/TPM selectivity under 30-minute unagitated swelling.

Overnight Swelling: PNB vs. TPM

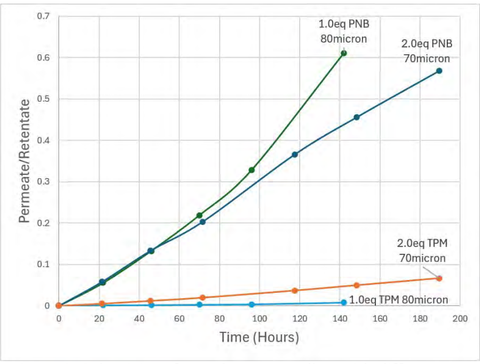


Figure 3. Selectivity of membranes swollen with different S_2Cl_2 equivalences overnight without agitation for 12 hours.

30 min. w/Agitation Swelling: PNB vs. TPM

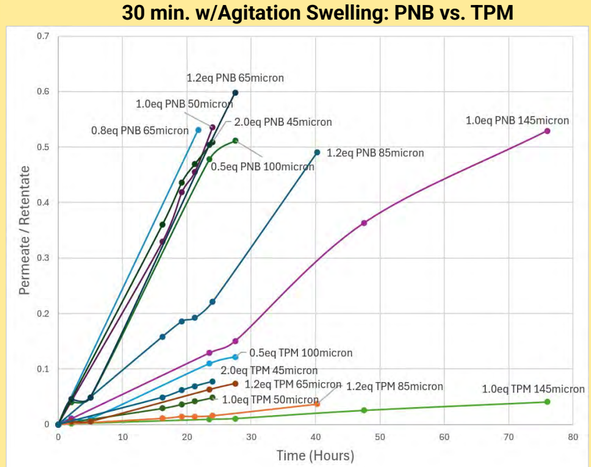


Figure 4. PNB/TPM Selectivity under 30-minute swelling with agitation in order to ensure reproducibility.

30 min. w/Agitation Swelling: Fatty Acids

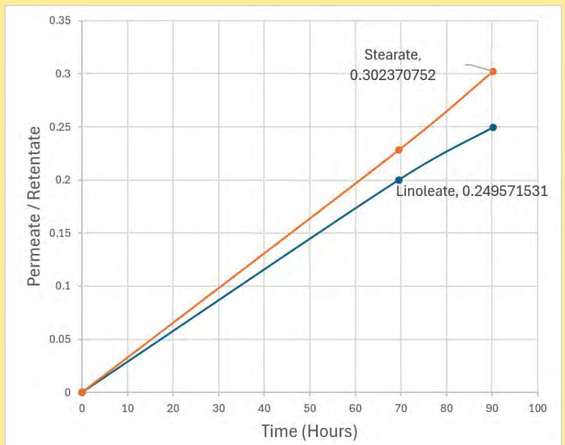


Figure 5. Separation of fatty acid methyl esters (Methyl Stearate/Methyl Linoleate) under 30-minute swelling with agitation.

Effect of S2Cl2 Equivalence (Agitated 30-minute Swelling) on Selectivity

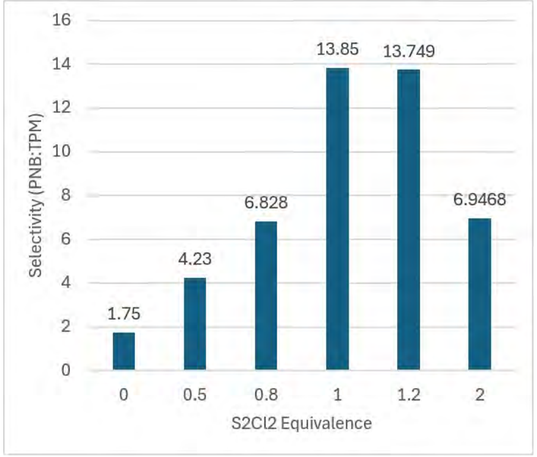


Figure 6. PNB/TPM selectivity as a function of S_2Cl_2 equivalence across 30-minute agitation trials. Highest selectivity occurs between 0.8x and 1.2x eq.

Conclusion

It was demonstrated that pDCPD membranes crosslinked with S_2Cl_2 are significantly more selective than raw pDCPD membranes, and that flux and selectivity can be controlled via swelling method and S_2Cl_2 equivalence. Results suggest a tradeoff between surface-concentrated and homogeneous crosslinking, though further characterization is needed to confirm. These membranes are not able to effectively separate C18 fatty acids and methyl esters, potentially requiring more selectivity through crosslinking.

Future Works

Investigate the effect of pressure on the flux and selectivity of ultra-thin S2Cl2-crosslinked pDCPD membranes. Investigate the effect of localized or homogenous crosslinking by quantitatively characterizing the degree of crosslinking throughout the membrane using FTIR or SEM.

Acknowledgements

Thank you to Jett Tjaden, Allen Ma, and Saurav Katuwal, and Professor Bowden for your valuable support throughout this program and for further inspiring my learning in chemistry.

References

Gilmer, C. M., & Bowden, N. B. (2018). Reactive epoxy nanofiltration membranes with disulfide bonds for the separation of multicomponent chemical mixtures. ACS Omega, 3(8), 10216–10224. https://doi.org/10.1021/acsomega.8b01323
Gilmer, C. M., Zvokel, C., Vick, A., & Bowden, N. B. (2017). Separation of saturated fatty acids and fatty acid methyl esters with epoxy nanofiltration membranes. RSC Advances, 7, 55626–55632. https://doi.org/10.1039/C7RA11642B
Long, T. R., Gupta, A., Miller, A. L., Rethwisch, D. G., & Bowden, N. B. (2011). Selective flux of organic liquids and solids using nanoporous membranes of polydicyclopentadiene. Journal of Materials Chemistry, 21, 14265–14276. https://doi.org/10.1039/C1JM11834D
Marchetti, P., Jimenez Solomon, M. F., Szekely, G., & Livingston, A. G. (2014). Molecular separation with organic solvent nanofiltration: A critical review. Chemical Reviews, 114(21), 10735–10806. https://doi.org/10.1021/cr500006j
Ranasinghe Arachchige, N. P. R., Xiong, N. W., & Bowden, N. B. (2023). Separation of C18 fatty acid esters and fatty acids derived from vegetable oils using nanometer-sized covalent organic frameworks incorporated in polyepoxy membranes. ACS Applied Nano Materials, 6(8), 6715–6725. https://doi.org/10.1021/acsanm.3c00442

Aging-Associated DNA Methylation Silences the FOXA2-PGR-HAND2 Pathway in Endometrial Cancer

Pinyan Panya Zhu[1]; Xiangbing Meng, PhD[2]; Shujie Yang, PhD[2]
[1]Portsmouth Abbey School, RI; [2]Department of Pathology, University of Iowa

Introduction

Endometrial Cancer

- The only major cancer with declining survival rates over the past 40 years.[1]
- Hormone therapy is most effective in tumors expressing progesterone signaling.[2,3]

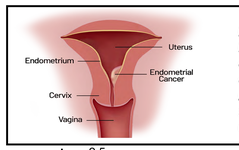


Figure 1. *Diagram of endometrial cancer. Picture retrieved from* ***Saint John's Cancer Institute***[4]

FOXA2-PGR-HAND2 Pathway

- **FOXA2** regulates progesterone receptor (PGR) expression.[2,5]
- **PGR** activates **HAND2**, a key suppressor of endometrial proliferation.[2,5]
- Disruption of this pathway contributes to endometrial cancer progression.[2,5]

Aging and Epigenetics

- **DNA methylation** is an epigenetic modification that regulates gene expression without altering the DNA sequence.[5]
- Aging is associated with aberrant DNA methylation that silences the **FOXA2–PGR–HAND2** pathway. [2,5]
- These epigenetic changes are potentially reversible.[5]
- **5-AZA** inhibits DNA methylation, while **Romidepsin** inhibits histone deacetylases, increasing chromatin accessibility.[3,5]
- Together, these epigenetic drugs may restore expression of the **FOXA2–PGR–HAND2** pathway and progesterone receptor (PR).[3,5,6]

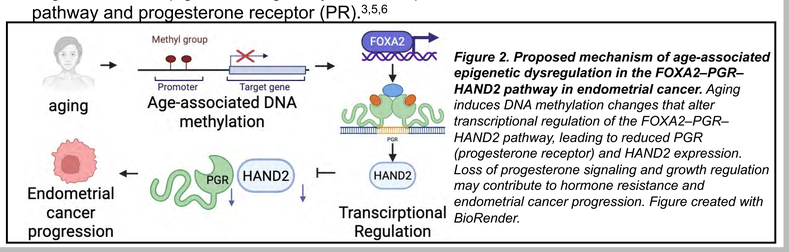


Figure 2. Proposed mechanism of age-associated epigenetic dysregulation in the FOXA2–PGR–HAND2 pathway in endometrial cancer. *Aging induces DNA methylation changes that alter transcriptional regulation of the FOXA2–PGR–HAND2 pathway, leading to reduced PGR (progesterone receptor) and HAND2 expression. Loss of progesterone signaling and growth regulation may contribute to hormone resistance and endometrial cancer progression. Figure created with BioRender.*

Objective

Research Question

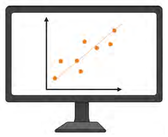
- How does aging influence DNA methylation and gene expression in the **FOXA2–PGR–HAND2** pathway?
- Does **5-AZA + Romidepsin** restore protein expression within this pathway?

Hypothesis

- Age-associated epigenetic alterations disrupt the **FOXA2–PGR–HAND2** pathway, reducing protein expression. Treatment with **5-AZA and Romidepsin** will restore expression of pathway proteins.

Methodology

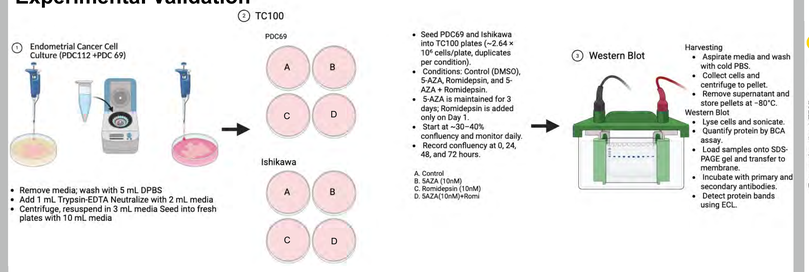
Data Analysis



- Download and clean four-gene methylation datasets from UCSC Xena (remove NAs).
- Generate lollipop plots (P < 0.05, Genomic Position, correlation).
- Create methylation vs. gene expression regression plots (remove 0 methylation).
- Identify inverse methylation-expression correlations.
- Generate CpG methylation vs. age box plots (20-year bins, outliers removed, patient count, P values).
- Generate gene expression vs. age box plots (outliers removed, P values).
- Generate FOXA2 vs. PGR, PGR vs. HAND2

All data generated using RStudio.

Experimental Validation



Results

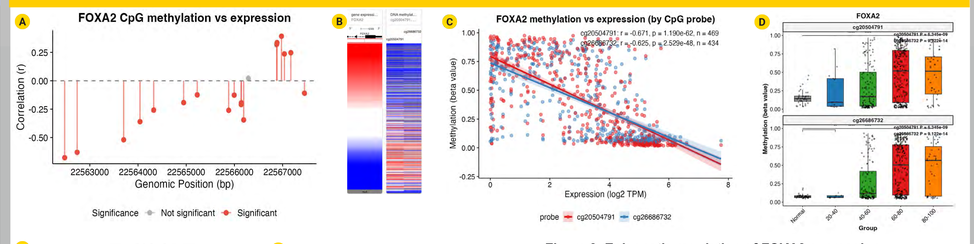


Figure 3. Epigenetic regulation of FOXA2 expression. ***(A)*** *Lollipop plot of CpG probes associated with FOXA2 (P < 0.05) vs. Genomic Position.* ***(B)*** *Heatmap of inverse methylation-expression correlations.* ***(C)*** Scatter plot confirming negative correlation (r < 0, *P* < 0.05). ***(D–F)*** *Methylation and expression across 20-year age bins, showing age-related hypermethylation and decline (P < 0.05). All analyses were performed using RStudio.*

FOXA2

- Inverse correlation between methylation and expression (r < 0, P < 0.05)
- Hypermethylation and expression decline with age (P < 0.05)

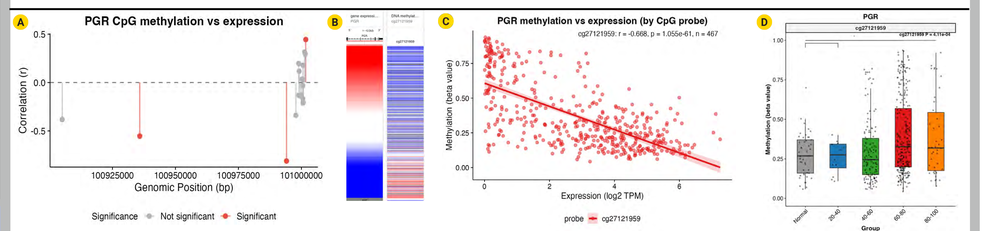


Figure 4. Epigenetic regulation of PGR expression. ***(A)*** *Lollipop plot of CpG probes associated with PGR (P < 0.05) vs. Genomic Position.* ***(B)*** *Heatmap of inverse methylation-expression correlations.* ***(C)*** *Scatter plot for cg27121959 (r = -0.668, P < 0.05).* ***(D–F)*** *Methylation and expression across 20-year age bins, showing age-related hypermethylation and decline (P < 0.05). All analyses were performed using RStudio.*

PGR

- cg27121959 shows strong inverse correlation (r = -0.668, P < 0.05)
- Methylation increases, and expression declines with age (P < 0.05)

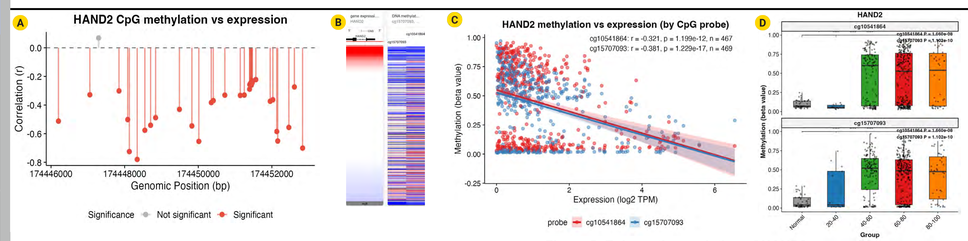


Figure 5. Epigenetic regulation of HAND2 expression. ***(A)*** *Lollipop plot of CpG probes associated with HAND2 (P < 0.05) vs. Genomic Position.* ***(B)*** *Heatmap of inverse methylation-expression correlations.* ***(C)*** Scatter plot confirming negative correlation (r < 0, *P* < 0.05). ***(D–F)*** *Methylation and expression across 20-year age bins, showing age-related hypermethylation and decline (P < 0.05). All analyses were performed using RStudio.*

HAND2

- Inverse correlation between methylation and expression (r < 0, P < 0.05)
- Hypermethylation and expression loss with age (P < 0.05)

Results(continued)

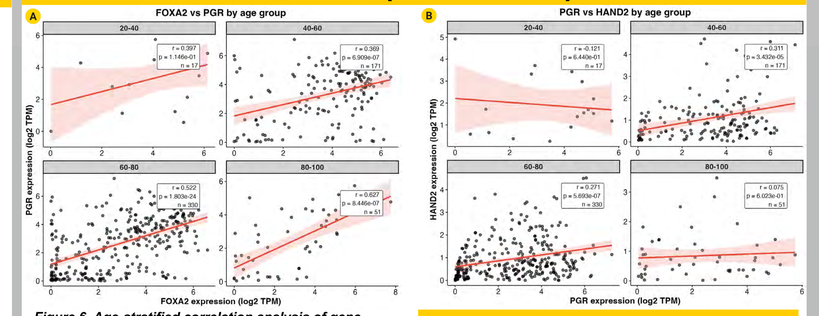


Figure 6. Age-stratified correlation analysis of gene expression. *Scatter plots displaying the correlation between (A) FOXA2 vs PGR and (B) PGR vs HAND2 expression across four age groups (20-40, 40-60, 60-80, 80-100 years). Each panel includes Pearson's correlation coefficient (r), p-value, and sample size (n). FOXA2-PGR correlation strengthens with age (r increasing from 0.397 to 0.627), while PGR-HAND2 correlation peaks in the 40-80 year groups (r ≈ 0.27-0.31) and diminishes in the oldest patients. All analyses were performed using RStudio.*

Age-dependent expression correlations in endometrial cancer

- FOXA2-PGR correlation increases with age
- PGR-HAND2 correlation peaks in middle age but is lost in the elderly

Western Blot

- Combined 5-AZA + Romidepsin treatment synergistically restored FOXA2, PR, and HAND2 expression while increasing PARP cleavage, supporting epigenetic reactivation of progesterone signaling.

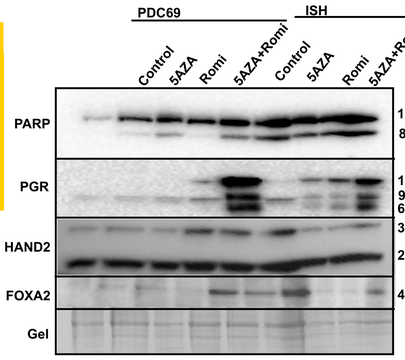


Figure 7. Western blot analysis of FOXA2, PGR, HAND2, and cleaved PARP protein expression in PDC69 cells following treatment with 5-Azacytidine (5-AZA), Romidepsin (Romi), or the combination. *Combined treatment produced the greatest restoration of FOXA2, PR, and HAND2 expression while increasing PARP cleavage, indicating synergistic epigenetic reactivation of the pathway.*

Conclusion

- **FOXA2–PGR–HAND2** pathway is a key aging-associated regulatory pathway in endometrial cancer.
- Age-associated DNA methylation is linked to reduced expression of the **FOXA2–PGR–HAND2** pathway in endometrial cancer.
- Hypermethylation correlates with transcriptional silencing, supporting an epigenetic mechanism underlying disease progression.
- Combined **5-AZA and Romidepsin treatment restored FOXA2, PR, and HAND2 protein expression and enhanced PARP** cleavage, demonstrating synergistic therapeutic activity.
- These findings support epigenetic therapy as a promising strategy to improve progesterone responsiveness and treatment outcomes in endometrial cancer.

Future Directions

- Validate pathway alterations in additional patient-derived models.
- Evaluate epigenetic therapies that restore **FOXA2-PGR-HAND2** signaling
- Develop age-associated methylation biomarkers to predict hormone therapy response.

Acknowledgments

I would like to express my sincere gratitude to Dr. Yang and Dr. Meng for their invaluable guidance and for providing the laboratory space used to conduct this research, as well as the Belin Blank Center for providing this amazing opportunity to conduct research. I also thank NIH R37-CA38274 (SY) and the Department of Pathology Start-Up Fund (ST) for their generous funding support.

IOWA

References